ABSTRACTS BOOKLET OF

CIF24

CHITOSE INTERNATIONAL FORUM 2024

September 3 - 4, 2024
Chitose Inst. of Sci. & Tech. (CIST),
Chitose, Japan

Sponsors and support

公立大学法人
公立千歳科学技術大学

特定非営利活動法人
ホトニクスワールドコンソーシアム

ARIM Japan

ARIM Biomaterials
名古屋大学
次世代バイオマテリアル 拠点

日本化学会北海道支部

高分子学会北海道支部

ACCESS TO CIST

From JR Sapporo Station, 33 minutes by Rapid Airport train to Minami-Chitose Station
From Minami-Chitose Station to the university, 9 minutes by free shuttle bus. Thus, from Sapporo Station to CIST it takes a total of 42 minutes!
From Tomakomai, 19 minutes by local train to Minami-Chitose Station + 9 minutes by free shuttle bus = a total of 28 minutes!

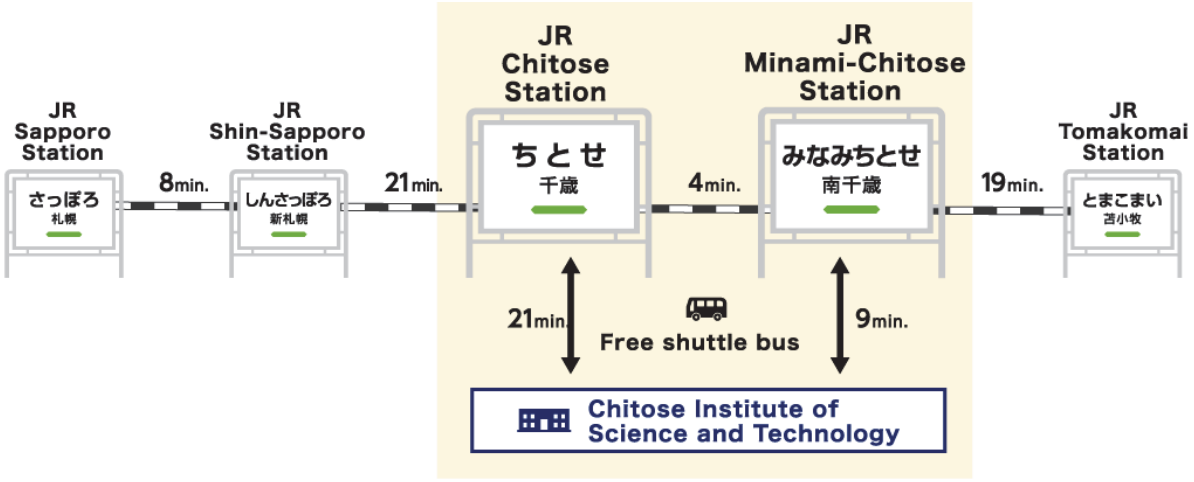

Free shuttle buses run from JR Chitose Station and Minami-Chitose Station to the university. The bus timetable can be found on the next page.
The free shuttle bus takes about 9 minutes from JR Minami-Chitose Station and about 21 minutes from JR Chitose Station to arrive at the CIST. Get off at the main campus.

■Chitose Sta. Bus Stop

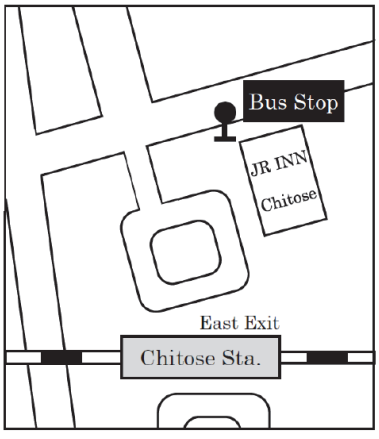

■Minami-Chitose Sta. Bus Stop

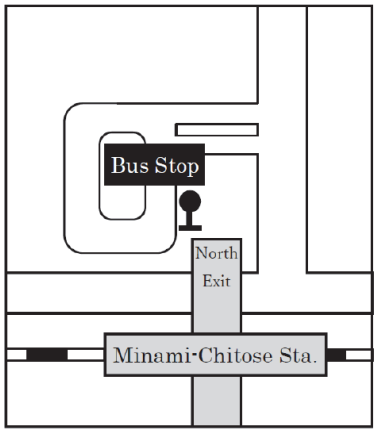

BUS TIMETABLE

Outward

Chitose Sta.	Minami-Chitose Sta.	RESEARCH CAMPUS	MAIN CAMPUS
7:55	8:05	8:13	8:16
8:30	8:40	8:48	8:51
9:18	9:28	9:36	9:39
10:15	10:25	10:33	10:36
10:44	10:54	11:02	11:05
11:39	11:49	11:57	12:00
12:45	12:55	13:03	13:06
13:28	13:38	13:46	13:49
14:28	14:38	14:46	14:49
15:18	15:28	15:36	15:39
16:15	16:25	16:33	16:36
17:18	17:28	17:36	17:39

Return

MAIN CAMPUS	RESEARCH CAMPUS	Minami-Chitose Sta.	Chitose Sta.
10:45	10:48	10:56	11:06
11:34	11:37	11:45	11:55
12:22	12:25	12:33	12:43
13:07	13:10	13:18	13:28
14:00	14:03	14:11	14:21
14:56	14:59	15:07	15:17
16:07	16:10	16:18	16:28
16:47	16:50	16:58	17:08
17:17	17:20	17:28	17:38
17:53	17:56	18:04	18:14
18:29	18:32	18:40	18:50
18:59	19:02	19:10	19:20
19:29	19:32	19:40	19:50
20:13	20:16	20:24	20:34
21:08	21:11	21:19	21:29

BY AIR

Section	Time required
Tokyo (Haneda Airport) → New Chitose Airport	Approx. 90 min.
Osaka (Kansai International Airport) → New Chitose Airport	Approx. 110 min.

BY CAR

Section	Time required
JR Minami-Chitose Station → Chitose Institute of Science and Technology	Approx. 5 min.
New Chitose Airport → Chitose Institute of Science and Technology	Approx. 7 min.
JR Chitose Station → Chitose Institute of Science and Technology	Approx. 15 min.

The main campus is the venue for CIF24.

MAP OF SITE

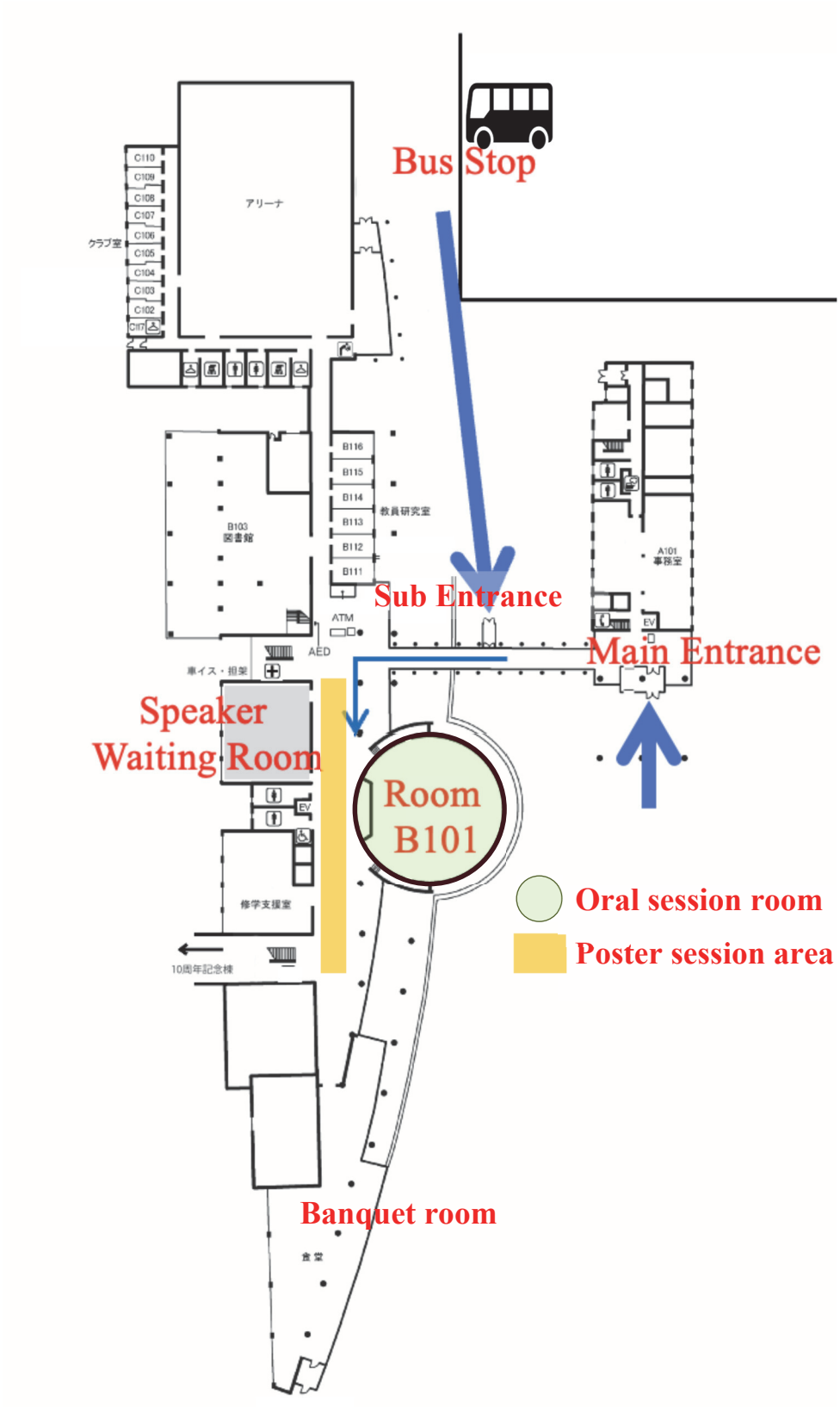
Bus Stop
Sub Entrance
Main Entrance
Speaker
Waiting Room
Room
B101
Oral session room
Poster session area
Banquet room
アリーナ
クラブ室
B103
図書館
教員研究室
A101
事務室
ATM
AED
車イス・担架
修学支援室
10周年記念棟
食堂

URL FOR ONLINE PARTICIPATION

https://us06web.zoom.us/j/89700964939?pwd=Am9bEiQ9ZuA4Z7lTDW9coD9VfsIRnl.1

Meeting ID: 897 0096 4939
Password: 134323

PROGRAM

September 3 (Tue)

13:00-13:10	**Opening** **Welcome Address** Prof. Yoshikazu Miyanaga President of Chitose Institute of Science and Technology (CIST)	
13:10-14:00	**Keynote Lecture** "Advanced Research Infrastructure for Accelerated Biomaterials and Biodevices R&D" Prof. Yoshinobu Baba, Nagoya University, Japan	**p.19**
14:00-14:30	**Tree Planting, Group Picture, Coffee Break**	
14:30-14:55	**Invited lecture 1** "The rise of Materials Informatics: Infrastructure to Materials Design" Prof. Keisuke Takahashi, Hokkaido University	**p.21**
14:55-15:20	**Invited lecture 2** "Data-driven materials science study based on atomic-resolution scanning transmission electron microscopy imaging" Dr. Kohei Aso, Assistant Professor, Japan Advanced Institute of Science and Technology (JAIST)	**p.23**
15:20-15:35	**Oral Presentation 1** "Charge Transport and Thermoelectric Properties in Electrochemically Doped Conducting Polymers" Dr. Hisaaki Tanaka, Associate Professor, CIST	**p.25**
16:00-17:30	**Poster Session**	
17:45-19:30	**Banquet / continued Poster viewing**	

September 4 (Wed)

10:00-10:25	**Invited lecture 3** "Sequence-defined glycopolymers for biomedical applications" Prof. Laura Hartmann, Freiburg Universiy, Germany	**p.26**
10:25-10:50	**Invited lecture 4** "Photoswitchable Bioactive Glass for Calcium Control in Enamel Remineralization" Dr. Enrique Ezra, Assistant Professor, Health Sciences University of Hokkaido	**p.27**
10:50-11:05	**Oral Presentation 2 (Online)** "Fabrication of VO2 micro/nanostructures by laser-induced hydrothermal synthesis" Dr. Christophe Pin, Okinawa Institute of Science and Technology	**p.29**
11:05-11:20	**Oral Presentation 3** "Chitin-chitosan hybrid materials: Effect of crosslinking type and density on mechanical properties" Leonard Genin, Universität Potsdam, Germany	**p.30**
11:20-11:35	**Oral Presentation 4** "Controlled drug-releasable novel dental restorative composite materials using nano-structured silica particles" Prof. Shigeaki Abe, Nagasaki University	**p.31**
11:35-11:50	**Oral Presentation 5** "Photopharmacology: Fundamentals and Applications" Dr. P. K. Hashim, Assistant Professor, Hokkaido University	**p.32**
11:50-13:00	**Lunch**	

13:00-13:25	**Invited lecture 5** "Studying transcription factor networks to unlock the production of phytoalexins in plants" Dr. Nik Kovinich, Associate Professor, York University, Canada	**p.33**
13:25-13:50	**Invited lecture 6** "Quantum emitters and hybrid integration" Prof. Andreas W. Schell, Johannes Kepler University Linz, Austria	**p.35**
13:50-14:05	**Oral Presentation 6** "Nanophotonics for photonic quantum technology" Dr. Hideaki Takashima, Associate Professor, CIST	**p.37**
14:05-14:20	**Oral Presentation 7** "Analysis of the barnacle exploratory behavior on precisely controlled different functional group surfaces by video analysis" Shota Asano, CIST	**p.38**
14:20-14:35	**Oral Presentation 8** "Corrosion resistance of Al materials after anodizing and pore sealing treatments under high humidity and temperature" Maho Yamaguchi, National Institute of Technology Asahikawa College	**p.39**
14:35-14:50	**Oral Presentation 9** "Near-infrared responsive soft actuators consisting of thermosensitive gels and photothermal conversion materials with wavelength selectivity" Satoshi Watanabe, National Institute of Technology Tomakomai College	**p.40**
14:50-15:10	**Coffee Break**	
15:10-15:25	**Oral Presentation 10 (Online)** "Research on Automation of Learning Support Advising using Large Language Model" Kana Sunahara, CIST	**p.41**

15:25-15:40	**Oral Presentation 11 (Online)** "Research on Visualization of Learning Reflection Data for Competency Evaluation" Rin Sano, CIST	**p.42**
15:40-15:55	**Oral Presentation 12 (Online)** "Research on Feature Detection from Time-Series Variations in Ultrasound Video Images" Keisuke Hirakawa, CIST	**p.43**
15:55-16:10	**Oral Presentation 13 (Online)** "Construction of Waste-battery Classification System using Generative Machine Learning Modeling" Ryusei Shihara, CIST	**p.44**
16:10-16:30	**Closing**	
16:10	**Student poster and oral presentation award**	
16:20	**Closing Remarks** Prof. Olaf Karthaus, Chairperson of CIF24	

POSTER PRESENTATIONS

P29	"Synthesis of Vinylidenecyclopropanes via Gold(I)-Catalyzed Cyclopropanation of Vinyl Arenes" Hiroto Mori1, Yusuke Ono1, Shota Nakagawa1, Sota Akima1, Miki Murakami2, Toshinobu Korenaga3, Tadashi NakajiHirabayashi2, Yoshikazu Horino*1 1 CIST (Japan), 2 Grad. Sch. of Sci. and Eng., Univ. of Toyama (Japan), 3 Iwate Univ. (Japan)	**p.74**
P30	"Stereoselective Synthesis of (Z)-anti-Homoallylic Alcohols Using Palladium-Catalyzed Three-Component Reaction" Ayumu Natsubori1 and Yoshikazu Horino*1 1 CIST (Japan)	**p.75**
P31	"Synthesis of 2-Vinylnapthalenes via Gold(I)-Catalyzed Cyclopropanation of Indenes" Shota Nakagawa1, Yoshikazu Horino*1 1 CIST (Japan)	**p.76**
P32	"Transition-Metal-Free Synthesis of Homopropargylic Alcohols" Haruya Hirano1, Yoshikazu Horino*1 1 CIST (Japan)	**p.77**
P33	"Synthesis of new reusable cage-shaped phosphine ligands" Mizuki Oda1, Yoshikazu Horino*1 1 CIST (Japan)	**p.78**
P34	"Evaluation of Source Code that Includes Perspectives of Ease of Handover Measured by Class Cohesion" Mayu Sudo1, Hiroto Yamakawa1 1 Grad. Sch. Sci. Tech., CIST (Japan)	**p.79**
P35	"Development and Implementation test of LTI Gateway System to Improve Interoperability of Educational Systems" Toshinobu Kamada1, Hiroto Yamakawa1 1 Grad. Sch. of Sci. and Tech., CIST (Japan)	**p.80**
P36	"Investigation of the inactivation effects of different UV intensity at 213 nm and irradiation time" Tatsuro Kagawa1, Kazuhiro Dainaka1, Nobuhiro Umemura1 1 CIST (Japan)	**p.81**

P37	"Elucidation of anomalous fluorescence properties of 2,4-bis(1,3-benzothiazolylphenol derivatives" Yuma Hirose1, Haruto Yamakawa1, Ken-ichi Sakai1, Tomoyuki Akutagawa2 1 CIST (Japan), 2 IMRAM, Tohoku Univ. (Japan)	**p.82**
P38	"Analysis of the Aggregated Structure of C3-Symmetric Molecules with a Cyclic Hydrogen Bonding Network" Akihiro Kakiyama1, Manami Uemura1, Ken-ichi Sakai1, Tomoyuki Akutagawa2 1 CIST (Japan), 2 IMRAM, Tohoku Univ. (Japan)	**p.83**
P39	"Thermal and Fluorescence Properties of Methyl Salicylate Derivatives with an Anchor Site for Self-Assembling" Kei Kobayashi1, Ken-ichi Sakai1, Takashi Nakanishi2 1 CIST (Japan), 2 NIMS (Japan)	**p.84**
P40	"Performance Verification of an RSSI Indoor Localization Technique using a Two-Step Estimation Algorithm" Reiya Muraguchi1, Yasuhiro Takano1, Hsuan-Jung Su2, Yoshiaki Shiraishi3 1 CIST (Japan), 2 NTU (Taiwan), 3 Kobe Univ. (Japan)	**p.85**
P41	"A Survey on Colorization Techniques for Near-Infrared Images" Shunsuke Shimada1, Yasuhiro Takano1, Yoshiaki Shiraishi2 1 Grad. Sch. of Sci. and Tech., CIST (Japan), 2 Grad. Sch. of Eng., Kobe Univ.(Japan)	**p.86**
P42	"Control of Photoinduced Electron Transfer via Supramolecular Complex Formation of Polymers with Electron-Donor Molecules" Hiroyasu Yamaguchi1*, Yilin Cao1, Hikaru Sotome2, Syoji Ito2 1 Grad. Sch. of Sci., Osaka Univ. (Japan), 2 Grad. Sch. of Eng. Sci., Osaka Univ. (Japan)	**p.87**

COMMITTEE

Honorary Chair	Yoshikazu Miyanaga, President, CIST
General Chair	Olaf Karthaus, CIST
Secretary General	Tomoya Takada, CIST
Technical Program Committee	Masanori Wakizaka, CIST Hirooki Aoki, CIST Hiroshi Fukuda, CIST Keiichi Kawano, CIST/ARIM Makito Haruta, CIST
Poster session	Makito Haruta, CIST
Financial Committee	Akihiro Shoji, CIST Shino Chiba, CIST
Media+Zoom	Yuji Hirai, CIST
Local Arrangement Committee	Yuji Hirai, CIST Hisaya Oda, CIST Tsuyoshi Kurashima, Photonics World Consortium
Publishing Committee	Shigeki Hagihara, CIST Hisaya Oda, CIST
Publicity Committee	Katsufumi Ohsumi, Nagoya University/ARIM Keiichi Nakamoto, Institute for Molecular Science/ARIM Yasutaka Matsuo, Hokkaido University/ARIM Tamami Maruyama, National Institute of Technology, Hakodate College Akihito Iguchi, Muroran Institute of Technology Makoto Chiba, National Institute of Technology, Asahikawa College Mio Suzuki, National Institute of Technology, Kushiro College Takashi Yasui, Kitami Institute of Technology Hiroyuki Kono, National Institute of Technology, Tomakomai College
Award Committee:	Kento Okoshi, CIST

*CIST: Chitose Institute of Science and Technology

*ARIM: Advanced Research Infrastructure for Materials and Nanotechnology in Japan

Advanced Research Infrastructure for Accelerated Biomaterials and Biodevices R&D

Yoshinobu Baba[1,2]

[1]Institute for Quantum Life Science, National Institutes for Quantum and Science and Technology (QST), Chiba 2638555, Japan
[2]Institute of Innovation in Quantum Chemistry, Nagoya University, Nagoya 4648603, Japan
*email: babaymtt@chembio.nagoya-u.ac.jp, baba.yoshinobu@qst.go.jp

Nagoya University is the Hub for next-generation biomaterials in the MEXT ARIM (advanced research infrastructure for materials and nanotechnology in Japan). We have been supporting the data-driven R&D for accelerated biomaterials and biodevices design, such as nanobiodevices for cancer diagnosis, quantum dots for *in vivo* imaging, biological quantum nanosensors, and bio-adaptive materials [1-15]. We have supported to develop nanowire devices, which are extremely useful to isolate extracellular vesicles from body fluids and vesicle-encapsulated microRNA analysis (Fig. 1). The device composed of a microfluidic substrate with anchored nanowires gives us highly efficient collections of extracellular vesicles in body fluids and *in situ* extraction for huge numbers of miRNAs (2,500 types) more than the conventional ultracentrifugation method. Nanowire devices gave us the miRNA date for several hundred patients and machine learning system based on these miRNA data

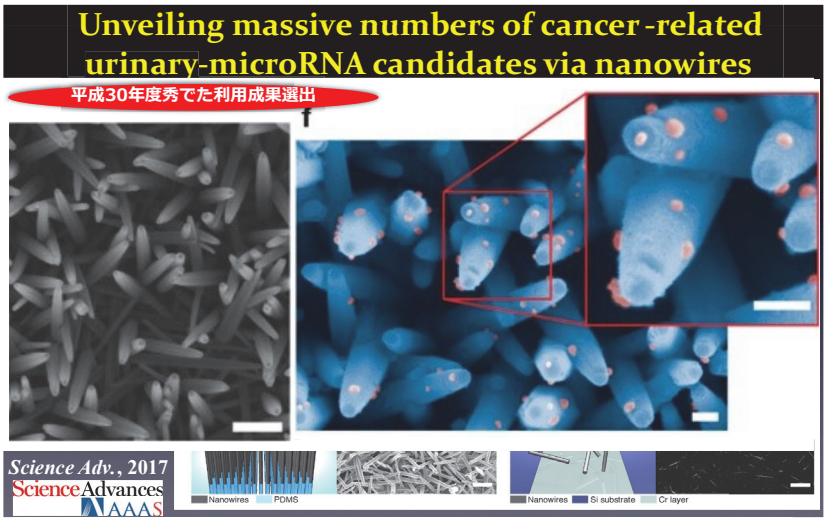

Figure 2. Nanowire devices for cancer diagnosis [1, 3]

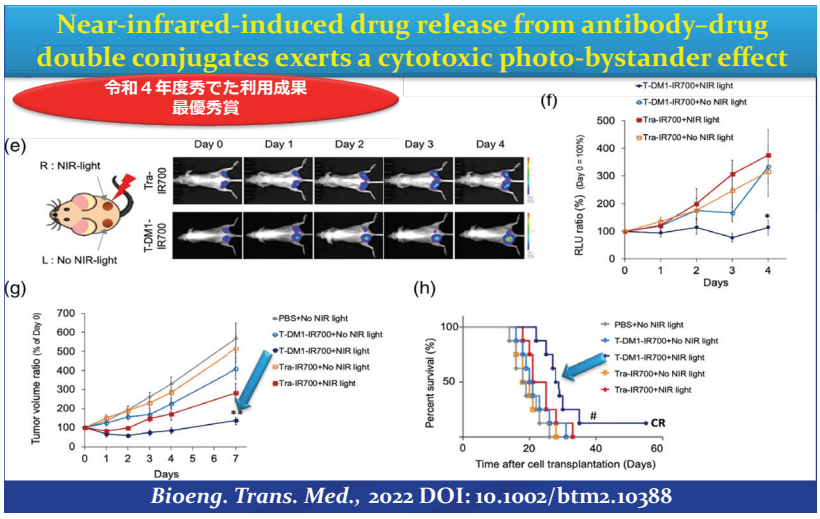

Figure 1. Quantum photo immuno-therapeutic devices for cancer [2, 6]

enabled us to develop the early-stage diagnosis for lung cancer, brain tumor, pancreas cancer, liver cancer, bladder cancer, prostate cancer, diabetes, heart diseases, and Parkinson disease. We have been supporting data-drive R&D for biological quantum nanosensors. Nanodiamonds, with nitrogen-vacancy centers, and quantum dots are applied to develop quantum sensors for quantum switching *in vivo* imaging for iPS cell (induced pluripotent stem cells) based regenerative medicine, and quantum photo immuno-therapeutic devices for cancer (Fig. 2). Since Kyoto University is the Hub for bio-adaptive materials in the MEXT DxMT (data creation and materials technology project), Nagoya University is collaborating with Kyoto University to support the data-driven R&D for accelerated bio-adaptive materials design. Cutting-edge MS technology enables us to collect big data for the amino acid sequences of proteins and peptides isolated from spider's silk. These sequence data are applied to the data-driven development for sustainable textiles, fiber materials, and so on.

References

[1] Y. Baba, R. Hanayama, H. Akita, T. Yasui (Ed), *Extracellular Fine Particles*, Springer Nature, 2024.

[2] H. Yukawa, K. Sato, Y. Baba, Theranostics applications of quantum dots in regenerative medicine, cancer medicine, and infectious diseases, *Adv. Drug Deliv. Rev.,* 200, 14863 (2023).

[3] T. Yasui, et al., *Science Advances*, 3 (2017) e1701133.

[4] T. Yasui, et al., *ACS Nano*, 13 (2019) 2262.

[5] M. Tsutui, et al., *Science Advances*, 8, eabl7002 (2022).

[6] K. Takahashi, et al., *Bioengineering Translational Medicine,* 7. e10388 (2022).

[7] A. Yokoi, et al., *Science Advances*, 9, eade6958 (2023).

[8] A. Yokoi, et al., *Nature Commun.*, 14, 6915 (2023).

[9] K. Chattrairat, et al., *ACS Nano*, 17, 2235 (2023).

[10] H. Takahashi, et al., *Biosens. Bioelec*, 234, 115318 (2023).

[11] K. Matsuo, et al., *eBioMedicine* (Part of THE LANCET Discovery Science), 95, 104737 (2023).

[12] Z. Zhu, et al., *ACS Appl. Mat. & Int.*, 15, 36866 (2023).

[13] K. Sitthisuwannakul, et al., *Biosens. Bioelec*, 254, 116218 (2024).

[14] Z. Min, et al., *ACS Appl. Mat. & Int.*, 16, 29570(2024).

[15] K. Chattrairat, et al., *Device*(Cell Press), 2, 100363 (2024).

[16] M. Tsutsui, et al., *ACS Nano*, 18, 15695 (2024).

The rise of Materials Informatics: Infrastructure to Materials Design

Keisuke Takahashi[1]*

[1] Department of Chemistry, Hokkaido University, Sapporo 060-0810, Japan

keisuke.takahashi@sci.hokudai.ac.jp

The emergence of materials informatics has had a significant impact on the design of materials and catalysts[1,2]. This approach leverages the field of informatics to extract valuable knowledge from data on materials and catalysts, enabling more effective and efficient design processes. This presentation provides a comprehensive overview of the role that materials informatics plays in the design of materials and catalysts. It covers various aspects, including the generation of big data through high-throughput experiments, the application of machine learning techniques, catalyst design using small data, the development of an informatics platform, and the use of computational material data[3,4].

High-throughput experiments generate large volumes of data by systematically exploring a wide range of material compositions and processing conditions. This big data is crucial for identifying patterns and correlations that inform material design. Machine learning techniques, such as neural networks and decision trees, are then applied to this data, enabling the prediction of material properties and accelerating the discovery of new materials with desired characteristics. In cases where data is limited, catalyst design can still benefit from advanced informatics techniques. Methods like transfer learning and active learning make efficient use of small datasets to optimize catalyst properties with fewer experiments.

The development of an informatics platform is another key aspect, providing tools for data management, analysis, and sharing. Such platforms often include databases, visualization tools, and interfaces for machine learning models, facilitating collaboration among researchers and streamlining the material design process.

Furthermore, the advent of artificial intelligence, such as ChatGPT, has the potential to revolutionize the way scientific research is conducted. This presentation will examine the various perspectives, concerns, and opportunities related to the use of artificial intelligence in scientific pursuits. AI can enhance data analysis, generate hypotheses, and even draft research papers, making scientific research more efficient and comprehensive. However, it also raises concerns about the attribution of patents when

AI discovers new materials and understanding the process by which AI makes these discoveries. This presentation aims to provide a balanced view of these issues, highlighting the transformative potential of AI while addressing the challenges it presents. In particular, oxidative coupling of methane is used as a case study.

References

[1]Keisuke Takahashi, Junya Ohyama, Shun Nishimura, Jun Fujima, Lauren Takahashi, Takeaki Uno, Toshiaki Taniike,
Catalysts informatics: paradigm shift towards data-driven catalyst design
ChemComm., 2023, 59, 2222-2238.
[2]Toshiaki Taniike, Keisuke Takahashi
The value of negative results in data-driven catalysis research
Nat. Catal., 2023, 6, 108–111.
[3]Keisuke Takahashi, Lauren Takahashi, Son Dinh Le, Takaaki Kinoshita, Shun Nishimura, and Junya Ohyama
Synthesis of Heterogeneous Catalysts in Catalyst Informatics to Bridge Experiment and High-Throughput Calculation
J. Am. Chem. Soc., 2022, 144, 34, 15735–15744.
[4]Keisuke Takahashi*, Jun Fujima, Itsuki Miyazato, Sunao Nakanowatari, Aya Fujiwara, Thanh Nhat Nguyen, Toshiaki Taniike, Lauren Takahashi
Catalysis Gene Expression Profiling: Sequencing and Designing Catalysts
J. Phys. Chem. Lett., 2021, 12, 30, 7335-7341

Data-Driven Electron Microscopy Studies for Nanomaterials

Kohei Aso

[1] School of Materials Science, Japan Advanced Institute of Science and Technology, 1–1 Asahidai, Nomi, Ishikawa, 923–1292, Japan

aso@jaist.ac.jp

Since materials' properties strongly correlate with their crystal structures, structural analysis is extremely important in materials science. Transmission electron microscopy (TEM) and scanning TEM (STEM) are powerful tools to visualize the structure at the atomic scale in real space. STEM and also TEM images nowadays are raster graphics that are formed from arrays of pixels, and therefore data analysis is necessary to extract materials' information, such as the distributions of crystal phases[1], defects[2], composition[3], and spatial change in interatomic distances leading to strain distribution[4]. Appropriate data science methods have to be chosen, combined, and/or developed depending on the material, imaging mode, and purpose.

For example, we have developed a method to measure sub-percent level strain distribution in nanomaterial from a STEM image[4]. Figure 1a shows an atomic resolution STEM image of a gold nanorod. Bright spots correspond to gold atoms aligned in the projection direction. By determining the atomic positions from the center of the spots, we analyzed the displacement of atoms from the ideal atomic positions. The displacement is expected to be continuous in single-crystal nanorods. However, the displacement map in Fig. 1b contains random noise, which is an obstacle in determining the strain by simply derivating the displacements.

To overcome this problem, we introduced Gaussian process regression (GPR), which is a data science method used in the fields of geostatistics and computational finance, to STEM image analysis. GPR assumes that the true state of the observed data is smooth and that the observed data contains Gaussian noise. The true state can be estimated from the observed data from these assumptions. By applying GPR to the displacement map in Fig. 1b, we succeeded in extracting the smooth displacement distribution that is the nature of the nanorod (Fig. 1c). Figure 1d maps the strain distribution by calculating the derivative of the displacement. To verify the precision of the developed method, Figure 1e compares the standard deviation of strain obtained directly from the original data to those obtained by applying GPR. While the original data has a standard deviation of 1.1%, the spread is narrowed to 0.2% by using GPR. High precision in strain detection was achieved by employing GPR.

A local expansion strain of about 0.5% occurs near the boundary between the body and the hemispherical cap of the nanorod. The cap is subjected to surface stresses perpendicular to the surface and inward to the nanorod. In the axial direction, the stress is accommodated by the entire nanorod. In the radial direction, on the other hand, the stress is accommodated only by the cap part. As a result, lattice contraction occurs at the cap in the radial direction and expansion strain in the axial direction due to the Poisson effect. We believe that this method developed by our group, which allows unprecedentedly precise analysis of atomic arrangements, will contribute to a better understanding of nanostructured materials and their functionalities.

Recently, the (S)TEM technique itself has also evolved to collect “big data”. Real-time atomic-resolution TEM observations of deforming gold nanowires have been achieved while applying force utilizing a mechanical nanoprobe mounted in a TEM sample holder [5,6]. A combination of STEM and a high-speed camera has been devised to acquire electron diffraction patterns at each sampling position. This scanning diffraction method enables observations of beam-sensitive materials such as zeolites[7] and polymers[8], on the scale of a few nanometers. With these methods, thousands and millions of images and diffraction patterns are obtained in a single experiment.

Data science methods have been successfully applied to these big data to extract materials properties otherwise inaccessible. For the case of real-time TEM observations of deforming gold wire, wire radius-dependent Young's modulus has been revealed by measuring the lattice spacing from the images and combining it with the simultaneously measured spring constant[6]. Scanning diffraction of polymers has visualized the orientation of polymer molecules by determining the position of diffracted spots[8]. In the future, by combining these advanced (S)TEM methods producing big data and data science analysis methods, we will deepen our understanding of the structure and properties of various materials at the atomic scale[9].

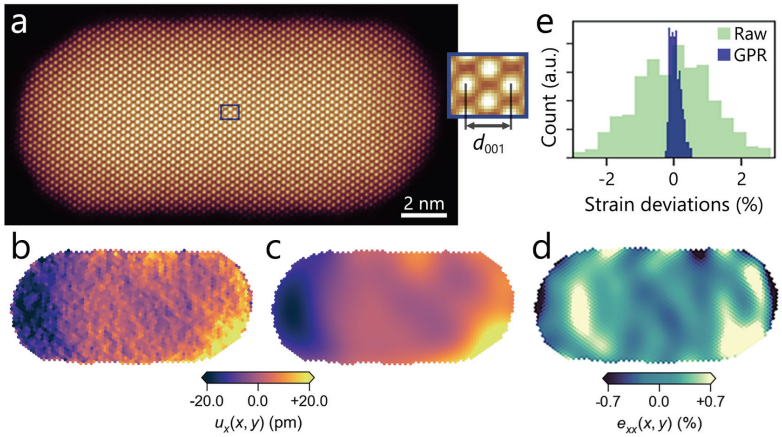

Figure 1. (a) STEM image of a gold nanorod. Center part is enlarged in the right panel. (b) Atomic displacement map obtained from the original data. (c) Smooth displacement estimated by GPR. These maps show displacement along the horizontal direction. (d) Strain map showing the contraction or expansion along the horizontal direction. (e) Strain deviations to compare the original (raw) and GPR-processed strain maps.

References

1 A. Belianinov, *et al.*, *Nature Communications* 6, 7801 1−8 (2015)

2 CH. Lee, *et al.*, *Nano Letters* 20, 3369−3377 (2020)

3 K. Aso, *et al.*, *Nanoscale* 14, 9842−9848 (2022)

4 K. Aso, *et al.*, *ACS Nano* 7, 12077−12085 (2021)

5 J. Zhang, *et al.*, *Physical Review Letters* 128 146101 1−7 (2022)

6 J. Liu, K. Aso, *et al.*, under review.

7 K. Mitsuishi *et al.*, *Scientific Reports* 13, 316 1−11 (2023)

8 D. Chatterjee, *et al.*, *Nano Letters* 23, 2009−2015 (2023)

9 K. Aso, *et al.*, submitted.

Charge Transport and Thermoelectric Properties in Electrochemically Doped Conducting Polymers

Hisaaki Tanaka

Department of Applied Chemistry and Bioscience, Chitose Institute of Science and Technology, 066-8655, Japan

h-tanaka@photon.chitose.ac.jp

Conducting polymers have been attracting much interest in terms of both scientific and technological viewpoints. Owing to the highly sophisticated material designs, various new high-mobility polymers have been synthesized with the carrier mobility approaching, or even exceeding, 1 cm^2/Vs. Carrier doping on such high-mobility polymers can thus cultivate various new applications such as wearable thermoelectric generators. However, charge transport mechanisms in these polymers have not been fully understood yet, especially in their doped states, due to the highly complicated film structure consisting of both crystalline domains and domain boundaries.

In the present talk, we introduce our recent studies on the charge transport and thermoelectric properties of electrochemically-doped semicrystalline polymers [1]. We adopt an electrolyte gating method, schematically illustrated in Figure 1a, to sensitively control the doping level up to high concentration regions by applying external gate voltages. We observed that a typical semicrystalline polymer PBTTT (Fig. 1a) underwent a macroscopic metal-like transition upon doping as shown in Fig. 1b, associated with a peak of the thermoelectric power factor, consistent with the recent theoretical studies. The structural optimization by DFT calculations revealed that the planarity of the polymer backbone was improved by the doping, promoting the inter-domain charge transport, which should be a key to realize macroscopic metal-like charge transport in semicrystalline polymers. We will also introduce our recent trial to extract the mobility in such electrochemically doped polymer films.

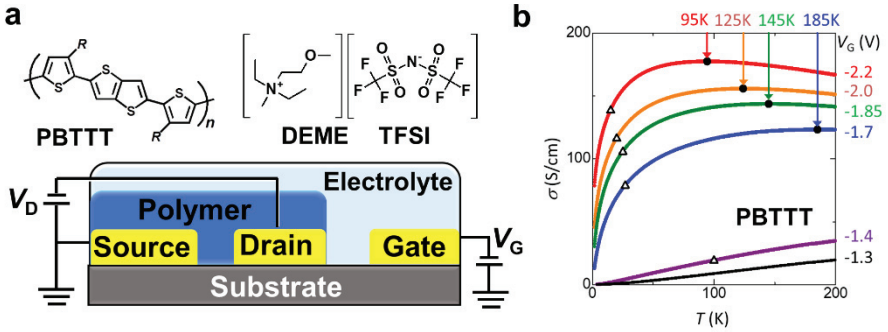

Figure 1. (a) Chemical structures of PBTTT and the electrolyte [DEME][TFSI] together with the schematic illustration of the device structure. (b) Temperature dependence of the electrical conductivity (σ) obtained at various gate-voltages.

References

1 H. Tanaka, K. Kanahashi, N. Takekoshi, H. Mada, H. Ito*, Y. Shimoi, H. Ohta, T. Takenobu, *Sci. Adv.* **6**, eaay8065 (2020).

Sequence-defined glycopolymers for biomedical applications

Laura Hartmann[1,2]*

[1] Institute of Macromolecular Chemistry, University of Freiburg, Germany
[2] Freiburg Center for Interactive Materials and Bioinspired Technologies, University of Freiburg, Germany
laura.hartmann@makro.uni-freiburg.de

Carbohydrates are an important part of our nutrition, they are used as materials e.g., cellulose or chitin, but they are also highly relevant in mediating various biological interactions, for example in cell-cell communication, immune responses and tumour formation. From a chemical point-of-view, carbohydrates are a highly diverse class of biomacromolecules using a great number of different building blocks that are assembled into linear and branched structures, oligomers, polymers and glycoconjugates. Intentionally reducing this complexity while maintaining the biological activity is achieved for so-called multivalent glycomimetics via the attachment of smaller glycan fragments onto synthetic scaffolds.
We have previously introduced sequence-defined glycopolymers as multivalent glycomimetics that can be easily varied in terms of their scaffold structure, composition as well as number and kind of glycan fragment attached, parameters known to affect ligand properties such as avidity and binding specificity. In order to mimic the structural diversity of carbohydrates, these glycomacromolecules can then be used again as building blocks to create more complex glycomimetic structures and materials e.g., through conjugation onto nanoparticles or proteins. The lecture will present the bottom-up synthesis of such glycopolymers and glycomimetic materials and will discuss their potential biomedical applications for example in inhibiting viral and bacterial infections.

References

1 U.I.M. Gerling-Driessen, M. Hoffmann, S. Schmidt, N.L. Snyder, L. Hartmann, *Chem. Soc. Rev.* **52**, 2617-2642 (2023).

Photoswitchable Bioactive Glass for Calcium Control in Enamel Remineralization

Zuniga Heredia E E[1*], Arteaga-Arteaga F[2,3], Sawamura M[2] and Iijima M[1]

[1]Division of Orthodontics and Dentofacial Orthopedics, School of dentistry, Health Science University of Hokkaido, [2]School of Sciences, Hokkaido University, [3]Institute for the Advancement of Higher Education, Hokkaido University.

ezra@hoku-iryo-u.ac.jp

Bioactive glasses (BG) have potential in promoting enamel remineralization and developing materials with site-selective functionalities. However, uncontrolled ion release has been a significant challenge. Previous studies have modified the composition to enhance network connectivity or created pH-responsive mechanism. In this study, we surface-modify BG with a photo-switchable macrocyclic structure containing an azopyridine group (P) to achieve controlled release and capture of calcium ions (Ca^{2+}) from the BG surface.

The modified bioactive glass (PBG) was synthesized and subjected to X-ray diffraction (XRD), scanning electron microscopy (SEM), energy/dispersive X-ray spectroscopy (EDX), transmission electron microscopy (TEM), Fourier transform infrared spectroscopy (FTIR) coupled with attenuated total reflection (ATR) and X-ray photoelectron spectroscopy (XPS) characterization techniques. To test the effectiveness of the photo-switchable ligands immobilized on the surface of the bioactive glass, PBG samples were dissolved in an artificial saliva solution and subjected to alternating UV and LED irradiation every 15 and 30 minutes, while monitoring the Ca^{2+} concentration using a Ca^{2+} sensor.

To evaluate the enamel remineralization potential of PBG, artificial demineralized lesion was created by treat enamel slices (N=5, 2x2x1mm) with 37% orthophosphoric acid for 15 seconds and immersed in artificial saliva containing PBG at a concentration of 1 mg/mL for 7 days. The hardness and elastic modulus of the samples were measured using a nanoindenter, and any differences were analyzed using ANOVA.

The BG was synthetized by sol-gel method, yielding particle size of 40nm and an appropriate composition of SiO_2, CaO, Na_2O, SrO and P_2O_5. The particle size and the amorphous structure indicated by the characteristic bump at 25 degrees in the XRD spectra, remained unchanged after functionalization with the photo-switchable macrocyclic structure.

The behavior of Ca^{2+} ions differed between BG and PBG samples. Specifically, in the BG samples, the concentration increased from 31 to 150ppm and continued to rise. In the PBG samples, the concentration increased from 31 to 72ppm and then exhibited a "zig-

zag" pattern during the 30-minute interval. UV light activation resulted in a decrease in Ca^{2+} concentration, whereas the use of LED light caused an increase (from 82-62 ppm)

The PBG samples demonstrated an ability to maintain their enamel remineralization potential, exhibiting increased hardness and elastic modulus when compared to etched. This difference was statistically significant (Fig. 1).

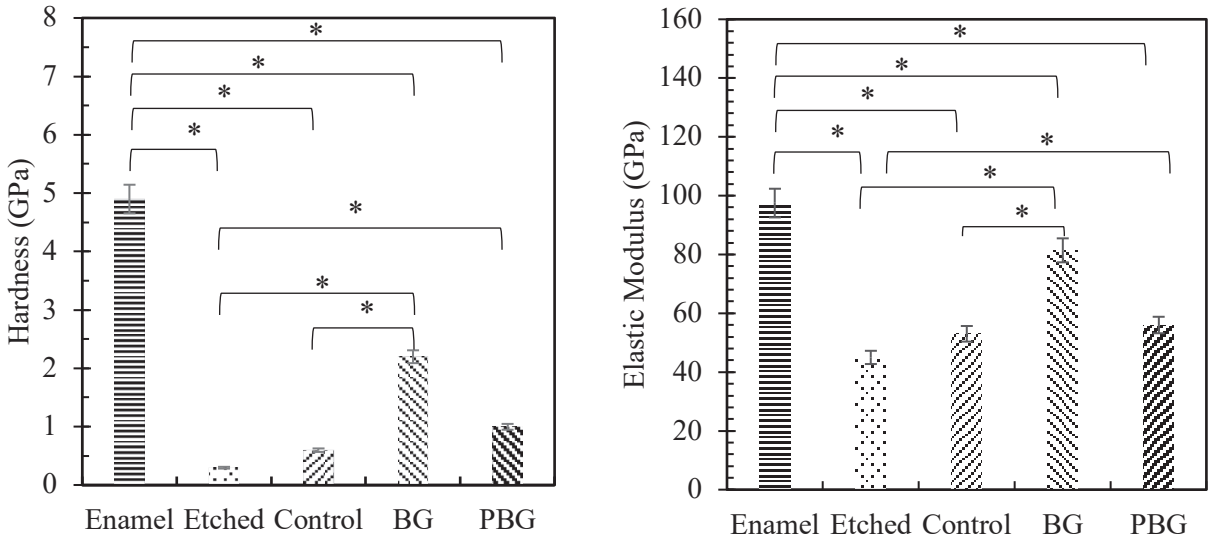

Fig 1. Hardness and Elastic modulus of enamel before and after 7 days of immersion with BG and PBG.

The trans and cis isomeric forms exhibited different affinities for Ca^{2+}, allowing efficient capture and release of Ca^{2+} under light irradiation. The modified bioactive glasses conserved their potential for hydroxycarbonate layer formation and buffer capacity.

References

1. A.Taha, M.P. Patel, R.G. Hill, P. S. Fleming. *J. Dent.* **67,** 9-17 (2017)
2. Raszewski Z, Chojnacka K, Mikulewicz M. *J.Funct. Biomater.* **15,** 119- (2024)

Fabrication of VO_2 micro/nanostructures by laser-induced hydrothermal synthesis

Christophe Pin[1]*, Hideki Fujiwara[2] and Keiji Sasaki[3]

[1] Light-Matter Interactions for Quantum Technologies Unit, Okinawa Institute of Science and Technology Graduate University, Onna, Okinawa 904-0495, Japan
[2] Faculty of Engineering, Hokkai-Gakuen University, 1-1, Nishi 11, Minami 26, Chuo-ku, Sapporo, Hokkaido, 064-0926, Japan
[3] Research Institute for Electronic Science, Hokkaido University, Kita 20, Nishi 10, Kita-ku, Sapporo, Hokkaido, 001-0021, Japan

christophe.pin@oist.jp

Vanadium dioxide (VO_2) has been intensively studied and used for its insulator-to-metal phase transition close to room temperature (~ 68 °C).[1,2] It is material of particular interest for designing nanoscale switching devices with highly tunable electronic and optical responses. Integrated VO_2 micro/nanostructures are usually fabricated using conventional top-down fabrication techniques.[2] To reduce the fabrication costs and enable the fabrication of more complex nanostructures, cost-effective, bottom-up fabrication techniques enabling well-controlled material synthesis are needed. Although solvothermal/hydrothermal synthesis of VO_2 nanoparticles, nanowires, and nanosheets has been reported,[2] the assembly and integration of dispersed nanomaterials in devices requiring nanoscale precision remains challenging.

We demonstrate here the laser-induced hydrothermal synthesis of VO_2 micro/nanostructures on gold thin films and gold nanostructures.[3,4] A 1064 nm infrared laser beam was focused onto the gold film/nanostructures at the surface of a glass substrate immersed in the precursor solution[5]. 1μm-large VO_2 structures were fabricated by locally heating a 30nm-thick alumina-coated gold film. It was found that the generation of a microbubble results in an improved crystallization of the synthesized material. VO_2 was similarly synthesized at the surface of gold nanodisks and nanorods. Enhanced, localized, polarization-controlled photothermal heating of the gold nanostructures was achieved via the excitation of localized surface plasmon resonances (LSPR), demonstrating efficient VO_2 synthesis by plasmon-assisted hydrothermal synthesis.[4]

References

1 Z. Shao, X. Cao, H. Luo, P. Jin, *NPG Asia Mater.* **10**, 581–605 (2018).
2 V. Devthade, S. Lee, *J. Appl. Phys.* **128**, 231101 (2020).
3 H. Fujiwara, T. Suzuki, R. Niyuki, K. Sasaki, *New J. Phys.* **18**, 103046 (2016).
4 H. Fujiwara, T. Suzuki, C. Pin, K. Sasaki, *Nano Lett.* **20**, 389–394 (2019).
5 R. Shi, J. Wang, X. Cai, L. Zhang, P. Chen, S. Liu, L. Zhang, W. Ouyang, N. Wang, C. Cheng, *J. Phys. Chem. C* **121**, 24877–24885 (2017).

Chitin-chitosan hybrid materials: Effect of crosslinking type and density on mechanical properties.

Leonard Genin[1], Yoshihiko Omura[2] and Olaf Karthaus[3]

[1] Universität Potsdam, Karl-Liebknecht-Straße 24-25, 14476 Potsdam, Germany
[2] Omura Toryo Inc., Chiyomi 3 Chome-87, Tottori 680-0911
[3] Department of Applied Chemistry and Bioscience, Chitose Institute of Science and Technology, Bibi 65-758, Chitose 066-8655, Japan

The negative environmental impact of mismanaged plastic waste, the depletion of fossil oil and consequently the increased carbon footprint demand greener and sustainable materials with less environmental impacts. One possible approach is the use of bioplastics made from renewable resources[1]. Several benefits have been attributed with the use of bioplastics, such as biodegradability, a lower carbon footprint, independence from crude oil, and generally fewer toxins[2]. In recent years there has been an increasing interest into materials derived from the polysaccharides chitin and chitosan as safe and biodegradable alternatives to already existing plastic materials[3]. The aim of this research was to produce both thin coatings and macroscopic specimen as biodegradable but durable alternatives. Chitosan was dissolved in diluted acetic acid with citric acid as a crosslinking agent, to control the mechanical and thermal properties. Additionally, chitin nano fibers can be added to tailor durability. Both glass and metal substrates were coated with different mixtures varying in the amount of acetic acid, citric acid, and chitin nano fibers, baked at 160~200°C, and characterized by FTIR, SEM, hardness testing, and contact angle measurement. The macroscopic specimen were produced by pressing a paste containing the components in a hot press and were characterized by FTIR and through stress-strain curves.

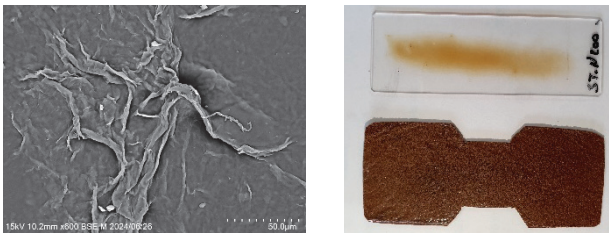

Figure 1. SEM image of chitin nano fibers embedded into the coating (left), coated microscope slide (up right) and macroscopic specimen (down right)

References

[1] S. Shah, F. Matkawala, S. Garg, S. Nighojkar, A. Nighojkar, A. Kumar, *Emerging Trend of Bioplastics and Its Impact on Society*, BJI, **24**, 4, 1-10 (2020)
[2] E. B. Arikan, H. D. Ozsoy, *A Review: Investigation of Bioplastics*, *JCEA*, **9**, 2, 188-192 (2015)
[3] I. Aranaz, M. Mengibar, R. Harris, I. Panos, B. Miralles, N. Acosta, G. Galed, A. Heras, *Functional Characterization of Chitin and Chitosan*, *Current Chemical Biology*, **3**, 2, 203-230 (2009).
[4] N. Wrońska, N. Katir, M. Nowak-Lange, A. El Kadib, K. Lisowska, *Biodegradable Chitosan-Based Films as an Alternative to Plastic Packaging*, *Foods*, **12**, 3519 (2023).

Controlled drug-releasable novel dental restorative composite materials using nano-structured silica particles

Yuko ERA[1], Sirus SAFAEE[2], Mahdis NESABI[2], Sayaka IWATA[2], Masahiro ENDO[2], Mizuki KINJO[2], Atsushi HYONO[3], Shigeaki ABE[1,*], Mariko NAKAMURA[4], Hiroshi MURATA[1] and Ikuya WATANABE[1]

[1] Saitama Prefectural University, Kawagoe 343-8540, Japan
[2] Graduate School of Biomedical Science, Nagasaki University, Nagasaki 095-8102, Japan
[3] National Institute of Technology, Asahikawa College, Asahikawa 072-8142, Japan
[4] Kyushu University of Medical Science, Nobeoka 882-8508, Japan
sabe_den@nagasaki-u.ac.jp

Recently, nano-structured materials have been received much attention by many researchers. Their nano scaled structures induce large surface area and reactive surfaces. Nano porous silica particles (NPS) is a typical nano-structured material. They have numerous of nano-pore with several nm in diameter. The nano-pore can be applied for capture-release molecule systems, such as drug molecules. Therefore, we prepared NPS contained dental resin composite (RC), and then investigated in their molecules-release properties to apply them for a newly drug-release systems. 15 mg of NPS was mixed into 0.3 g of RC paste (5 wt% at concentration), then specimen (ϕ10 x 1 nm) were prepared by light-cure. The obtained specimen was immersed to 1 wt% of model-drug aqueous solution for 24 hrs. After immersion, the sample was immersed to distilled water for a week. Then the samples were moved to a new distilled water every week. The samples can release the model-drugs with positive charge for several weeks. In contrast, RC without NPS sample eluted lower amount of the compounds compared with NPS-RC and the amount deceased rapidly. In case of negative charged one, the released amount also decreased rapidly. The results suggested to apply for a newly drug-released dental materials.

Photopharmacology: Fundamentals and Applications

P. K Hashim*

Research Institute for Electronic Science, Hokkaido University,
001-0020, Sapporo-shi, Hokkaido, Japan

hashim@es.hokudai.ac.jp

Over 85% of small molecule drugs in clinical trials are discarded due to insufficient selectivity and the resulting side effects. One promising approach to enhance drug selectivity is "photopharmacology," which involves using drugs with light-responsive components (photoswitches) that can be activated or deactivated by light.[1] Photoswitches are molecules that change between different structural forms (isomers) in response to light. However, most photoswitches require UV light for this process, which can be harmful to living cells. For effective photopharmacology, the light used must be non-toxic and able to penetrate deeply into tissues to ensure optimal activation of the target drug. This talk will explore the development of photoswitches that are activated by visible light[2] for applications in photopharmacology.

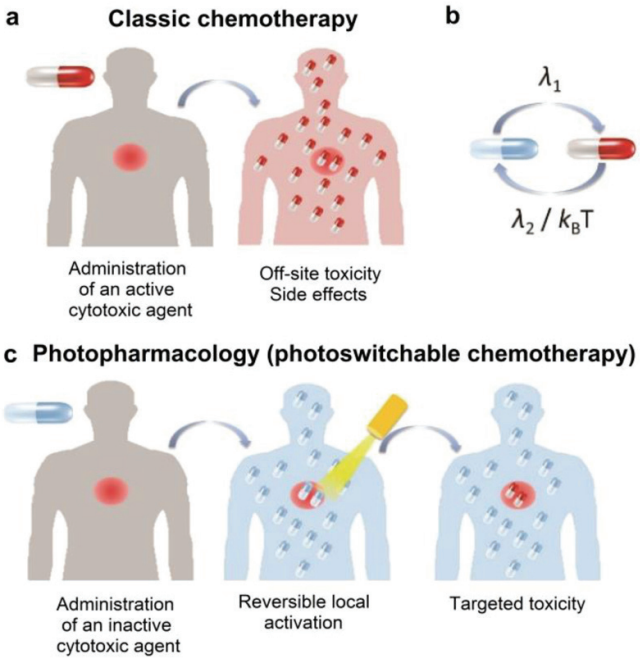

Figure 1. Overview of the classic- and phot-chemotherapy.

References

1 W. A. Velema, W. Szymanski, B. L. Feringa, *J. Am. Chem. Soc.*, 136, 2178 (2014).
2. R. Lin, P. K. Hashim, N. Tamaoki et al. *J. Am. Chem. Soc.*, 145, 9072 (2023).

Studying transcription factor networks to unlock the production of phytoalexins in plants

Jie Lin[1], Ivan Monsalvo[1], Melissa Ly[1], Md Asraful Jahan[2], Dasol Wi[1], Izabella Martirosyan[1], Nik Kovinich[1]

[1] Department of Biology, Faculty of Science, York University, Toronto, Canada
[2] Department of Genetic Engineering and Biotechnology, Shahjalal University of Science and Technology, Bangladesh

kovinich@yorku.ca

Plant materials serve as the source of numerous clinical pharmaceuticals. Phytoalexins comprise a wide variety of plant specialized metabolites that are biosynthesized *de novo* in response to pathogens. They have important uses in crop protection, as antibiotics in animal agriculture, and as clinical and prospective pharmaceuticals. The problem is that phytoalexins are produced only transiently and in low amounts in plant tissues in response to pathogen elicitation. Further, the complexity of many phytoalexin molecules prevents their economical synthesis using chemistry methods. In plants, the biosynthesis of phytoalexins is controlled mainly at the level of transcription of the biosynthetic genes. Thus, we are studying and manipulating using genetic engineering approaches the networks of transcription factors that regulate phytoalexin biosynthesis. Our research thus far has identified a complex network of both positive and negative regulators that have conserved roles in regulating the biosynthesis of chemically diverse phytoalexins. We discuss how multigene engineering of the transcription factor network as an avenue to unlock phytoalexin production in plant materials.

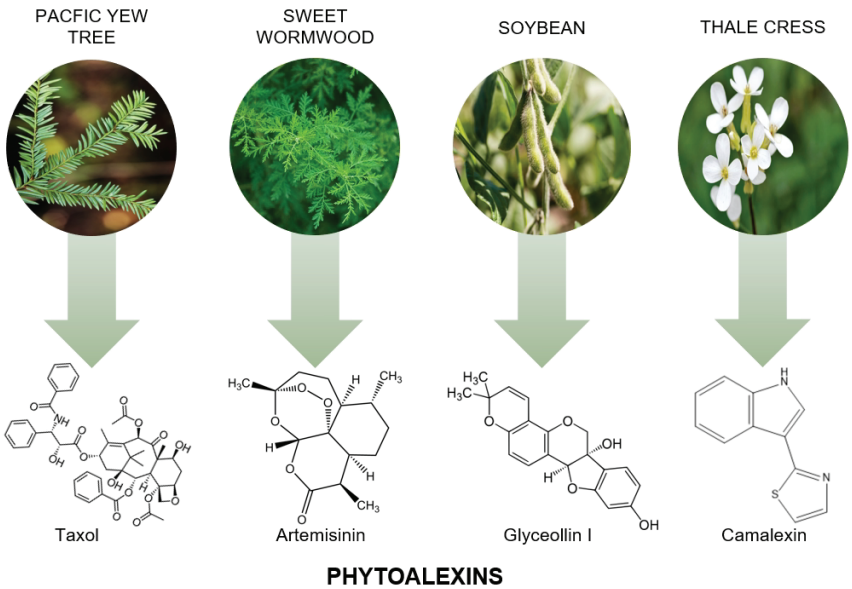

Figure 1. Phytoalexins are diverse chemicals that are produced by plants in response to pathogens. Theres is a need to enhance accessibility to phytoalexin molecules since they are produced only in low amounts in plants.

References

1. Jahan MA, Harris B, Lowery M, Infante AM, Percifield RJ, Kovinich N (2020) Glyceollin Transcription Factor GmMYB29A2 Regulates Soybean Resistance to Phytophthora sojae. *Plant physiology* 183: 530-546
2. Lin J, Monsalvo I, Ly M, Jahan MA, Wi D, Martirosyan I, Kovinich N (2023) RNA-seq dissects incomplete activation of phytoalexin biosynthesis by the soybean transcription factors GmMYB29A2 and GmNAC42-1. *Plants* 12: 545
3. Monsalvo I, Lin J, Kovinich N (2024) Phytoalexin Gene Regulation in Arabidopsis thaliana-On the Verge of a Paradigm Shift? *Current Plant Biology*: 100367

Optical Quantum Technology with Solid-State Single Photon Emitters

Andreas W. Schell[1]

[1] Johannes Kepler University Linz, Altenberger Str. 69, 4040 Linz, Austria

andreas.schell@jku.at

Optical quantum technologies promise to be much more powerful than classical optical technologies in a number of research fields such as computing [1], secure quantum communication [2], and sensing tasks [3].
One possible implementations of such quantum technologies is based on using single particles of light, so called single photons. Such single photons can be created for examples non-linear optics using crystals or by atoms or atom-like systems. The latter offer many advantages, as their properties can be tailored ans as they can be integrated into optical chips. In this presentation, we like to address these two advantaged by (a) introducing advances spectroscopy techniques for the understanding of the properties of such single photons emitters in solid-state systems, and by (b) showing our efforts to optical interface these systems in order to facilitate chip-integrated devices.

At first, we are reporting on our ongoing efforts to understand nano-sized solid-state quantum emitters such as defect centers in diamond and hexagonal boron nitride, quantum dots, and molecules. A variety of optical spectroscopy techniques is used to achieve this goal, such as time resolved single photon correlation spectroscopy, multi-photon and cryogenic microscopy, and multi-wavelength excitation [4,5].
In our experiments we are extending the wavelength range as well as the number of investigated emitters in order to provide reliable information on the emitter properties for their use in quantum technologies.

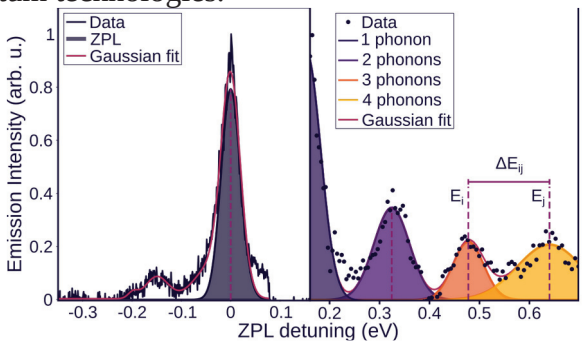

Figure 1. Emission (left part) and excitation spectrum of a single emitter in hexagonal boron nitride.

Secondly, we will show our ongoing efforts to implement a quantum photonic platform using the so called hybrid approach for the assembly of quantum photonic elements. In the hybrid assembly approach, structures and emitters from different materials are combined in order to exploit the specific strength of the individual material while avoiding possible disadvantages by use of complementary other materials. This

approach is highly flexible and can be adapted to many different material systems and structures. In particular, we will introduce techniques based on scanning probe microscopy [6] and three-dimensional laser writing [7]. The hybrid quantum photonic elements assembled with these approached include emitter coupled to on-chip resonators and waveguides, different kinds of fiber integrated cavities and incorporate a variety of emitter such as NV centers, quantum dots, and defects in two-dimensional materials, such as hexagonal boron nitride.

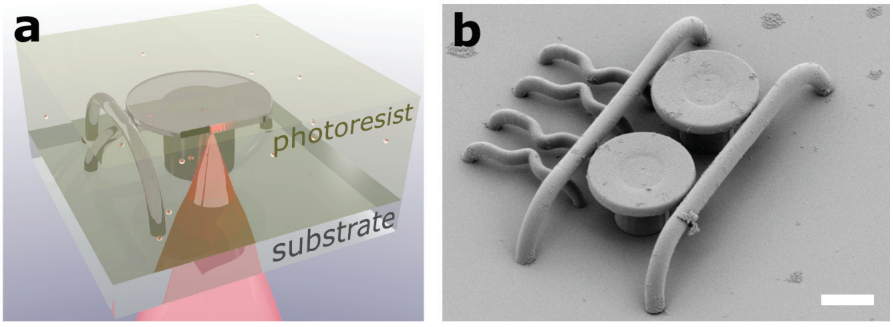

Figure 2. Two-photon polymerization process of a diamond containing hybrid photoresist (a, left) and a fabricated structure (b, right). Scale bar is 10 μm.

References

1 Ladd, T. D., Jelezko, F., Laflamme, R., Nakamura, Y., Monroe, C., & O'Brien, J. L. Quantum computers. Nature, 464(7285), 45-53 (2010).

2 Pavičić, M., Benson, O., Schell, A. W., & Wolters, J. Mixed basis quantum key distribution with linear optics. Optics express, 25(20), 23545-23555 (2017).

3 Degen, C. L., Reinhard, F., & Cappellaro, P. Quantum sensing. Reviews of modern physics, 89(3), 035002 (2017).

4 Tieben, P., & Schell, A. W. Fingerprinting Defects in Hexagonal Boron Nitride via Multi-Phonon Excitation. Advanced Optical Materials, 2302700 (2024).

5 Schell, A. W., Svedendahl, M., & Quidant, R. Quantum emitters in hexagonal boron nitride have spectrally tunable quantum efficiency. Advanced materials, 30(14), 1704237 (2018).

6 Schell, A. W., Kewes, G., Schröder, T., Wolters, J., Aichele, T., & Benson, O. A scanning probe-based pick-and-place procedure for assembly of integrated quantum optical hybrid devices. Review of Scientific Instruments, 82(7) (2011).

7 Schell, A. W., Kaschke, J., Fischer, J., Henze, R., Wolters, J., Wegener, M., & Benson, O. Three-dimensional quantum photonic elements based on single nitrogen vacancy-centres in laser-written microstructures. Scientific reports, 3(1), 1577 (2013).

Nanophotonics for photonic quantum technology

Hideaki Takashima[1]

[1] Chitose Institute of Science and Technology,
758-65, Bibi, Chitose, Hokkaido, 066-8655, Japan

h-takash@photon.chitose.ac.jp

Nanophotonic devices coupled with single-photon emitters have been attracted attention to realize photonic quantum information technology, such as photonic quantum computers, quantum networks, and quantum sensors. As the nanophotonic devices, we have recently developed nanofiber Bragg cavities (NFBCs), which are optical nanofibers embedded a microcavity in it [1, 2, 3, 4]. NFBCs can realize the high coupling efficiency of photons into single-mode fibers [1, 2]. They can also ultra-widely tune more than 20 nm resonant wavelengths by applying mechanical tension [1, 4]. Here, we report the fabrication method of the NFBCs with the high-quality factor using a helium-focused ion beam. Besides these results, we will report our recent results on the NFBCs.

We gratefully acknowledge financial support from JSPS KAKENHI Grants (Nos. 24H00195, 21H04444, 26220712, 23K22426, and 19K03686), JST CREST (JPMJCR1674), JST PRESTO (JPMJPR2257), MEXT Q-LEAP (JPMXS0118067634), JSPS Bilateral Program Number JPJSBP120242003, and a research granted from Murata Science and Education Foundation. A portion of this work was supported by the "Nanotechnology Platform Project" of MEXT (Nanotechnology Open Facilities in Osaka Univ.).

References

1. A. W. Schell, H. Takashima, S. Kamioka, Y. Oe, M. Fujiwara, O. Benson and S. Takeuchi, Sci. Rep., 5, 9619 (2015).
2. H. Takashima, M. Fujiwara, A. W. Schell, and S. Takeuchi, Opt. Express, 24, 15050 (2016).
3. H. Takashima, A. Fukuda, H. Maruya, T. Tashima, A. W. Schell, and S. Takeuchi, Opt. Express, 27, 6792 (2019).
4. H. Takashima, A. W. Schell, and S. Takeuchi, Opt. Express, 31, 13566 (2023).

Analysis of the barnacle exploratory behavior on precisely controlled different functional group surfaces by video analysis

Shota Asano[1 *], Shuren Sugawara[2], Takayuki Murosaki[3], Yasuyuki Nogata[4], Yuji Hirai[2]

[1]Graduate School of Science and Technology, Chitose Institute of Science and Technology, 758-65 bibi, Chitose Hokkaido 066-0012, Japan. [2]Chitose Institute of Science and Technology, [3]Asahikawa Medical University, [4]Central Research Institute of Electric Power Industry. Email : m2230010@photon.chitose.ac.jp

Barnacles can easily adhere to the intake channels of power plants and the bottoms of tanker ships. This causes the reduction in energy efficiency and fuel efficiency. In the past, antifouling paints were used to prevent this problem. However, they were prohibited due to their endocrine disrupting effects on other marine organisms. Therefore, there is a demand for developing new antifouling materials with less environmental impact. In our previous study, we investigated the barnacle settlements on the surfaces modified with self-assembled monolayers (SAM) of the several kinds of terminal functional groups. We found that the settlement rate was lowest on the OH surface and highest on the COOH surface among the tested SAMs [1]. Furthermore, when conducting settlement tests on patterned SAM substrates with OH and COOH terminal functional groups, the settlement rates were more influenced by OH pattern geometry than by the OH modified ratio. The settlement rate was lower in case of a continuous OH surface (Fig. 1). In this study, we focused on the exploratory behavior with adhesion proteins before settlement, and attempted to clarify the influence of SAM on barnacle settlement rates by analyzing video of the exploratory behavior. The SAM substrates were prepared by modifying the gold substrate with thiol reagents with OH or COOH terminal functional groups. Experiments were then performed using three types of SAM substrates: OH, COOH and 25 μm stripe (OH/COOH) patterned SAMs with these functional groups. The videos were recorded for 8 hours per day for 3 consecutive days.

As a result of imaging, exploratory behavior was observed 4 times each on the COOH and OH group SAM, and 6 times on the stripe patterned SAM. Two types of exploratory behaviors such as walking and change of direction were observed. Comparing the number of actions for each surface, there was a marked difference in the number of walks between the COOH and stripe patterns, and in the number of direction changes between the COOH and OH patterns (Fig. 2). Therefore, it is suggested that the OH group and the stripe patterned SAM affect the exploratory behavior of cypris larvae, which could be factors that reduce the adhesion rate.

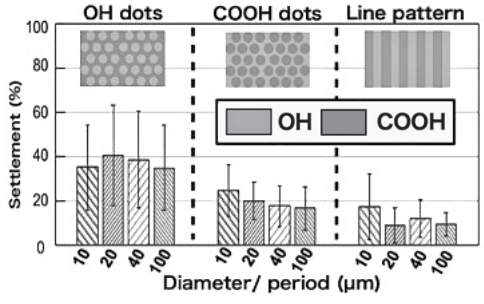

Fig. 1 Results of settlement tests on patterned SAM substrates. Modification ratio of OH and COOH were both 50 % (N = 6, Error bars = S.D.)

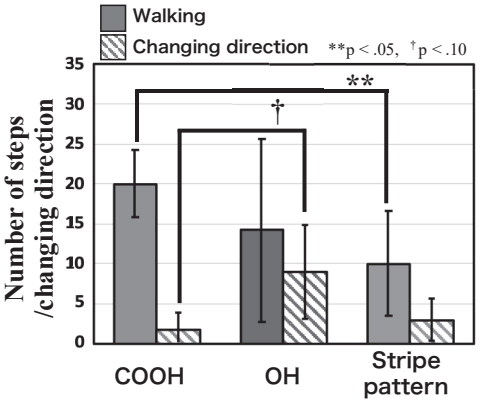

Fig. 2 Comparison of average action number on each surface.

References

[1] Ai Momose et al., Sessile Organisms , 37 (1), 1-9, 2020.

Corrosion resistance of Al materials after anodizing and pore sealing treatments under high humidity and temperature

Maho Yamaguchi[1], Koki Saito[1] and Makoto Chiba[1,*]

[1] National Institute of Technology Asahikawa Collage,
Shunkodai 2-2-1-6, 071-8142, Japan

*makoto@asahikawa-nct.ac.jp

Al material is widely used for many products, because the weight of this material is light and the price of this is inexpensive. However, due to its low corrosion protection, surface treatment for improvement of the corrosion protection is required for use this as a product. Anodizing and pore sealing treatment is one of the most popular techniques for improvement of corrosion protection of pure aluminum. An oxide film with many pores arranged regularly can be formed by anodizing. After that, these pores of oxide film are sealed with hydrated oxide by immersing the boiling water, as pore sealing treatment. However, corrosion protection of aluminum alloy, not pure Al, is not improved, significantly. Thus, in our research group, new type of pore sealing treatment for improvement of corrosion protection of Al alloy is proposed. As pore sealing treatment, Al alloys after anodizing is keep in the chamber with high temperature and humidity for long term. In this study, we investigated the corrosion protection of pure Al and Al alloys after anodizing and new type of pore sealing treatment.

Pure Al (purity: 99.98%) and 1050-Al (purity: 99.51%) were used as samples. After electrolytic polishing as pretreatment, anodizing was performed for 60 minutes in a 2wt%-$(COOH)_2$ solution with 200Am^{-2} of constant current density. After that, pore sealing treatment was performed under the following two conditions. One is the immersing in boiling water for 20 minutes, this is a traditional condition. The other one was kept in the camber with hot and high humidity conditions for 30 hours. The corrosion protection of these samples after anodizing and pore sealing treatment were evaluated by electrochemical impedance spectroscopy (EIS).

Fig. 1 shows a Nyquist plot obtained by EIS measurements of pure Al and Al alloy after anodizing and pore sealing in boiling water. From these plot, the corrosion resistance of pure Al and 1050-Al after sealing in boiling water, is 110.2 kΩ and 72.8kΩ, respectively. From these results, it is clear that the corrosion protection of pure Al is higher than that of Al alloy after anodizing and pore sealing in boiling water. The surface of anodized Al alloy has many defects and these may be caused the generation of cracks on the surface layer. The generation of these cracks will make a low corrosion protection of Al alloy.

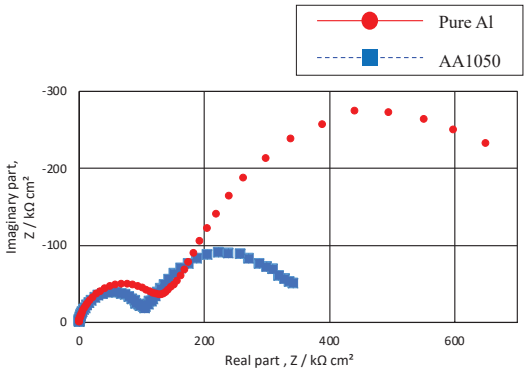

Fig. 1 Nyquist plot of pure Al and Al alloy after anodizing and pore sealing in boiling water obtained by EIS measurements

Near-infrared responsive soft actuators consisting of thermosensitive gels and photothermal conversion materials with wavelength selectivity

Satoshi Watanabe[1], Kazuki Arikawa[2], Hiroshi Era[2], Masashi Kunitake[2]

[1]Division of Applied Chemisty and Biochemistry, Tomakomai KOSEN, Tomakomai city, Hokkaido 059-1275, Japan.
[2] Department of Material Science and Applied Chemistry, Kumamoto University

watasato@tomakomai-ct.ac.jp

Near-infrared responsive soft actuators of thermosensitive gels and photothermal conversion nanofillers have attracted much attention for applying micromachines in bioliving. However, conventional nanofillers such as graphene and carbon nanotubes limit control of the actuators to the optical scanning which does not work on micromachines. In this study, we demonstrate wavelength selective control systems by replacing conventional photothermal conversion materials with lanthanoid materials having narrow bandwidths, high durability, and being harmless to bio living.

Thermosensitive gels and lanthanoid materials were composited by the calcination-free[1] or complexation crosslinking[2] techniques. Figure 1 shows photographs of the soft actuators in water at 30 °C (b) without and under light irradiation at (a) 808 nm and (c) 980 nm, respectively. The 808 nm irradiation got the bending motion of the Nd_2O_3 nano particle-incorporated part of the actuators. After turning off the light, the actuator returned to the original shapes. The 980 nm irradiation got the bending motion of the Yb_2O_3-nanopaticle-incorporated part of the actuators. The repeated experiments yielded the same responses and gave no damage of the gels and the lanthanoid materials.

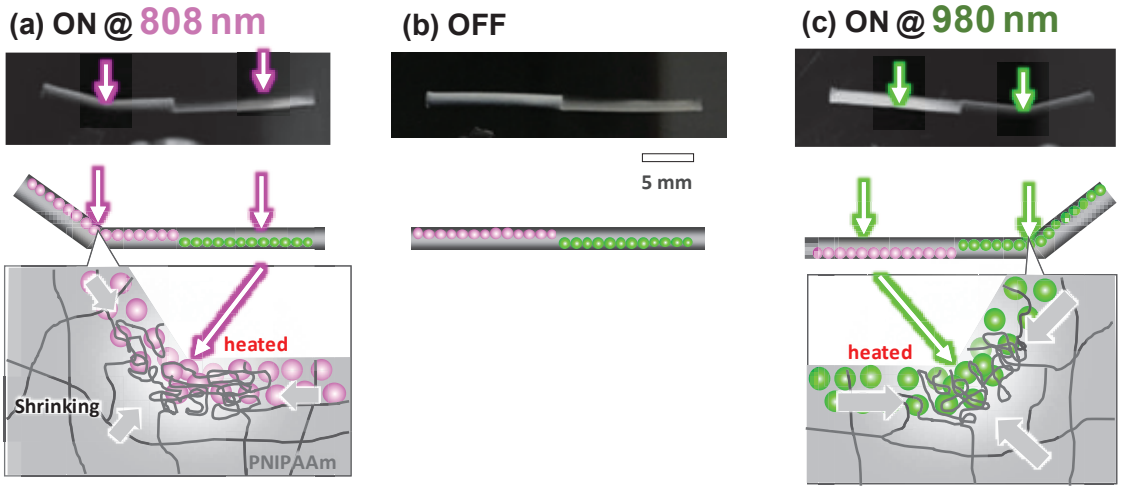

Figure 1. Photographs of the soft actuators in water at 30 °C (b) without and under light irradiation at (a) 808 nm and (c) 980 nm, respectively.

References

1 S. Watanabe, *Adv. Funct. Mater*. **21**, 4264 (2011); **25**, 4390 (2015).

2 S. Watanabe, *Chem. Lett*. **49**, 1111 (2020); *Soft Smart Mater. submitted* (2024).

Research on Automation of Learning Support Advising using Large Language Model.

Kana Sunahara[1*], Yasuomi Takano[1], Gingi Someya[1], Taketo Tsurube[1], Haruki Ueno[2], Hiroshi Komatsugawa[1]
[1] Graduate School of Science and Engineering, Chitose Institute of Science and Technology
[2] Faculty of Science and Technology, Chitose Institute of Science and Technology
m2240310@photon.chitose.ac.jp

Recently, Japanese higher education emphasizes the importance of shifting the educational approach from traditional teaching to autonomous learning for which it is necessary to arrange the educational environment where students can learn proactively. For students who are not accustomed to the proactive learning, teachers should provide learning support such as a scaffolding. However, it is challenging for teachers to grasp the situation of every student and provide individualized scaffolding. In the previous study, we have been verifying the automatic generation of learning advisement based on learning logs and learners' reflection writings using Large Language Models.

In this study, we have developed a learning support system that can provide personalized learning advice when students engage in reflection. The system automatically generates learning advice by combining learning history data with data from students' reflections and goal setting. As reflection items, we set task achievement, participation in group work, whether goals were achieved, and the specific reasons. Figure 1 shows a part of the reflection input screen in the advising system. After entering these sections, advice is displayed. Students can review the advice and set their next goals.

The system was applied to a programming class, and we performed a case study of the class. Questionnaire surveys were conducted with the students. The survey responses were collected from 75, and the usefulness of the advice in learning support was evaluated. The results obtained from the case study indicate that the system gives a certain contribution to support learners' own learning.

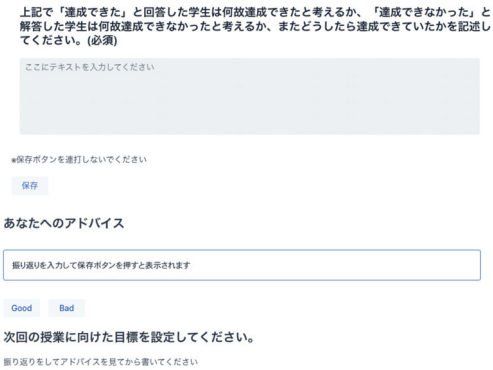

Figure 1. system concept diagram

References

1 Yasuomi Takano, Taketo Tsurube, Haruki Ueno and Hiroshi Komatsugawa, " A Proposal and Evaluation of Learning Advising using a Generative AI ", 31th International Conference on Computers in Education Work In Progress Posters Proceedings, pp. 872-874

Research on Visualization of Learning Reflection Data for Competency Evaluation

Rin Sano[1], Haruki Ueno[2] and Hiroshi Komatsugawa[1]

[1] Graduate School of Science and Engineering, Chitose Institute of Science and Technology, Chitose 066-8655, Japan
[2] Chitose Institute of Science and Technology, Chitose 066-8655, Japan

m2240250@photon.chitose.ac.jp

We analyze and visualize the tendency of teachers' evaluation and the characteristics of learners' reflections based on learning reflection data. In previous study, we used machine learning modeling to extract the evaluation viewpoint based on tacit knowledge, which depends on the teachers' experience in education, from a large dataset of learning reflections. In this study, we develop a feedback sheet for teachers and learners (Figure 1) as an effective tool for data analysis and visualization of competency evaluation. The feedback sheet provides the results of the analysis of teachers' evaluation tendency towards all learners and evaluation result for each learner. We investigated validity of the contents of the sheet through the interview for teachers at the institutions.

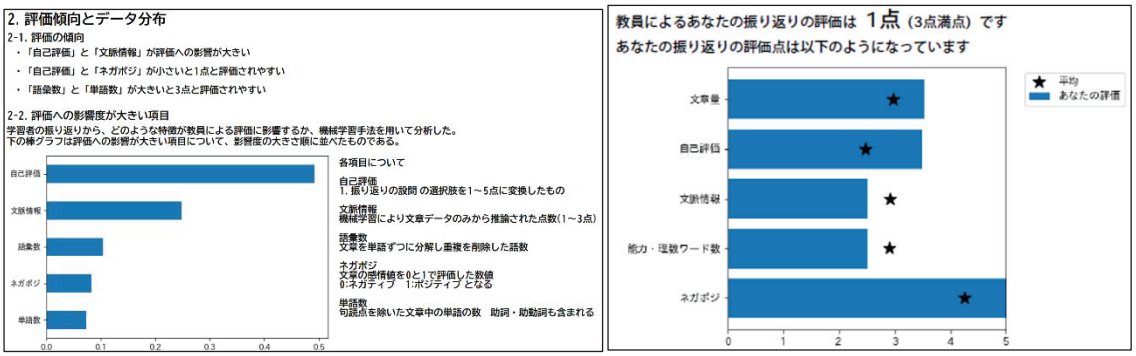

Figure 1. a part of feedback sheet for teachers(left) and for learners (right)

References

1 Allen Momiji, Mitsuru Kawazoe and Hiroshi Komatsugawa:
Analysis of Teachers 'Tacit Knowledge-based Evaluation of Learner Competencies Using Machine Learning Approach,
IIAI2023 To be published

2 Tanizuka et al:
『教職ｅポートフォリオの活用による教育実習生の自己評価および相互コメントの効果』，日本教育工学会論文誌, 39巻3号 p.235-248 (2015),
https://www.jstage.jst.go.jp/article/jjet/39/3/39_39041/_pdf/-char/ja

Research on Feature Detection from Time-Series Variations in Ultrasound Video Images

Keisuke HIRAKAWA[1*], Ueno HARUKI[2] and Hiroshi KOMATSUGAWA[1]

[1]Graduate School of Science and Engineering, Chitose Institute of Science and Technology
[2] Chitose Institute of Science and Technology
[*] m2240390@photon.chitose.ac.jp

In the medical field, ultrasound video images are used in echo-guided punctures mainly for distinguishing between arteries and veins. Basically, the identification of each vessel is determined by the temporal changes in the shape of the vessels induced by the operation of punctures. However, the ultrasound images are unclear, and the distinction is challenging for beginners of healthcare professionals. The purpose of this study is to make a site determination of time-series shape changes in ultrasound video images by utilizing machine-learning algorithms. For this purpose, we focus on YOLO, which can recognize images in real time. Specifically, we utilize YOLOV which is an extended YOLO to handle videos and construct a machine learning model trained and inferred from the ultrasound images including arteries and veins. We then evaluate the classification accuracy of this model.

In this study, we created a dataset annotated with arteries and veins in ultrasound video images. The dataset was created with the cooperation of Hokkaido University of Science and was captured using ultrasound equipment from seven students at our university. Among these, data from five students were used for training, and data from two were used for evaluation. The captured videos were converted into images at a rate of four frames per second. A total of 5,032 images were used for training, and 1,291 images were used for evaluation. The model was trained and inferred using videos with a duration of 7 to 8 seconds per session. We also utilized the YOLOX machine learning algorithm, for conventional image analysis to compare its performance with video analysis and highlight the advantages of the latter. In the current study, we used Intersection Over Union (IoU) and Average Precision (AP) as evaluation metrics.

The results of the comparative evaluation of detection accuracy between YOLOX and YOLOV are shown in Table 1.

Table 1: Evaluation Results of YOLOX and YOLOV

model	Artery AP(IoU=0.5)	Vein AP(IoU=0.5)
YOLOX	0.416	0.202
YOLOV	0.388	0.347

Comparing the AP values of YOLOX and YOLOV, the AP value for arteries does not change significantly, with YOLOX achieving 0.416 and YOLOV achieving 0.388. On the other hand, the AP value for veins increases, with YOLOX at 0.202 and YOLOV at 0.347. This is veins exhibit considerable shape changes in the ultrasound video time series, while arteries do not undergo the changes. Healthcare professionals use the fact to make judgments when distinguishing the vein and the artery. In our study we found that YOLOV also captured the features of time-series vein change in the same way that the professionals do.

Construction of Waste-battery Classification System using Generative Machine Learning Modeling.

Ryusei Shihara and Hiroshi Komatsugawa

Graduate School of Science and Technology, Chitose Institute of Science and Technology 758-65 Bibi, Chitose, Hokkaido, Japan

M2230180@photon.chitose.ac.jp

At recycling sites, waste batteries are manually classified by skilled workers according to differences in shape, labeling, dirt, and damage. With the recent advances in image recognition by AI, it is expected to improve the efficiency of manual work through automatic detection and classification. However, collecting enough data on waste batteries to train AI is not easy due to legal regulations.

In this study, we aim to construct an object detection model for waste batteries characterized by the augmentation of the data using an image generation model, while the actual small dataset. For this purpose, data augmentation is performed using Stable Diffusion [1], which can generate and convert images from text descriptions. Specifically, additional training is performed on the pre-trained model of Stable Diffusion using a small amount of captured waste battery data. Subsequently, a large number of images are generated for training the object detection model to classify waste batteries.

We verified whether the constructed model (hereafter referred to as the "generated image learning model; GLM") could handle waste batteries. Based on the study in [2], we constructed an object detection model trained only on new battery data (hereafter referred to as the "existing model; EM") for comparison with the results of the GLM. Using these models, we flowed waste batteries with various dirt on a conveyor belt and verified how many could be detected. In this process, the camera was set to capture the label. Using 2642 frames obtained from 60 batteries, detection was performed with each model. As a result, the GLM detected 2345 frames (88.76%), while the EM detected 1126 frames (42.62%), an increase of approximately 2.08 times. In the EM, we determined that the battery cannot distinguished to prevent false positives when less than 10% of the total frames are detected [2]. We also verified the number of units detected under this condition. As a result, the GLM detected 57 units (95.0%), while the EM detected 29 units (48.3%), an increase of approximately 1.96 times.

From these results, the GML was confirmed to be more adaptable to waste batteries than the EM. Future research will be conducted to optimize the model so that it can be applied to other types of batteries.

References

1 Stability. Stable diffusion v1.5 model card, https://huggingface.co/runwayml/stable-diffusion-v1-5

2 R. Shihara, H. Ueno, H. Komatsugawa: "Construction and verification of a was te battery classification system using object detection", AI2023-36.

Foam material preparation of natural and synthetic polymers

Taiyo Nagai[1], Olaf Karthaus[1]*
[1]Graduete school of Science and Engineering, Chitose Institute of Science and Technology, Chitose 066-8655, Japan
*Corresponding author. E-mail; kart@photon.chitose.ac.jp

Introduction

There is a waste problem where Styrofoam used for shiitake mushroom log cultivation in forests is left uncollected. Therefore, we have developed a novel foam material made out of biodegradable chitosan, but it has been found that foam made solely from chitosan decomposes faster than shiitake mushroom growth under certain conditions.

Therefore, in this experiment, chitosan was blended with poly(vinyl alcohol), PVA, to prepare a foam material that is biodegradable and has excellent dimensional stability.

Method

In this study, a chitosan-citric acid solution was prepared using the fact that chitosan is soluble in weak acid. The chitosan-PVA foam was made by adding an aqueous PVA solution (7%) and a cross-linking agent, sodium phosphate monohydrate, to the 5% chitosan solution and then adding sodium bicarbonate as a foaming agent to form a porous chitosan PVA foam.

Fig.1 Photograph of a sample

Results and discussion

The foamed materials were analysed using FT-IR and compressive stress tests to determine whether cross-linking occurred. The spectra obtained did not change with the presence or absence of the cross-linker, but a change occurred in the graph of the results of the compressive stress test.

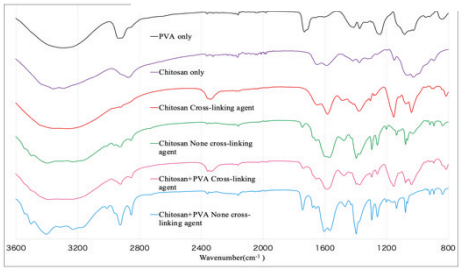

Fig.2 FT-IR spectra

Current issues include the decrease in elasticity of the foamed material over time and the need to improve dimensional stability. It is necessary to study the ratio and type of materials and the foaming method in order to address these issues.

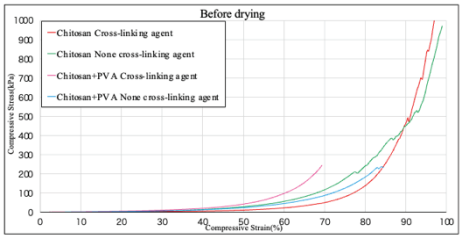

Fig.3 Compression testing before baking

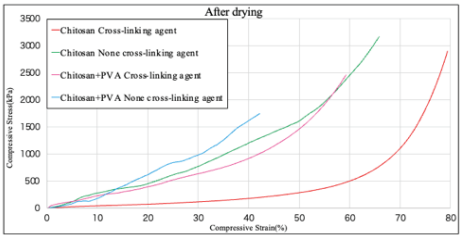

Fig.4 Compression testing after baking

Evaluation of chitosan decomposition by mold

Akihiro Mizuyma[1], Tomohisa Suzuki[1], Taiyo Nagai[1] and Olaf Karthaus[1]*

[1] Graduate School of Science and Engineering, Chitose Institute of Science and Technology, 758-65 Bibi, Chitose Hokkaido 066-8655, Japan

m2230340@photon.chitose.ac.jp

Biodegradable plastics using chitin and chitosan, which are natural polymers, have been produced to reduce the environmental burden that is caused by synthetic polymers. Chitosan solution is used in the fabrication process, and ,surprisingly, mold growth was observed in the solution. However, chitosan is generally considered to be antimicrobial, and should inherently resistant to mold growth. By studying the degradation of chitosan by such mold, it is possible to control the degradation of materials derived from chitosan. In this study, we analyzed molds and evaluated the degradability of chitosan-derived biodegradable plastics by molds.

Molds cultured in chitosan solution were observed by FE-SEM and Czapek-dox medium was prepared for identification. To analyze the degradation of chitosan solution, the viscosity of chitosan solutions during mold growth was measured. In parallel, the BOD was measured. In addition, mold-infected chitosan solutions were dropped onto biodegradable plastic derived from chitin and chitosan, and their degradation by mold was observed under a stereomicroscope and FE-SEM.

The mold cultivated in the chitosan solution was found to be Aspergillus (Fig. 1). Three-week BOD measurements showed that the duration of mold growth and the amount of mold growth varied with the concentration of the chitosan solution (Fig. 2). This is dependent on the concentration of the chitosan solution. Surface degradation was also observed after about 4 months (Fig. 3). Therefore, it can be said that the fungus is capable of reproducing and degrading in the presence of chitosan.

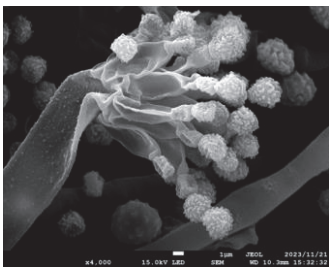

Fig 2 SEM image of mold

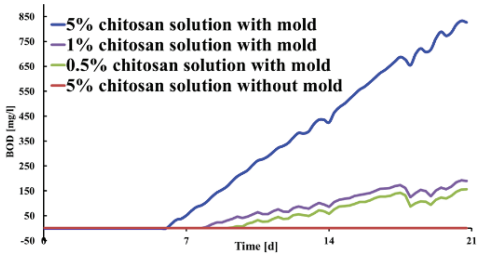

Fig 1 Result of BOD

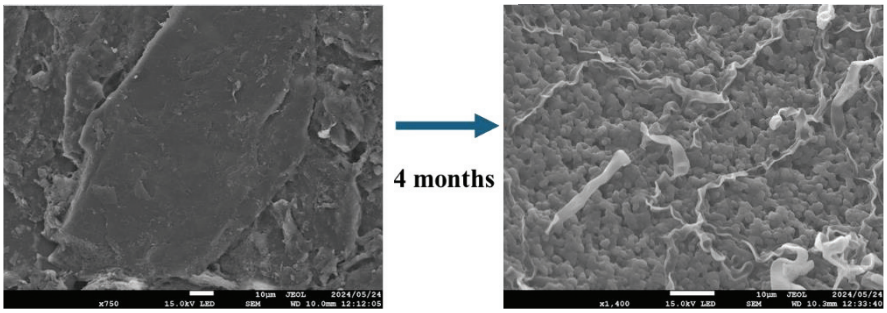

Fig 3 Decomposition image by mold

Basic research for the preparation of alternative materials for plastics of *Fomes Fomentarius*

Ryuya Abe[1], Tomohisa Suzuki[1], Olaf Karthaus[1]*

[1]Graduate School of Science and Engineering, Chitose Institute of Science and Technology, Chitose 066-8655, Hokkaido, Japan

kart@photon.chitose.ac.jp

Today, the problem of plastic waste is becoming more and more serious on a global scale. Although plastic hurts the environment, it is an inseparable part of our daily lives. Therefore, we would like to make it possible to use plants, which can be a sustainable resource, as an alternative material to plastics. Here, we focus on a fungus, *Fomes Fomentarius*, that is widespread in Hokkaido. It has a porous base and a cross section of channels leading to the bottom. The body is as hard as hardwood. It is sometimes used as a natural herbal medicine, but it is not currently used as a cellulose material.

In this study, the dried and powdered *Fomes Fomentarius* were used. The powder consisted mainly of cellulose microfibers with a circular cross-section which could be mixed with water, a cross-linking agent, and chitosan to make a paste, which was then hot-pressed at 90°C for 30 minutes at 60 MPa using a JIS-K7139 type mold to produce dumbbell-shaped test pieces. The test pieces were then tensile tested for strength, and stress-strain curves were collected for several preparation conditions, and the cross sections were imaged by SEM.

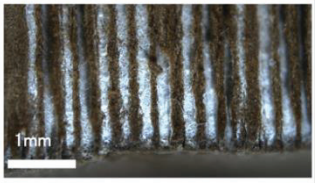

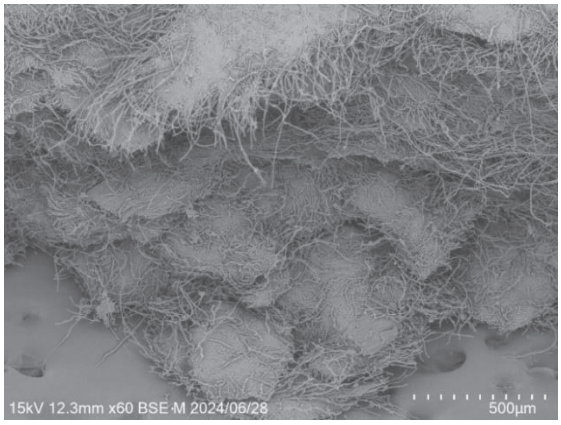

Microscopic structure of VUV-irradiated cycloolefin-polymer substrates by transmission electron microscopy and spectrum imaging

Koichi Higashimine[1,*], Shoko Kobayashi[1], Taro Arimoto[2,3]

[1] JAIST, 1-1, Asahidai, Nomi, Ishikawa, Japan
[2] Ushio Inc., 1194, Sazuchi Bessho-cho, Himeji, Hyogo, Japan
[3] Osaka University, 2-1 Yamadaoka, Suita, Osaka, Japan
koichi@jaist.ac.jp

Advances in adhesive technology are expected to increase adhesive strength while maintaining a flat interface between metals and resin substrates. One method to enhance adhesion strength is by pretreatment of the resin substrate surface with vacuum ultraviolet (VUV) irradiation (λ = 172 nm) using an excimer lamp [1]. This treatment leads to the formation of oxygen-related functional groups at the surface, as confirmed by using infrared absorption spectrometry. However, the microscopic structure of the resin substrate surface including these groups remains unclear. In the present study, we conducted transmission electron microscopy (TEM) observations and electron energy loss spectroscopy-spectrum imaging (EELS-SI) measurements on cross-sectional samples of VUV-irradiated cycloolefin polymer (COP) substrates. We adopted the iodine ion staining method to stain the functional groups for TEM samples. As shown in Figs. 1 and 2, the results suggest the presence of a modified layer near the COP surface. It is noted that a relatively high concentration region of oxygen-related functional groups exists at a depth of several hundred nanometers, marked as "B" in Fig. 1 and shown with a two-way arrow in Fig. 2(e). Such functional groups' distribution might affect the formation of metal plating.

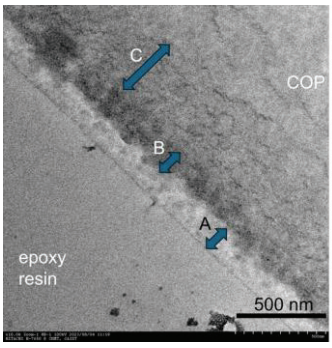

Fig. 1 A cross-sectional TEM image near the surface of VUV-irradiated COP stained with iodine ion, in which the dark contrast indicates oxygen-related functional group distributions.

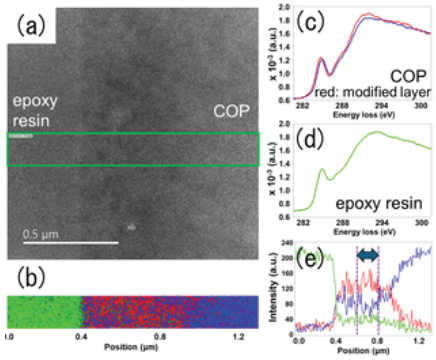

Fig. 2 Results of EELS-SI measurement and multivariate analysis of VUV irradiated COP. (a) survey image, (b) distribution map, (c) COP area, (d) epoxy resin area, (e) integrated line profile of (b).

Acknowledgment
This work was partly supported by the ARIM_JAPAN project under Grant Numbers JPMXP1222JI0012, JPMXP1223JI0009, and JPMXP1223JI0055.

References

[1] T. Arimoto et al. 18th IMPACT Conference, Proceedings 247 - 250 (2023).

Examination of a Water Filter Containing *Populus alba* Leaves

Konoha Ueda[1], Shinon Takahashi[1], Yoshihiko Omura[2], Chiharu Hayashida[3] and Hiroshi Kunimori[3], Olaf Karthaus[1*]
[1]Department of Applied Chemistry and Bioscience, Chitose Institute of Science and Technology, 65-758 Bibi, Chitose 066-8655, Japan. [2]Omura Toryo Inc., 3-87 Chiyomi, Tottori 680-0911, Japan. [3]Aoya Washi Koubou, Aoyacho Yamane 313, Tottori 689-0514, Japan

b2210380@photon.chitose.ac.jp

This study aims to develop a pollutant adsorbent paper filter using leaves of White poplar (*Populus alba*), a naturalized tree in Hokkaido, as a solution for water pollution. White poplar leaves have a dense fiber layer especially at the underside of the leaves that are both highly hydrophobic and lipophilic.

Previous research has shown that intact leaves can absorb various organic dyes from an aqueous solution[1]. To improve the usability of the material as a filter, the crushed leaves were incorporated in paper by combining them with Japanese 'washi' paper using various preparation techniques. Figure 1 shows the electron micrograph of a filter paper produced by mixing Washi fibers made from gampi (*Diplomorpha sikokiana*) and *populus alba* crushed leaves. The crushed leaves are randomly incorporated into the washi fiber network, and there was no observable preferred orientation or aggregation.

By using a simple filtration system driven by capillary force and gravity, we investigated the adsorption of Rhodamine B on washi with or without *P. alba*. Compared to washi made by simply mixing washi raw materials and *P. alba*, the two-layer structure with the mixed washi overlaid on top of the washi resulted in a faster filtering rate. Washi made from *D. sikokiana* were more compatible with *P. alba* and easier to make than those made from paper mulberry (*Broussonetia kazinoki*). The filtering speed was also faster.

In conclusion, the possibility that natural cellulose fibers can function as an adsorbent was demonstrated. In the presentation, detailed conditions for dye adsorption on *P. alba* and the adsorption mechanism will also be discussed.

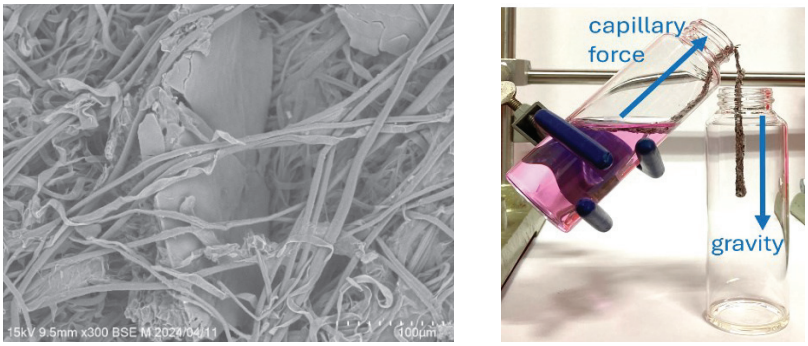

Figure 1. A filter paper (left) and a filtration system (right)

References

1 Shinon Takahashi, Ryota Iida, Tatsuki Saito, Masayoshi Tabata, Thomas Berberich, Olaf Karthaus: "Structure of Cellulose Microfibers on the Lower Side of *Populus Alba* Leaves and their Use in Materials", CIF22, Sept. 30, 2022, Chitose, Japan.

Surface modification of nanofibrillated bacterial cellulose: anionization by TEMPO-catalyzed oxidation

Hijiri Takeda, Ryota Kishimoto, Sayaka Fujita, and Hiroyuki Kono*

Division of Applied Chemistry and Biochemistry, National Institute of Technology, Tomakomai College, Tomakomai, Hokkaido 059-1275, Japan

th23819@stu.tomakomai-ct.ac.jp (H.T.)

Nanofibrillated bacterial cellulose (NFBC) is expected as a functional nanofibrous carrier because of its excellent properties such as high aspect ratio, high mechanical strength, biodegradability, and biocompatibility. However, the NFBC surface has only hydroxyl groups and no highly reactive functional groups for surface modification or graft polymerization. Carboxymethylation is one of the popular methods for modifying cellulose, but the reaction is performed in a mixture of aqueous sodium hydroxide solution and isopropanol, which is accompanied by fiber swelling[1]. TEMPO-catalyzed oxidation, on the other hand, can rapidly convert the primary hydroxyl groups of cellulose dispersed in water to the carboxyl groups[2]. In this study, the conversion of primary hydroxyl groups on the surface of NFBC to carboxyl groups using TEMPO-catalyzed oxidation was investigated for the purpose of functionalizing NFBC (Figure 1). When laccase was used as cofactor in the oxidation reaction of NFBC, the primary hydroxyl groups on the NFBC surface were efficiently converted to the carboxyl groups. The aqueous solution of the TEMPO-oxidized NFBC (TONFBC) improved its permeability and its zeta potential negatively shifted. TONFBC is expected to be applied to thickeners and binders, and to form polyelectrolyte complexes with polycations such as chitosan, which has potential applications as antimicrobial nanofibers in medical materials and food packaging materials.

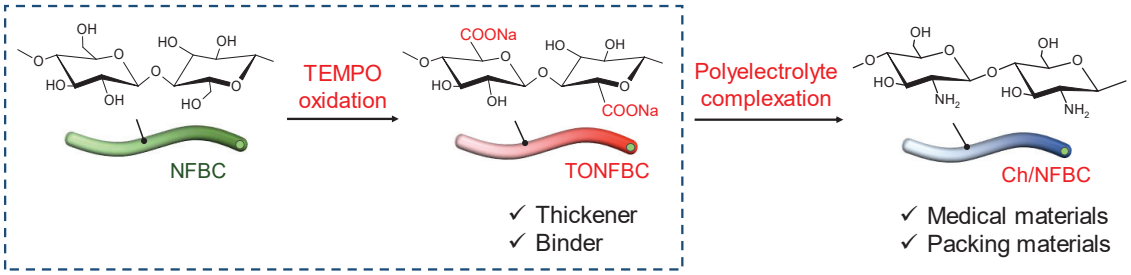

Figure 1. Preparation of TEMPO-oxidized NFBC (TONFBC) and its polyelectrolyte complexation with chitosan

Acknowledgments

This study was partially supported by the JSPS KAKENHI Grant Number JP24K08548, JST SATREPS Program Grant Number JPMJSA2206, and F-REI Grant Number JPFR23020106.

References

1. H. Kono *et al.*, *ACS Omega,* **6** (2021) 34107-34114.
2. J. Jiang *et al., Biomacromolecules* **18** (2017) 288-294.

Biodegradable resin composites reinforced with the nanofibrillated bacterial cellulose

Airi Yokokawa, Kennosuke Takaya, and Hiroyuki Kono*

[1]National Institute of Technology, Tomakomai College, Tomakomai, Hokkaido 059-1275, Japan

ya23833@stu.tomakomai-ct.ac.jp (Y.A.)

Biodegradable resins such as polycaprolactone (PCL) and polybutylene succinate (PBS) are promising alternatives to petroleum-based plastics. However, the application of these biodegradable polyester resins is limited because of their low mechanical properties. Therefore, this study investigated the improvement of mechanical property of PCL and PBS by compositing nanofibrillated bacterial cellulose (NFBC). NFBC has excellent properties such as homogenous fiber width and a long fiber length. Due to its three-dimensional network structure, NFBC shows high mechanical strength and Young's modulus, and thus it is expected as a nanofiller for fiber-reinforced composite resins[1)]. Herein, surface-modified NFBCs were prepared from neat NFBC dispersed in aqueous solution by silane-coupling reaction with 3-aminopropyltrimethoxysilane to enhance interfacial adhesion between NFBC and resins[2)]. The surface-modified NFBC (APC) was well dispersed in these resins by melt kneading method, and the elasticity and Young's modulus of the composites were enhanced with increasing APC content (Figure 1). From these results, it is concluded that the surface-modified NFBC is effective for enhancing the mechanical properties of the biodegradable resins.

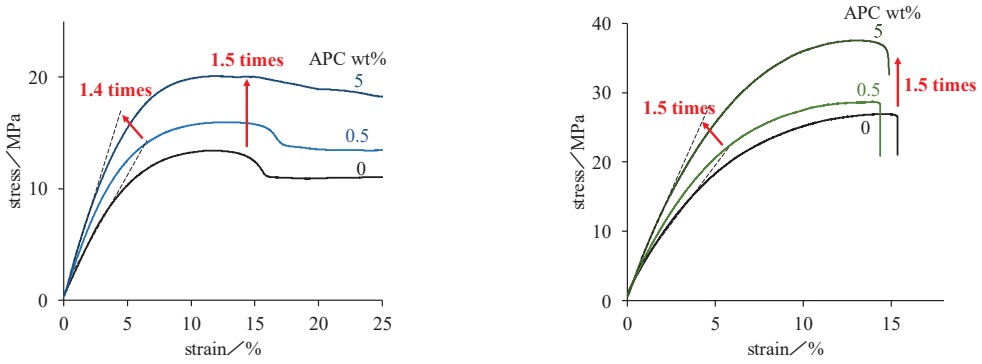

Figure 1. Stress-strain curves of APC-reinforced PCL (left) and PBS (right) composites.

Acknowledgments

This study was partially supported by the JSPS KAKENHI Grant Number JP24K08548, JST SATREPS Program Grant Number JPMJSA2206, and F-REI Grant Number JPFR23020106.

References

1. H. Kono *et al.*, *ACS Omega,* **5**, 29561-29569 (2020).

2. H. Kono *et al., Nanomaterials*, **12**, 537 (2022).

Formation of novel crystalline chitin nanoribbons by self-assembly of chitin oligohexamer in aqueous solution

Ayumu Izutsu[1], Yuya Nagaoka[1], Takeshi Hattori[2], Taiiti Usui[3], Takuya Isono[4], Makoto Ogata[2], Hiroyuki Kono[1,*]

[1]Division of Applied Chemistry and Biochemistry, National Institute of Technology, Tomakomai College, Nishiki-oka 443, Tomakomai, Hokkaido 059-1275, Japan
[2]Faculty of Food and Agricultural Sciences, Fukushima University, 1 Kanayagawa, Fukushima, Fukushima 960-1296, Japan
[3]Faculty of Agriculture, Shizuoka University, 836 Ohya, Suruga-ku, Shizuoka 422-8529, Japan
[4]Faculty of Engineering, Hokkaido University, N13W8, Kita-ku, Sapporo 060-8628, Japan

ia23803@stu.tomakomai-ct.ac.jp (I.A.)

Proteins and nucleic acids form regular structures in aqueous solution through self-assembly processes. Chitin also forms regular hierarchical structures via hydrogen bonding of molecular chains, but its self-assembly process is still unknown[1, 2]. In this study, we found that among water-soluble chitin oligosaccharides, only chitin hexamer (GN6) shows a reversible sol-gel transition at high temperature (Figure 1, left). The transition temperature (T_g) shifted to the lower temperature side with increasing GN6 concentration, especially the T_g of aqueous GN6 solution with 2.0–2.5 wt% concentration was almost same as the biological temperature. The formed gel consisted of plate-like nanoribbon aggregates about 200 nm wide and 3 nm thick and water, and the nanoribbons had a highly crystallized α-chitin structure. The direction of fiber growth of the generated nanoribbons was orthogonal to the *c*-axis (fiber axis) of the α-chitin crystal, indicating that the nanoribbons grew along the *b*-axis of the α-chitin crystal; the GN6 molecules were aligned perpendicular to the nanoribbon growth direction and the adjacent GN6 molecules were aligned inversely parallel. The GN6 nanoribbon growth direction corresponds to a hydrophobic surface and is considered to be self-assembled by hydrophobic interactions. These results indicate that the plate-like nanoribbons formed by the self-assembly of GN6 molecules can be used as pure α-chitin crystals, and the

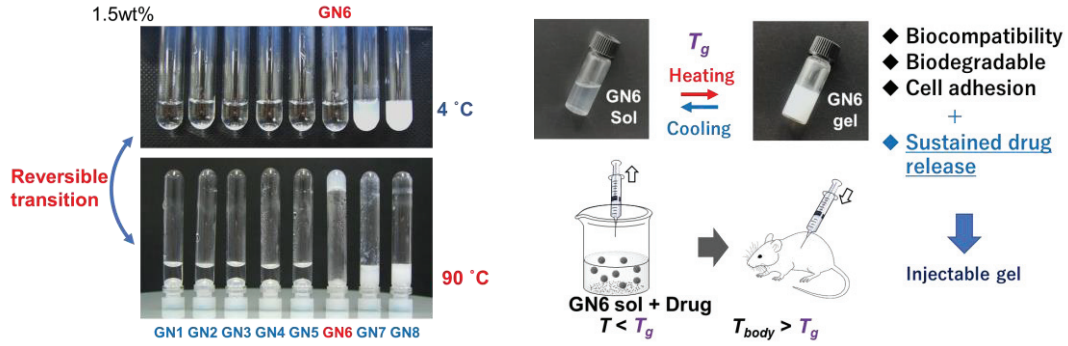

Figure 1. Water solubility of chitin oligomers (GNn) at 4 ˚C and 90 ˚C (left). GN6 shows the reversible phase change from solution to gel upon heating. Biomedical application of GN6 gels (right).

nanoribbon formation mechanism is very useful information for understanding the mechanism of hierarchical structure formation from the assembly of chitin molecules. Furthermore, the thermoreversible gelation exhibited by GN6 aqueous solution is expected to be applied to biomaterials such as thermoresponsive injectable gels that combine chitin-derived biocompatibility and cell adhesion (Figre 1, right).

Acknowledgments

This study was partially supported by the JSPS KAKENHI Grant Number JP24K08548, JST SATREPS Program Grant Number JPMJSA2206, and F-REI Grant Number JPFR23020106.

References

1. Barikani, M. *et al., Iran. Polym. J. Eng. Ed.* **23,** 307–326 (2014).
2. Serizawa, T. *et al*., *ACS Macro Lett*. **9**, 301–305 (2020).

Selective synthesis of conductive graphitic nanomaterials using local laser-heating

Hideki Fujiwara,[1] Christophe Pin,[2] Hideo Kaiju,[3] Kenji Hirai,[4] and Hiroshi Uji-i[4,5]
[1] Faculty of Engineering, Hokkai-Gakuen University
[2] LMIQT Unit, Okinawa Institute of Science and Technology Graduate University
[3] Faculty of Science and Technology, Keio University
[4] Research Institute for Electronic Science, Hokkaido University
[5] Department of Chemistry, KU Leuven, Belgium
h-fujiwara@hgu.jp

Graphene/graphite films are expected to have a wide variety of applications, including energy storage, electromagnetic shielding, thermal control materials, and electronic circuits. However, because existing synthesis methods such as mechanical exfoliation, silicon carbide pyrolysis, and alcohol chemical vapor deposition require high processing temperatures, long processing times, and expensive equipment, a facile and low-cost method is needed. In addition, several methods have been proposed for the direct and site-specific deposition of graphitic carbon nanomaterials using nanoscale-patterned or nanoscale-masked catalytic metal films, enabling the synthesis of graphitic carbon nanomaterials at arbitrary sites. However, these methods also employ expensive lithographic equipment, requiring extra pre- and post-processes for patterning catalytic metals and mask removal. In this study, we focus on the method proposed by Zhou *et al*., who synthesize a graphite film in a few seconds by quenching high-temperature Ni foils in ethanol [1], and report the results of an attempt to locally synthesize graphitic nanomaterials by heating Ni substrates by focused laser irradiation instead of heating Ni foils in a high-temperature furnace [2].

In the experiment, a glass substrate coated with NiFe thin film (thickness ~120 nm) by sputtering technique was immersed in ethanol as a carbon source. A multimode 405-nm CW laser was focused onto the back of the NiFe thin film through the glass substrate using a 10× objective lens (NA 0.5) to generate localized heat at the ethanol−NiFe interface. To optimize the fabrication conditions, we explored laser power, duration time, and the number of bursts of radiation. After laser irradiation, the NiFe substrate surface was evaluated using Raman spectroscopy and the current map and local I−V characteristics of carbon materials were investigated by conductive atomic force microscopy (c-AFM).

Figures 1(a) and 1(b) show the distributions of Raman signal intensity at the G (1600 cm^{-1}) band and of the Raman signal intensity ratio of D (1300 cm^{-1}) and G bands specific to carbon materials, when the site on the NiFe thin film was irradiated at a laser power of 180 mW for 10 s. Figure 1(c) shows the photograph of the laser-irradiated spot and the white dotted line indicates the measurement area of Raman signal intensity distribution. Figure 1(d) shows the position-dependent Raman spectra (indicated by the numbers in the Figure). It can be seen that these characteristic peaks appear at the center of the laser irradiation spot (②) and that the quality of Raman peak response deteriorated outside the spot (③). In addition, a ring-shaped distribution appears around the irradiation spot, and a strong D-band signal can be confirmed (③).

These results suggest that high-quality graphite is not synthesized outside the spot due to the temperature drop. However, clear G, D, and 2D band peaks can be observed inside the irradiated spot, indicating that graphite-like materials can be synthesized at the irradiated spot by appropriate laser irradiation conditions. Thus, we proposed a new approach for the selective synthesis of high-quality graphite on a NiFe thin film using local laser heating and succeeded in the site-specific synthesis of conductive graphitic nanomaterials at the targeted area.

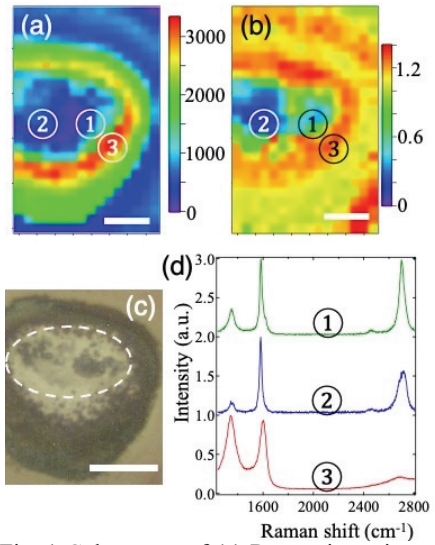

Fig. 1 Color maps of (a) Raman intensity at the G band (1580 cm^{-1}) and (b) the D/G intensity ratios. (c) Microscopy image of the laser- irradiated spot. White line shows the measurement area. (d) Raman spectra obtained at different positions indicated by numbers 1−3 in (a) and (b).

We acknowledge financial support from JSPS KAKENHI (JP23K26518), Advanced Research Infrastructure for Materials and Nanotechnology in Japan (ARIM) of MEXT (JPMXP1223HK0126), and Amada Foundation (AF-2021226-B3).

[1] T. Zhou *et al.*, ACS Nano **14**, 3121 (2020).

[2] H. Fujiwara *et. al*., ACS Appl. Nano Mater. **6**, 13885 (2023).

Effect of Biomorphic Design Elements of Virtual Environment on Virtual Walking

Misuzu Hasegawa[1], Mana Nakai[1], and Daiji Kobayashi[2]

[1]Graduate school of Chitose Institute of Science and Technology, Hokkaido, 066-8655, Japan
[2]Chitose Institute of Science and Technology, Hokkaido, 066-8655, Japan

m2240360@photon.chitose.ac.jp

In recent years, virtual reality (VR)-based services for art museum visits and shopping experiences have become increasingly prevalent. These services are distinguished by their ability to allow users to experience a virtual environment as if they are walking through it. Generally, VR controllers are used to navigate these environments. However, users often lack recognition of spatial information because they perceive movement only visually. As a result, users may have difficulty remembering the virtual space and are more likely to get lost. To address this issue, users need to pay more visual attention to virtual spaces. We focus on biomorphic design to enhance visual attention in virtual spaces. This design is characterized by curvilinear and fluid forms that imitate natural elements such as creatures and water. Mirkia et al. (2022) found that visual attention was enhanced in spaces with biomorphic design, leading to improved spatial memorability [1]. Therefore, this study aimed to investigate the impact of biomorphic design elements on navigation within a virtual space. For this investigation, we asked subjects to navigate five mazes with progressively varying amounts of biomorphic design and recorded differences in the time to complete the mazes. Additionally, we gathered participants' opinions. These results suggest that biomorphic design elements in virtual spaces affect navigation, but the impact varies depending on the amount of biomorphic design, which requires further examination.

References

1 H. Mirkia, M.S.C. Nelson, H.C. Abercrombie, K. Thorleifsdottir, A. Sangari, A. Assadi, *Recognition Memory for Interior Spaces with Biomorphic or Non-Biomorphic Interior Architectural Elements. Journal of Interior Design.* **47(3)**, 47-66 (2022).

Impact of External Human-Machine Interface on Pedestrian Situation Awareness in Autonomous Delivery Vehicle Scenarios

Yuga Kato[1] and Daiji Kobayashi[2]

[1] Graduate School of Chitose Institute of Science and Technology, Hokkaido 066-8655, Japan
[2] Chitose Institute of Science and Technology, Hokkaido 066-8655, Japan

m2240180@photon.chitose.ac.jp

The shortage of drivers in the transportation industry has led to the integration of autonomous driving technology to supplement this workforce. Autonomous delivery vehicles (ADVs) are predicted to assume the role of last-mile transportation. However, the absence of a driver in autonomous vehicles limits communication with other road users, resulting in reduced situation awareness. According to Endsley, situation awareness involves the perception of elements in the environment, comprehension of their meaning, and projection of their status in the near future. To enhance the situation awareness of other road users, an external human-machine interface (eHMI) has been studied and developed to improve communication with other road users. This study focused on pedestrians and investigated the impact of eHMI on their situation awareness when interacting with ADVs. The experiment involved two conditions: with eHMI and without eHMI. Fourteen participants interacted with ADVs as pedestrians under both conditions in a virtual environment. The situation awareness of the participants was measured using the Situation Awareness Rating Technique (SART) and the Situation Awareness Global Assessment Technique (SAGAT). The results showed that in the SART, understanding of the situation and overall scores were significantly higher with eHMI compared to without eHMI. In the SAGAT, confidence in situation awareness was significantly higher with eHMI compared to without eHMI. Additionally, participants expressed that "the eHMI made it feel like they could communicate with the ADVs" and "the eHMI showed that the ADVs were aware of their surroundings." Therefore, eHMI improved the situation awareness of pedestrians, and it is assumed that eHMI could resolve communication issues in ADVs as well.

References

1 A. M. Schuster, S. Agrawal, N. Britt, et al, *Technology in Society, Will automated vehicles solve the truck driver shortages? Perspectives from the trucking industry.* **74(3)**, 102313 (2023).

2 S. Dabic-Miletic, *J. Ind Intell, Autonomous Vehicles as an Essential Component of Industry 4.0 for Meeting Last-Mile Logistics Requirements*, **1(1)**, 55−62 (2023).

3 M. R. Endley, *Proceedings of the Human Factors and Ergonomics Society Annual Meeting, Design and Evaluation for Situation Awareness Enhancement,* **32(2)**, 97−101 (1988).

Virtual Training Workspaces for Assembly Workers: A Case Study on Office Chair Assembly

Naomi Kuwata[1], Ryusei Fukuda[1] and Daiji Kobayashi[2]

[1] Graduate School of Chitose Institute of Science and Technology, Chitose, 066-8655 Japan
[2] Chitose Institute of Science and Technology, Chitose, 066-8655 Japan

m2240200@photon.chitose.ac.jp

Automobile manufacturers have pioneered the development and implementation of virtual training workspaces for assembly workers[1]. Utilizing information technology for training, especially through immersive environments such as virtual reality (VR), has proven to be effective in improving training outcomes. Songjia et al. (2021) examined the impact of varying levels of immersion on training effectiveness by providing assembly instructions via video, mobile VR, and VR[2]. Their findings revealed that instructions delivered through mobile VR and VR significantly reduced training time, validating the efficacy of VR-based training. However, it is crucial to verify that the trainee's performance in a virtual environment translates effectively to the real workplace.

This study aims to experimentally clarify the potential and challenges of designing and setting up a virtual workspace for assembling an office chair using motion analysis. Specifically, we focused on evaluating how different virtual workspace layouts affect work efficiency.

Participants were trained on how to navigate the virtual environment and assemble an office chair through a video tutorial. After practicing the assembly task, they performed the experimental assembly task five times. In the initial setup, termed Workspace A, participants' movements were tracked and analyzed to identify inefficiencies. Analysis of Workspace A revealed that excessive movement was a significant factor in reducing work efficiency. The redesigned Workspace B, which minimized unnecessary movements, resulted in significantly shorter assembly times. Additionally, participants reported significantly lower discomfort levels in Workspace B, as measured by the Subjective Fatigue Scale (SFF). These results demonstrate that optimizing the layout of a virtual workspace can enhance work efficiency and reduce trainee fatigue. The results demonstrate the effectiveness of analyzing hand movements to enhance the design of virtual training workspaces. By reducing unnecessary movements and optimizing the layout, trainees were able to complete tasks more efficiently with less fatigue.

References

1 “Audi uses modular solution for virtual-reality training”, Audi MediaCenter, (https://www.audi-mediacenter.com/en/press-releases/audi-uses-modular-solution-for-virtual-reality-training-10767).

2 S. Sonjira, C. Hsiang-Ting, R. William, and L. W. Tuck, *Effects of Level of Im mersion on Virtual Training Transfer of Bimanual Assembly Tasks, Virtual Re ality and Human Behaviour*, **2**, (2021)

Comprehensive analysis of metabolic pathways involving MBW-transcriptional complex in *Marchantia polymorpha*

Akari Harada[1], Haruka Arai[2], Kazuya Yanagiura[2] and Kengo Morohashi[1]
[1] Graduate School of Science and Technology, Chitose Institute of Science and Technology, 758-65 Bibi, Chitose, Hokkaido, 066-8655, Japan
[2] Department of Applied Biological Science, Faculty of Science and Technology, Tokyo University of Science, 2641 Yamazaki, Noda, Chiba, 278-8510, Japan
k-moroha@photon.chitose.ac.jp

A genotype reflects a phenotype through the regulation of gene expression by a set of transcription factors known as gene expression networks (GRNs). Since GRN is a process of gene regulation, it is invisible, whereas the phenotype is clearly visible. Thus, elucidating the role of GRNs from an evolutionary perspective is challenging. In *Marchantia polymorpha*, which belongs to the basal part of terrestrial plant evolution, transcription factors *MpMYB02* and *MpMYB14* have been reported to contribute to secondary metabolism (1) as components of the MYB-bHLH-WD (MBW) complex, which is widely conserved in plants. We previously reported that *MpBHLH12* participates in organ development and metabolic pathways (2). Although MpMYB02 and MpMYB14 are thought to interact with MpBHLH12 in the MBW complex, it is unclear how the MBW complex regulates secondary metabolic pathways through GRNs. Therefore, we focused on the GRN of metabolic pathways involving MBWs. We generated various recombinant *M. polymorpha,* in which the expression of *MpMYB14* or *MpBHLH12* was modified. Comprehensive analyses of the metabolic profiles and gene expression in these recombinants revealed that *MpBHLH12* is involved in isoquinoline alkaloid production. Currently, we are conducting a detailed analysis of genes involved in these biosynthetic pathways.

References

1. H. Kubo, S. Nozawa, T. Hiwatashi, Y. Kondou, K. Saito, K. Takanashi, T. Kohchi, K. Ishizaki, J. Plant Res. **131**, 849-864 (2018).
2. H. Arai, K. Yanagiura, Y. Toyama, K. Morohashi, J. Plant Res. **132**, 197-209 (2019).

Developing a novel method for protein identification using RNA aptamer

Yuma Ogata[1], Kengo Morohashi[1]

[1] Graduate School of Science and Technology, Chitose Institute of Science and Technology, 758-65 Bibi, Chitose, Hokkaido, 066-8655, Japan

k-moroha@photon.chitose.ac.jp

Drugs principally exert their effects by binding to their target proteins. Despite this demand, the identification of target proteins of drugs is technically challenging, because a highly sensitive protein identification method is required to accurately detect the target proteins of drugs. An RNA aptamer is a single-stranded RNA that binds to a specific target. It has been reported that an RNA aptamer strongly binds to a histidine tag (His-tag) (1). We hypothesized that an RNA aptamer could be used to identify the target proteins of drugs by expanding RNA aptamer-binding peptides. In this study, we aimed to develop a new protein identification method using an RNA aptamer that specifically binds to the FLAG-tag, which is widely used in antibody-based methods (Figure 1). First, we screened for RNA aptamers bound to FLAG-tags. We then validated whether the RNA aptamers bind to the FLAG-tag by comparison with the existing aptamer for His-tags. Currently, we are investigating the affinities of novel RNA aptamers for the FLAG-tag using recombinant proteins fused with a FLAG-tag and His-tag. In addition, we are examining the binding of known small molecule–protein interactions *in vitro*.

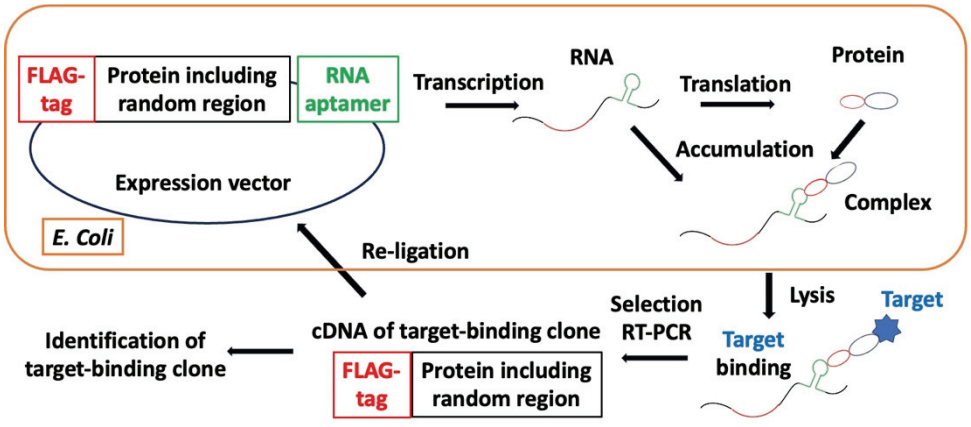

Figure 1. Principle of protein identification method using RNA aptamer

Reference

1. S. Tsuji, M. Yamashita, T. Kageyama, T. Ohtsu, K. Suzuki, S. Kato, J. Akitomi, M. Furuichi, and I. Waga, *PLoS One*. **8**, e83108 (2013).

Towards the development of odor biosensors: Evaluation of gene expression responses in *Escherichia coli* to a volatile organic compound by a novel aeration-culture based system

Riki Inui[1], Taiga Kamio[2], Kengo Morohashi[1,2]

[1] Graduate School of Science and Technology, Chitose Institute of Science and Technology, 758-65 Bibi, Chitose, Hokkaido, 066-8655, Japan
[2] Department of Applied Biological Science, Faculty of Science and Technology, Tokyo University of Science, 2641 Yamazaki, Noda, Chiba, 278-8510, Japan

k-moroha@photon.chitose.ac.jp

In recent years, the quantification of the human senses such as sight, hearing, taste, touch, and smell has progressed with the development of various sensors, but the quantification of the sense of smell has been delayed owing to the complexity of the many types of volatile organic compounds (VOCs) that are the source of odors. Given the complex nature of smell, this study focused on leveraging microorganisms, known for their sensitive VOCs detection capabilities, to advance biosensor technology (1,2). Therefore, we aimed to develop a biosensor using microorganisms by utilizing the mechanisms of gene expression changes. Previously, we isolated sequences from *Escherichia coli(E. coli)* that responded to the VOC, 2-phenylethanol (2-PE), in solid medium. However, the response to 2-PE in a solid medium is insufficient to develop a VOCs sensor that detects volatiles in air. Therefore, we developed an aeration culture system that continuously exposes *E. coli* to VOCs (Fig. 1). Using this system, we assessed a previously identified recombinant *E. coli* clone, PERS52, which can survive in cultures containing antibiotics only under 2-PE, since the 2-PE responsive sequence is located on the promoter of the antibiotic resistance gene. We confirmed that the number of viable PERS52 cells was increased in the presence of 2-PE (Fig. 2). Thus, we concluded the development of an aeration culture system to detect VOCs. Next, we utilize this system to screen novel sequences that respond to various VOCs.

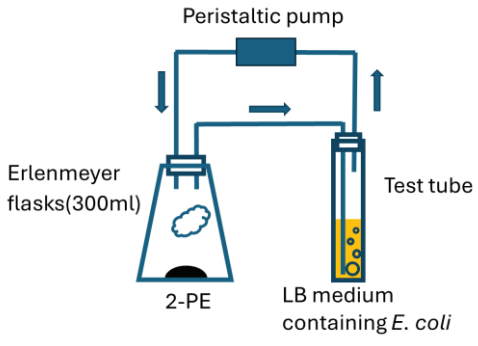

Figure 1. Aeration culture system

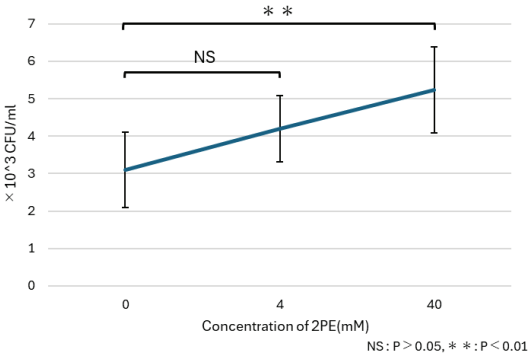

Figure 2. PERS52 aeration results

References

1 Sharma, U.K., and Chatterji, D. *FEMS Microbiol. Rev.* **34**, 646–657 (2010).

2 Wang, D., Ding, X., and Rather, P.N. *J. Bacteriol.* **183**, 4210–4216 (2001).

Attempts to identify target proteins of polyphenols

Ami Yakushijin[1], Kengo Morohashi[1]

[1] Graduate School of Science and Technology, Chitose Institute of Science and Technol −ogy, 758-65 Bibi, Chitose, Hokkaido, 066-8655, Japan

k-moroha@photon.chitose.ac.jp

Leukemia is one of the most common forms of cancer in young people. The main treatment for leukemia is chemotherapy with anticancer drugs, although these drugs have significant side effects, especially in the young generation. In recent years, polyphenols, which have anticancer effects, have been attracting attention; however, treatment with a single polyphenol has limited effects and does not meet practical requirements. Unlike drugs, which act strongly on a few target proteins, polyphenols are known to act moderately on many proteins; the effects of polyphenols are relatively mild compared to those of drugs. Thus, we sought to address the limited action of polyphenols by combining multiple polyphenols in a focused biological pathway. Therefore, we attempted to identify direct target proteins of certain polyphenols that exhibit strong synergistic effects. We generated a cDNA library from leukemia cells and screened for proteins that were directly associated with a given polyphenol. In this study, we report a vector-incorporated random cDNA (Figure 1).

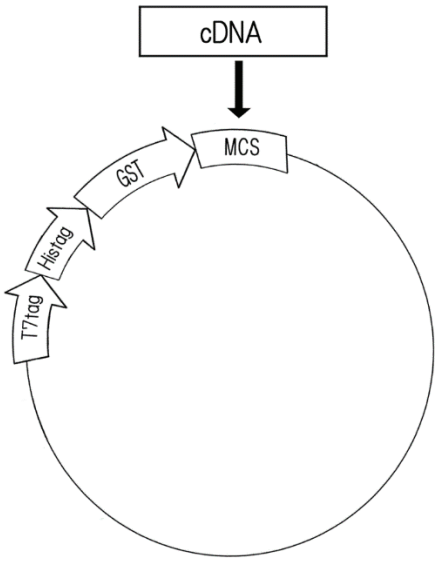

Figure 1. Schematic diagram of the vectors created for this project

An Integrated Network Analysis to Exploring the Potential of Flavonoid Combinations in Food for Drug-like Effects

Koyo Fujisaki[1], Osei Horikoshi[2], Yukitoshi Nagahara[2], and Kengo Morohashi[1*]

[1]Faculty of Science and Technology, Department of Applied Chemistry and Bioscience, Chitose Institute of Science and Technology, Chitose, Hokkaido, Japan
[2]Division of Life Science, School of Science and Engineering, Tokyo Denki University, Ishizaka, Hatoyama, Hiki-gun, Saitama 350-0394, Japan

k-moroha@photon.chitose.ac.jp

Flavonoids, a class of polyphenols found in vegetables and fruits, have been associated with various health benefits, including improved endothelial function, reduced risk of heart disease, and anticancer effects. However, the mechanisms through which flavonoids exert their effects differ from those of drugs approved by the Food and Drug Administration (FDA). While drugs interact with a small number of proteins with high affinity, flavonoids tend to interact with a broad range of proteins with moderate affinities, resulting in their nontoxic nature when consumed in the diet. Recent studies have employed network pharmacology to investigate the relationships among drugs, proteins, and biological functions, suggesting that flavonoid combinations can be explored by examining their interactions with biological networks. In this study, we comprehensively predicted the effects of flavonoids by analyzing drug-flavonoid associations using an integrated protein-compound network (Figure 1). To better understand the consequences of flavonoid combinations in food, we investigated the relationship between drug and flavonoid interactions and the flavonoid content in food. Previous epidemiological studies have shown that this relationship is correlated with the degree of association between drugs and flavonoids as well as the flavonoid content of the food in question. Our findings provide insights into the potential of foods containing optimal flavonoid combinations to produce drug-like effects, thereby opening new avenues for the development of flavonoid-based therapies and functional foods.

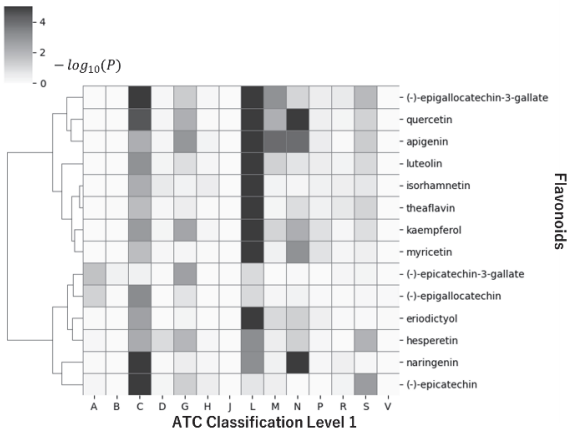

Figure 1. A heat map showing the relationship between flavonoids and drug classification (the ATC classification level 1). The vertical axis represents flavonoids, and the horizontal axis represents the ATC classification level 1. The ATC classification level 1 is as follows: A: Alimentary tract and metabolism, B: Blood and blood forming organs, C: Cardiovascular system, D: Dermatologicals, G: Genito urinary system and sex hormones, H: Systemic hormonal preparations, excl. sex hormones and insulins, J: Antiinfectives for systemic use, L: Antineoplastic and immunomodulating agents, M: Musculo-skeletal system, N: Nervous system, P: Antiparasitic products, insecticides and repellents, R: Respiratory system, S: Sensory organs, V: Various.

Output light emitted from POF cutting-faces finished by different facet terminations

Akaru OKAZAKI [1], Kotaro TAKAHASHI[1], Kimio OGUCHI[2], and Masashi EGUCHI[1*]

[1] Department of Opto-Electronic System Engineering, Chitose Institute of Science and Technology 758–65 Bibi, Chitose-shi, 066–8655 Japan
[2] Heterogeneously-integrated Silicon Photonic Integration (HiSiPIC), National Taiwan University of Science and Technology, No.43, Sec.4, Keelung Rd., Taipei, 106335, Taiwan
*megu@paical.spub.chitose.ac.jp

In order to verify which technique is appropriate for cutting and facet finishing of POF, we have compared various facet finishing techniques. In this study, commercially available SI-POFs (Super ESKA SK-40 by Mitsubishi Chemical Corporation) were used. The fiber length was 3 meters and different fibers were used for each experiment to prevent the fibers from becoming too short due to polishing or cutting. The incident end face was cut with a box cutter, then manually polished with sandpapers (#800 to #10,000), and fixed thereafter. Measurements were taken by changing only the conditions of the output end face.

For comparison based on the particle size of sandpaper, five types of sandpapers (#800, #1000, #1500, #2500, #3000) were tested. In polishing with each sandpaper, pre-polishing was done in the order from #800, e.g., for measuring with #1500, in the order of #800, #1000, and #1500. In addition, manually polishing with a polishing tool for glass optical fibers was also attempted. Next, a method using a hot plate for end face finishing was measured at temperatures from 70 to 120℃.

Fig.1 shows a measurement setup. Here, a laser diode module operating at 635nm was used. As an example, end faces manually polished by sandpapers are shown in Fig.2. Figs.2(a) and 2(b) correspond to polishings with #800 and #3000, respectively. It can be seen that in using a coarse sandpaper polishing flaws remain on the end face, wheareas in using a fine sandpaper the end face is polished smoothly. As a result, it is considered appropriate to finish the end face of POF by cutting with a box cutter, then polishing with a tool using a sandpaper around #3000.

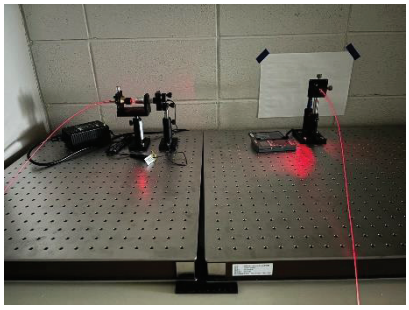

Fig.1 Measurement setup.

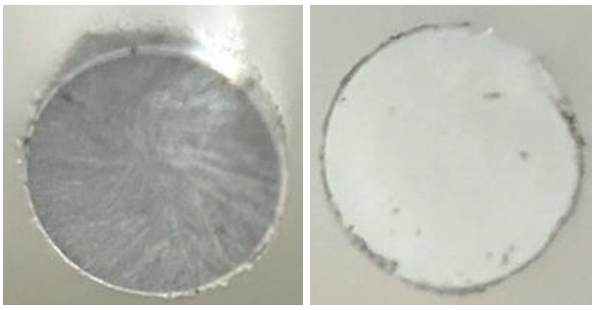

(a) #800 (b) #3000

Fig.2 POF end faces polished with sandpapers.

Developing a GUI for experimental design with Bayesian optimization and case study

Yoshiki Hasukawa, Mikael Kuwahara, Lauren Takahashi, and Keisuke Takahashi

Department of Chemistry, Hokkaido University, North 10, West 8, Sapporo 060-8510, Japan

hasukawa.yoshiki.i7@elms.hokudai.ac.jp

Catalyst informatics utilizes data science techniques, such as preprocessing, visualization, and machine learning, to analyze large datasets and identify hidden trends, patterns, and periodicities from features like reaction conditions, structures, and experimental variables. This approach treats catalytic reactions as an inverse problem for catalyst design. Although catalysts remain unchanged before and after a reaction, they undergo dynamic changes during the process, making it challenging to elucidate reaction mechanisms. However, even when the reaction mechanism is not fully understood, machine learning can reveal data-driven trends and patterns, making informatics particularly useful in the context of catalytic reactions. Especially, bayesian optimization, coupled with Gaussian process regression and acquisition functions, has proven to be a powerful tool in the field of experimental design. Despite its potential, the use of catalyst informatics poses significant challenges for researchers, as it requires a combination of data science skills such as statistics, mathematics, and machine learning and a broad knowledge of chemistry related to catalysis. To address these challenges and improve the catalyst development environment, this study developed a graphical user interface for experimental design using machine learning within the Catalyst Development Platform (CADS)[1], a user-friendly environment for handling data science tasks. The utility of the experimental design method is demonstrated by applying it to methanol synthesis data using zeolite catalysts. [2]

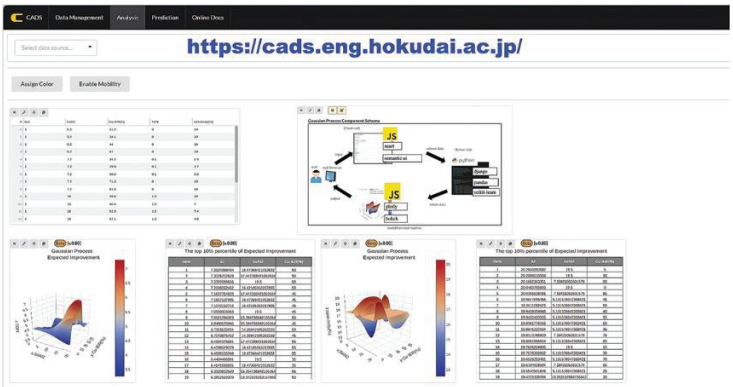

Figure 1. GUI for experimental design with Bayesian optimization

References

1 Fujima, J., Tanaka, Y., Miyazato, I., Takahashi, L., & Takahashi, K. (2020). *Re action Chemistry & Engineering*, *5*(5), 903-911.

2 Hasukawa, Y., Kuwahara, M., Takahashi, L., & Takahashi, K. (2024). *Science and Tec hnology of Advanced Materials: Methods*, *4*(1), 2300252.

Designing Catalyst Descriptors for the Water-Gas Shift and the Oxidative Coupling of Methane Reactions

Fernando Garcia-Escobar[1] and Keisuke Takahashi[1]

[1] Department of Chemistry, Hokkaido University, North 10, West 8, Sapporo 060-8510, Japan

escobarfernando.garcia.u8@elms.hokudai.ac.jp

The incorporation of Machine Learning-assisted methodologies has proven successful in the development of efficient catalysts for various applications, as the candidate screening can speed up the testing and discovery of candidate materials. This research presents two approaches toward Descriptor design in the construction of regression models that predict catalyst performance for the Water-Gas Shift (WGS) [1] and Oxidative Coupling of Methane (OCM) [2] reactions.

For the WGS reaction, CO conversion is predicted as a function of catalyst material and reaction conditions using a previously reported literature dataset. The representation of the catalyst materials in the model was explored in two ways: through one-hot encoding of the components in a Random Forest Regression model, and through physical and chemical properties of the metallic element components of the catalysts' in a Support-Vector Regression model.

On the other hand, for the OCM reaction, C2 yield is predicted as a function of catalyst composition only across fixed experimental conditions. Here, a feature-engineered data set containing 3289 descriptor variables and the performance of 200 catalysts for the oxidative coupling of methane (OCM) is used to develop a descriptor search algorithm based on the workflow of the Basin-hopping optimization methodology to sample descriptors that better fit a predictive model.

In conclusion, we propose an approach toward descriptor design and search that has been applied to predict catalyst performance for the WGS and OCM reactions. For the WGS reaction, high CO conversion candidates are predicted to be are promoted $Au/CeO_2–ZrO_2$, Au/CeO_2, Ru/CeO_2, and Rh/CeO_2 candidates, with $Yb/Au/CeO_2–ZrO_2$ to be of interest for WGS applications at low temperatures. For the OCM reaction, models with average cross-validation r^2 scores of 0.8268 and 0.6875 for Linear and Support-Vector Regression models, respectively could be constructed, which are higher than those obtained with common wrapper descriptor selection methodologies.

References

1 F. Garcia-Escobar, S. Nishimura, K. Takahashi, *J. Phys. Chem. C. Defg*. **127**, 6152-6166 (2023).

2 F. Garcia-Escobar, T. Taniike, K. Takahashi. *J. Chem. Inf. Model*. **64**, 1512-1521 (2024).

Effect of the chemical bonding state on the porous carbon surface on the persulfate activation and decomposition of organic dyes

Ryusuke Urushidate[1], Shuhei Shimoda[2], Keita Suzuki[3], Atsushi Fukuoka[2], Ken-ichi Shimizu[2], Tomoya Takada[1]
[1]Chitose Institute of Science and Technology, Chitose, Japan.
[2]Institute for Catalysis, Hokkaido University, Sapporo, Japan.
[3] Laboratory of XPS Analysis, Faculty of Engineering, Hokkaido University, Sapporo, Japan.

M2230060@photon.chitose.ac.jp

Advanced oxidation processes using persulfate (PS) and carbon catalysts have been widely studied in recent years.[1-2] One of the reasons why the decomposition efficiency differs depending on the type of carbon material is the difference in the chemical state of the surface. First, we prepared porous carbons with different surface chemical states and investigated their chemical structures by XPS and Boehm titration. Next, we investigated the efficiency of decomposing organic dyes using each catalyst and identified the best chemical structure for the surface.

The details of the chemical structure will be announced on the day. In brief, most of the carboxyl and lactone groups were eliminated by heat treatment, whereas the carboxyl groups were increased by ozone treatment. The decomposition efficiency of organic dyes was promoted by heat treatment and suppressed by ozone treatment. The longer the processing time, the more pronounced is the above tendency. Therefore, PS can be efficiently activated by removing excess acidic functional groups from the surface.

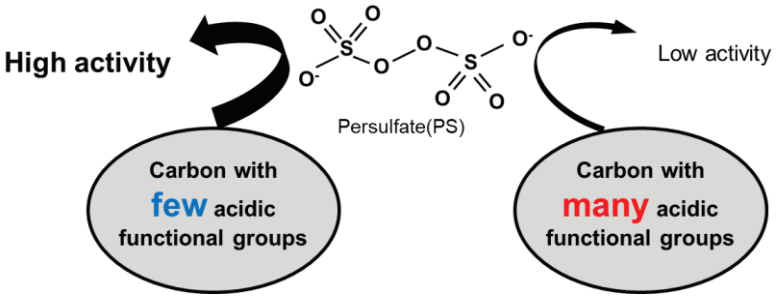

Fig. 1 Difference in the efficiency of PS activation.

This study was supported by the Joint Usage/Research Center for Catalysis and "Advanced Research Infrastructure for Materials and Nanotechnology in Japan (ARIM)," the Ministry of Education, Culture, Sports, Science, and Technology (MEXT).

References

1. X. Cheng, H. Guo, Y. Zhang, X. Wu, Y. Liu, Water Res. 2017, 113, 80-88
2. X. Duan, H. Sun, J. Kang, Y. Wang, S. Indrawirawan, S. Wang, ACS Catal. 2015, 5, 4629-4636

Antimicrobial Substances Produced by Broccoli Infected with Soft Rot

S. Doigawa, K. Okoshi*

Department of Applied Chemistry and Bioscience, Chitose Institute of Science and Technology, Chitose 066-8655, Japan

It is known that many plants in nature produce defense substances to cope with external stresses such as feeding damage from insects, ultraviolet rays from sunlight, and pathogens. The types of these defense substances vary depending on the type of plant and the source of stress, and to date, numerous attempts have been made to identify the defense substances. However, the antimicrobial substances in broccoli have not yet been elucidated.

Following standard protocols for food analysis [1-5], five fresh broccoli plants were sampled regularly for 6 days, and the same procedure was used to sample broccoli with soft rot. These were minced with a knife, grinded in a mortar, extracted with a 1:1 water/methanol solvent, and LC-MS measurements of the extracts were performed. These analyses were performed using Agilent MassHunter software and a data analysis software called MS-DIAL developed by RIKEN. Principal component analysis allowed clustering of each sample, with a cumulative contribution of 58% (Figure 1). Using the results of the factor loadings analysis, we narrowed down the components that were characteristic of broccoli with soft rot to three (Figure 2) and performed LC/MS/MS measurements for each. Component identification using the metabolite database resulted in the identification of two components. For the remaining one component, we predicted the compound from the obtained fragment pattern and synthesized a candidate compound.

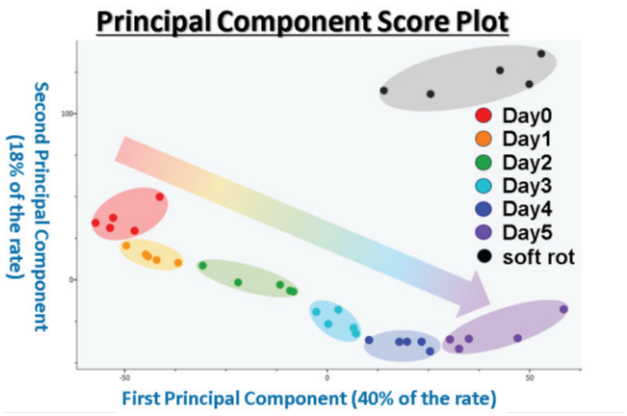

Fig.1 – Results of principal component analysis of aging process and soft rot

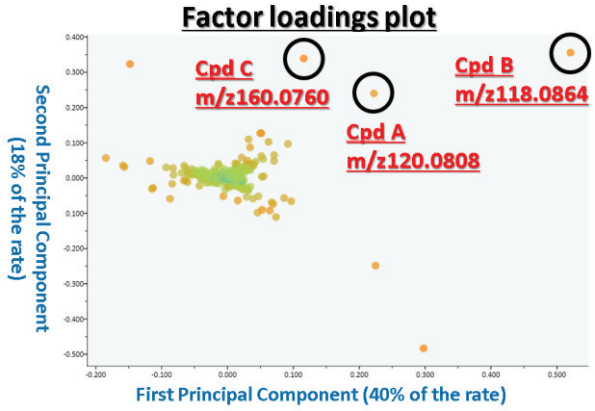

Fig.2 – Results of factor loadings analysis of aging process and soft rot.

References

[1] A. Trredoux, A. de Villiers, P. Májek, F. Lynen, *J. Agric. Food Chem.* **56** (2008) 4286
[2] M. P. Martí, O. Busto, J. Guasch, *J. Chromatogr. A* **1057** (2004) 211
[3] G. Botelho, A. Mendes-Faia, M. C. Climaco, *J. Agric. Food Chem.* **56** (2008) 7393
[4] Y. Fang, M. C. Qian, *J. Agric. Food Chem.* **54** (2006) 8567
[5] V. Arbona, D. J. Iglesias, *J. Agric. Food Chem.* **57** (2009) 7338

Nanopatterning Using the Smectic Phase of Rod-Like Polymers as a Template

Johanna Beck, Yoshitaka Sugiyama, and Kento Okoshi*

Department of Applied Chemistry and Bioscience, Chitose Institute of Science and Technology, Chitose 066-8655, Japan

k-okoshi@photon.chitose.ac.jp

It is theoretically predicted that when spherical particles are mixed with rod-like particles that form the smectic phase, an entropic interaction called the depletion effect selectively segregates the spherical particles between the layers of the smectic phase, stabilizing the phase.[1] We have demonstrated that spherical molecules are selectively stored in the interlayer when a rod-like polymer (polysilane) with a narrow molecular weight distribution that forms the smectic phase is mixed with a small compound (tetraalkylsilane) that can be regarded as spherical.[2] By using the stripe-like phase-separation structure with 10-100 nm intervals formed by this mixture system as a template, nanopatterning of the underlying substrate can be expected. By using the stripe-like phase-separation structure with 10-100 nm intervals formed by this mixture system as a template, it is expected to perform nano-patterning of the substrate.

We washed and dried silicon wafers (10x10 mm), spin-coated a chloroform solution (1.5 mg/mL) of a mixed sample of polysilane (Mw=125,600, Mw/Mn=1.17) and tetradecylsilane (20wt%) onto the and subjected to thermal annealing at 100°C for 20h. The substrate was subjected to CF4 (methane tetrafluoride) plasma etching for 1 min, and then chloroform:20 min ultrasonic cleaning was performed to remove polysilane, followed by reduced-pressure drying. AFM and SEM observations (Figure. 1) showed that the stripe structure was transferred onto the substrate in a layer-like segregated manner.

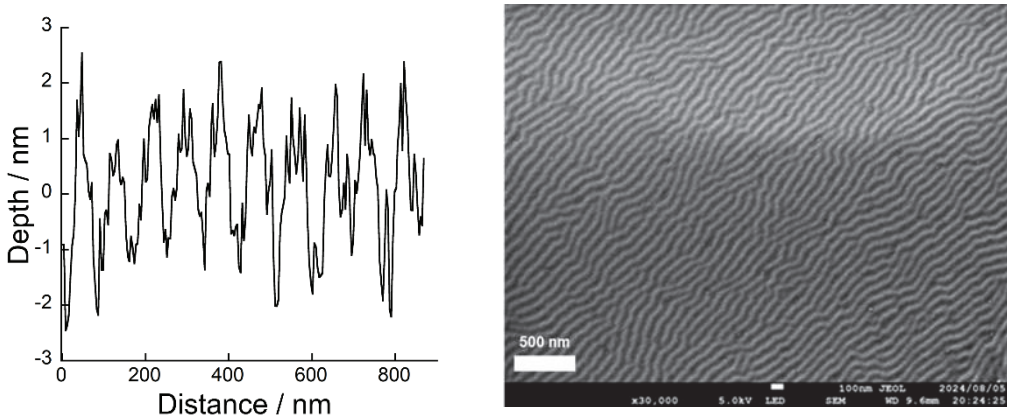

Figure 1. AFM cross-sectional profile (left) and SEM image (right).

References

1 T. Koda, M. Numajiri, S. Ikeda, *J. Phy. Soc. Jpn.,* **65**, 3551 (1996).

2 T. Tanaka, I. Kato, K. Okoshi, *J. Research Updates Polym. Sci.,* **7**, 1 (2018).

Structural Study on Rod-Coil-Coil Block Copolymers with polyacetylene as the hard segment

T. Onishi, K. Okoshi

Department of Applied Chemistry and Bioscience, Chitose Institute of Science and Technology, Chitose 066-8655, Japan

Although it is still not possible to predict the behaviour of a liquid crystal from its chemical structure, computational studies on liquid crystalline (LC) phases formed by coarse-grained rod-like particles have shown that the most commonly observed nematic-smectic-columnar LC phase sequence can be reproduced in simple rod-like particle systems.[1-3] Such theoretical treatment may reveal the essence of liquid crystal formation other than the intermolecular interaction specific to the molecular structure. This theoretical approach has been extended to systems of end-tethered rod-like particles to show rich phase behaviours, including wavy lamellae, zig-zag lamellae, perforated lamellae, smectic C, and bilayer arrowhead structures, which could occur depending on the relative coil fraction and the aspect ratio of the rods.

Some of these theoretically predicted structures have been prepared experimentally with rod-coil or coil-rod-coil block copolymers by balancing the mutual repulsion between immiscible blocks and the local packing of blocks of different shapes. However, there has been no systematic quantitative verification of the theoretical predictions by synthesizing block copolymers with precisely controlled molecular weights and molecular weight distributions, although such synthesis is essential for refining the theoretical models.

Polyacetylenes, whose main chain backbone is polyene composed of sp2 carbons, are known as one of the representative helical polymers, and a living polymerization method for phenylacetylenes using a multi-component catalyst system consisting of a rhodium complex, aromatic boronic acid derivatives, and diphenylacetylene derivatives has been reported.[4]

In this study, we report the synthesis of a macroinitiator bearing an atom transfer radical polymerization (ATRP) initiator at the end of a rigid rod-like helical polyacetylene with a very narrow molecular weight distribution and the ATRP of styrene monomer to extend the flexible coil from the ends (Figure 1) (Figure 2). Such a block copolymer could be used to quantitatively verify the theoretical predictions.

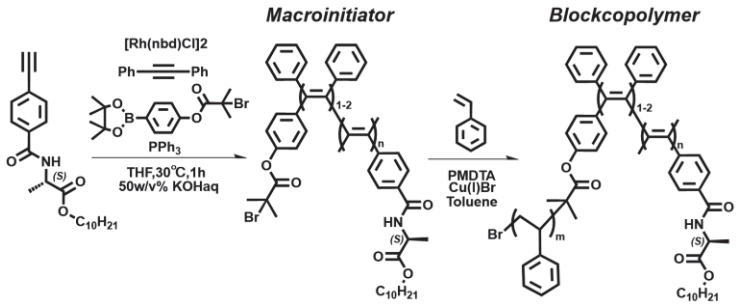

Figure 1. Synthesis scheme.

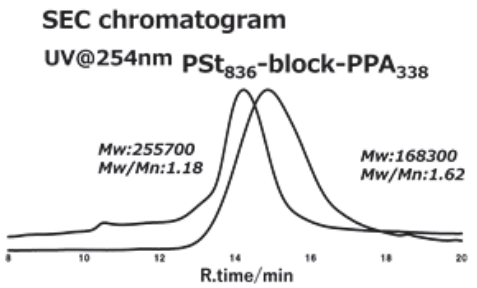

Figure 2 SEC of block copolymer.

References

1. A. Stroobants, H. N. W. Lekkerkerker, D. Frenkel, Phys. Rev. A: At., Mol., Opt. Phys. 36 (1987) 2929
2. J. A. C. Veerman, D. Frenkel, Phys. Rev. A: At., Mol., Opt. Phys. 43 (1991) 4334
3. P. Bolhuis, D. Frenkel, J. Chem. Phys. 106 (1997) 666
4. K. Maeda et al., Angew. Chem Int. Ed., 59, 8670 (2020).

Heterogeneous Structure in PMMA Synthesized by Bulk Polymerization

N. Suehiro, K. Okoshi

Department of Applied Chemistry and Bioscience, Chitose Institute of Science and Technology, Chitose 066-8655, Japan

Flexible and easy-to-handle plastic optical fibers are required to meet the demands of today's high-speed, high-capacity information communication networks. Therefore, amorphous polymers that do not have a non-uniform structure of refractive index in the crystalline region have been actively studied. TANIO Laboratory has been developing extremely transparent PMMA (polymethyl methacrylate) to minimize the transmission loss of plastic optical fibers. However, when PMMA polymerized under various conditions was evaluated by light scattering, it was found that a refractive index inhomogeneous structure on the order of tens of nm existed, which prevented high transparency [1].We have been analyzing the refractive index inhomogeneous structure of PMMA in collaboration with TANIO Laboratory, and comparing the transparency of PMMA samples at different polymerization temperatures and times, we have found that the refractive index inhomogeneous structure grows with polymerization time when polymerization is performed below 110°C, which is the glass transition temperature. In addition, AFM observation confirmed a spherical structure, which is considered to be correlated with the inhomogeneous structure.

In this study, we report the change in the size of spherical structures by AFM observation. Observation of samples with polymerization temperature and polymerization time increased to 70°C and 70°C, respectively, showed that the spherical structure tended to increase in size with the passage of time (Figure 1). AFM observation of samples with a polymerization time of 96 hours and varying polymerization temperatures showed that the spherical structure became larger as the temperature approached 110°C, the glass transition temperature (Figure 2).

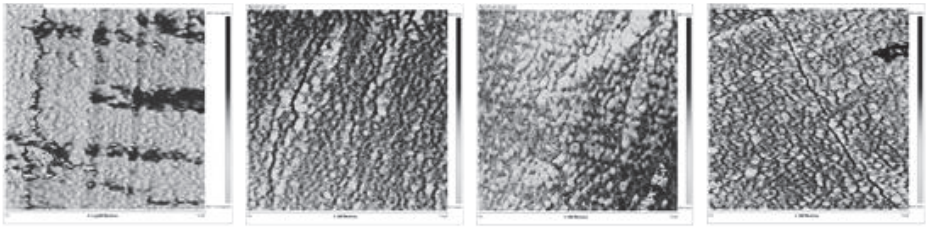

Fig1. AFM elastic modulus mapping of PMMA t_p 96,480,600,720 h

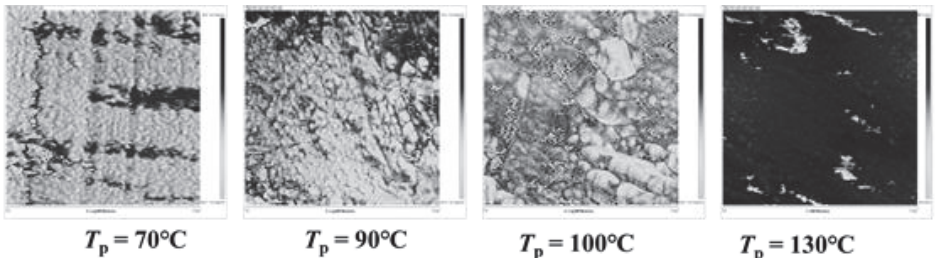

Fig2. AFM elastic modulus mapping of PMMA T_P 70,90,100,130 °C

References

[1] N. Tanio, H. Obata, A. Okada, S. Segawa, R. Takemura, R. Kaneko *Kobunshi Ronbunshu.* **66**, 1-9 (2009).

Formation of Unique Structure Expressed in Coil-Rod-Coil Block Copolymers

Tatsuhiro Kojima, and Kento Okoshi*

Department of Applied Chemistry and Bioscience, Chitose Institute of Science and Technology, Chitose 066-8655, Japan

We have been studying coil-rod-coil block copolymers, in which a coiled flexible polymer, polystyrene, is elongated at the end of a very rigid and nonpolar rod-like helical polymer, polysilane, and have shown that this coil-rod-block copolymer forms a smectic phase due to segregation of the flexible chains (Figure 1).[1] Computer simulations using mechanical models have revealed that such rod-shaped particles with flexible chains at both ends form a variety of structures depending on their rod/coil volume ratio and rod aspect ratio.[2] However, few experimental studies have been reported to substantiate these theoretical predictions. A coil-rod-coil block copolymer was synthesized by elongating polystyrene from both ends of rigid polysilane using the ATRP method, and its degree of polymerization was 646 of polystyrene, compared to 43 of polysilane (Figure 2).

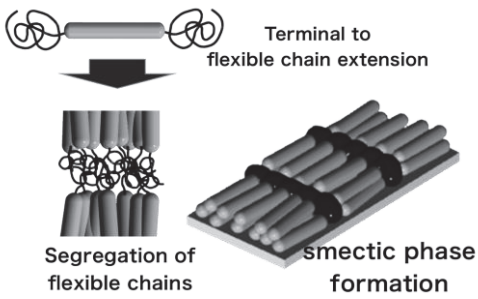

Figure 1. Smectic phase formed by coil-rod-coil block copolymers

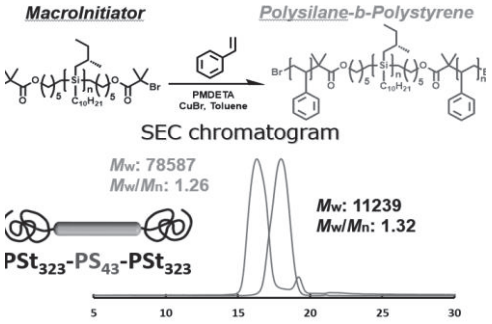

Figure 2. Example of synthesis of coil-rod-coil block copolymer

The coiled-rod coil block copolymer did not form the smectic phase, but instead a peculiar structure appeared, in which two lines are adjacent to each other (Figure 3), and disappeared when polystyrene included as an impurity was removed (Figure 4). This phenomenon is thought to be due to the depletion effect caused by the addition of flexible chains, which is to be elucidated.

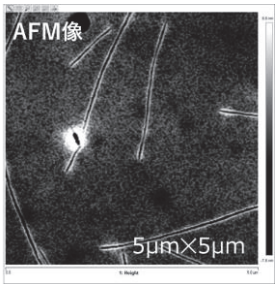

Figure 3. AFM image of synthesized coil-rod-coil block copolymer

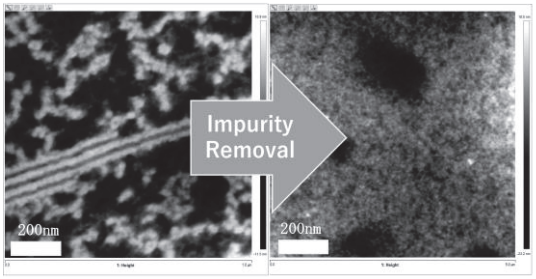

Figure 4. AFM image after removing impurities

References
1. I. Kato, T. Tanaka, K. Okoshi, *Chemistry Letters*, **49**, 347-349 (2020).
2. M. A. Horsch, Z. Zhang, S. C. Glotzer, *Soft Matter*, **6**, 945-954 (2010).

A Study of ZMP-Disturbance Estimation Based on Image-based Visual Servo for Biped Robot

Konosuke Ichiba and Naoki Oda
Chitose Institute of Science and Technology
m2240070@photon.chitose.ac.jp

Recently, Japan has been facing the problem of declining working population due to the progression of low birth rates and an aging society. As a result, various kinds of robots are being introduced in various situation to assist with daily life and working efficiency. Among them, biped robots are especially expected to adapt to human living environments.

Biped robots require highly reliable stabilization control, and in human living environments, where environmental changes occur rapidly, real-time performance is also crucial. In our laboratory, a camera is attached to the waist of the biped robot as shown in Fig.1, and visual servo is performed to keep a specified target at the center of the image plane. The robot's current posture and external forces are estimated from the image information, and stabilization control is performed. In previous research [1], the displacement of the Zero Moment Point (ZMP), which is a stability indicator for biped robots, was defined as the "ZMP-Disturbance", representing disturbances acting in the acceleration dimension on the image. Then, ZMP-Disturbance Observer (ZMP-DOB) was proposed and its effectiveness was demonstrated. However, the accuracy of the estimated value was not confirmed for stabilization control yet.

In this research, the robustness of visual servo is aimed to be improved by using Vision Space Observer, and ZMP-Disturbance is also estimated with the enhanced ZMP-DOB. The estimation results of the ZMP-Disturbance in the research are shown in Fig.2. In the figure, the blue line represents the ZMP acceleration calculated by force sensors, and the orange line represents the ZMP-Disturbance estimated by ZMP-DOB. As can be seen from the figure, the ZMP-Disturbance closely matches the profile of actual value, which shows that the accuracy of the ZMP-DOB has been improved. In the future, we plan to use this estimated value for ZMP stabilization control.

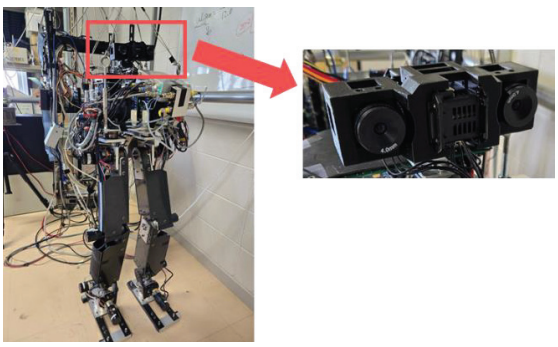

Fig.1 Biped Robot

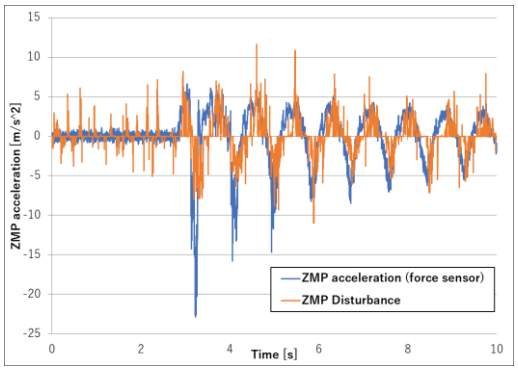

Fig.2 ZMP-Disturbance estimation results

References

[1] K.Matsumori, "A ZMP Disturbance Estimation and Recovery Control for Bipe d Walking Robot by Image-based Visual Servo", Chitose Institute of Science and Technology, Master's Thesis (2022) (in Japanese)

Development of 7DOF Redundant Robot Arm Equipped with Twin Drive System

Naruki Sugawara, Naoki Oda
Chitose Institute of Science and Technology, Chitose 066-8655, Japan
m2240270@photon.chitose.ac.jp

In recent years, the robots have been used in a variety of situations to improve work efficiency and save labor, and many robot arms have been developed using remote operation technology. However, the remote operation systems currently being developed require users to acquire specialized skills, making it difficult to control robot arms as dexterously as their own arms. In our laboratory, a robot hand, which can be reproduced the movement of human hand, is being developed [1]. Moreover, we make a robot arm part by using 3D printer. The arm is designed with 7 degrees of freedom (DOF) to reproduce the complicated movements of the human arm. Additionally, the "Twin Drive System" was introduced to develop a robot arm for sufficient torque drive with appropriate motion range and lightweight. This system enables high torque output in a small-limited joint structure by using two motors for each DOF.

In this research, the target angle range of motion of the arm joints is specified in Table 1, and developed 7DOF robot arm achieving the target range is shown in Fig1. The disturbance observer is employed for robust motion controller. The performance of joint motion by twin drive system is verified by several experimental results.

Table 1. target angle range

Joint	Motion	Joint Range(degree)
Shoulder	Flexion and Extension	0~180
	Adduction Abduction	0~180
Elbow	Flexion and Extension	0~150

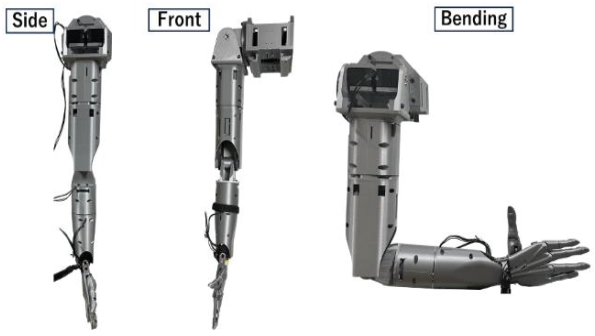

Fig 1. 7DOF robot arm

References

[1] Kunio Sakaki, Naoki Oda, "Developments of wire-driven haptic glove and robotic hand with considering tension control", 2023

Synthesis of Vinylidenecyclopropanes via Gold(I)-Catalyzed Cyclopropanation of Vinyl Arenes

Hiroto Mori[1], Yusuke Ono[1], Shota Nakagawa[1], Sota Akima[1], Miki Murakami[2], Toshinobu Korenaga[3], Tadashi NakajiHirabayashi[2], and Yoshikazu Horino*[1]

[1]Department of Applied Chemistry and Bioscience Chitose Institute of Science and Technology, Chitose 066-8655, Japan
[2]Graduate School of Science and Engineering, University of Toyama, 930-8555, Japan
[3]Department of Applied Chemistry and Bioscience, Iwate University, 020-8551, Japan

y-horino@photon.chitose.ac.jp

Research on gold-alkylidene and gold-vinylidene-mediated carbon–carbon bond forming reactions, such as olefin cyclopropanation, has been well developed.[1)] However, the gold(I)-coordinated allenylidene-mediated carbon–carbon bond forming reaction is underdeveloped due to lack of catalytic methods to access to such intermediates. We found for the first time a new method for the catalytic generation of gold(I)-coordinated allenylidene species by the combination of gold-induced 1,2-stannyl rearrangement of stannylated alkynes and subsequent bimolecular *anti*-specific elimination. We herein report the unprecedented generation of gold(I)-coordinated allenylidene species, applied for the cyclopropanation of vinyl arenes.

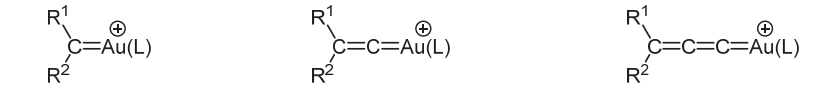

Figure 1. Gold(I)- carbene

The reaction of **1** and vinyl arene **2** in the presence of $(Ph_3P)AuCl/AgSbF_6$ (5 mol%) in CH_2Cl_2 at 25 °C afforded the desired VDCP **3** as a mixture of diastereomers (eqn 1). To obtain detail information on the mechanism of cyclopropanation, the DFT calculations were performed. Although concerted cyclopropanation was proposed in the previously reported reaction of styrene with gold(I)-coordinated benzylidene, it was found that the cyclopropane ring was constructed by a stepwise mechanism in the present case. The vinyl arene **2** attacks to Cα of the gold(I)-stabilized propargyl cation **B** not the predicted form **A** to give a benzylic carbocation intermediate. The detail of this reaction mechanism will be presented.

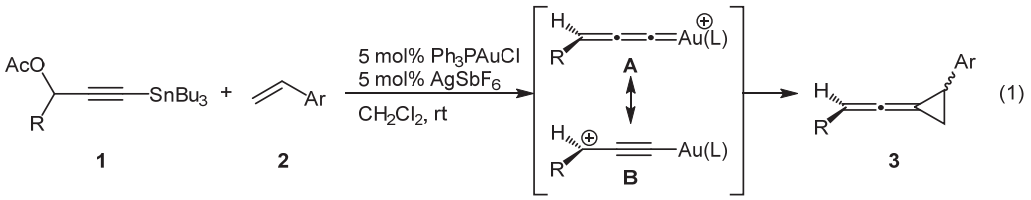

References

1) D. Benitez, N. D. Shapiro, E. Tkatchouk, Y. Wang, W. A. Goddard, F. D. Toste, *Nat, Chem.* **2009**, *1*, 482.

Stereoselective Synthesis of (*Z*)-*anti*-Homoallylic Alcohols Using Palladium-Catalyzed Three-Component Reaction

Ayumu Natsubori[1] and Yoshikazu Horino*[1]

[1] Department of Applied Chemistry and Bioscience Chitose Institute of Science and Technology, Chitose 066-8655, Japan

y-horino@photon.chitose.ac.jp

Three-component reactions are useful synthetic methods as they not only shorten the reaction process but also enable efficient stereoselective synthesis of target molecules. We have previously reported the palladium-catalyzed three-component reaction of benzaldehyde (**1a**), 3-(pinacolatoboryl)allyl acetates **2a**, and triorganoboranes (**3a**) to provide (*Z*)-*anti*-homoallylic alcohol **4aaa** (eqn. 1).[1)] However, the method offers narrow functional group tolerance as the trialkylboranes used in this reaction was prepared by hydroboration of the corresponding alkenes. On the other hand, organozinc reagents are easily prepared by either the direct insertion of zinc metal or transmetallation with zinc salts. In this study, we report a three-component reaction using organozinc reagents instead of the trialkylboranes, and found that a highly diastereoselective three-component coupling reaction proceeded to give (*Z*)-*anti*-homoallyl alcohols (eqn. 2).

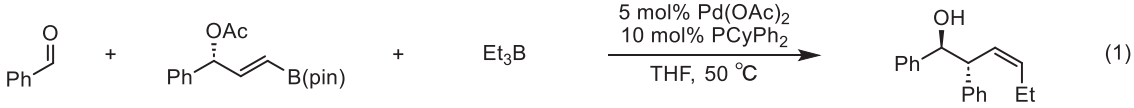

(1)

1a (*R*)-**2a** (99% *ee*) **3a** (1*S*, 2*R*)-**4aaa** 76%, 81% *ee*, 81% *es*

We initially examined the reaction of **1a**, **2a**, and commercially available diethyl zinc (**5a**) in the presence of catalytic amounts of $Pd(OAc)_2$ and $(4\text{-}CF_3C_6H_4)_3P$ (eqn. 2). We were pleased to find that the corresponding (Z)-*anti*-homoallylic alcohol **4aaa** was obtained in 76% isolated yield. The transfer of chiral information from chiral substrates to products (chirality transfer reaction) can generate enantiomerically enriched molecules, but the control of stereochemistry often proves challenging. Interestingly, while moderate chirality transfer was observed in our previous study (eqn. 1), the present system showed the excellent chirality transfer (94.5 %*es*). The detail of this reaction mechanism and scope of organozinc reagents as well as chirality transfer reaction will be presented.

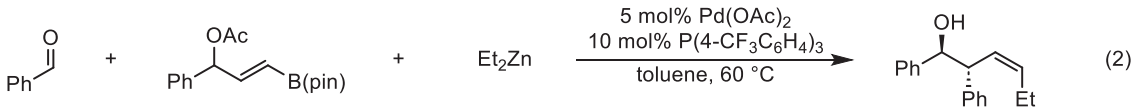

(2)

1a **2a** **5a** (*Z*)-*anti*-**4aaa**, 76%

Reference

1) Y. Horino, A. Aimono, H. Abe, *Org. Lett.* **2015**, *17*, 2824-2827.

Synthesis of 2-Vinylnapthalenes via Gold(I)-Catalyzed Cyclopropanation of Indenes

Shota Nakagawa[1] and Yoshikazu Horino*[1]

[1] Department of Applied Chemistry and Bioscience Chitose Institute of Science and Technology, Chitose 066-8655, Japan

y-horino@photon.chitose.ac.jp

We previously reported that the reaction of propargylic esters **1** having stannyl group at alkyne terminus with vinyl arenes**2** in the presence of a cationic gold(I) catalyst affords vinylidenecyclopropanes (VDCPs) **3** as a mixture of diastereomers (eqn 1).[1)] It was found that gold(I)-stabilized propargyl cation species **B** is generated rather than gold(I)-coordinated allenylidene species **A** in this system.

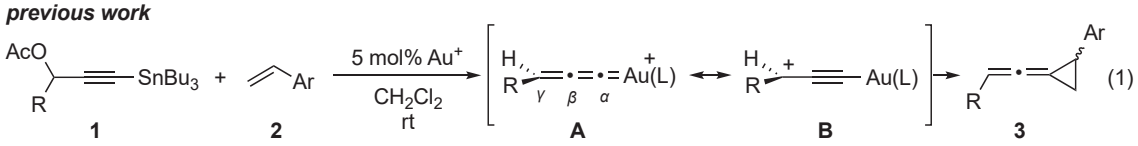

VDCPs are synthetically valuable molecules due to their extraordinary properties. For example, the estimated strain energy of VDCP is 50.9 kcal/mol, while that of cyclopropane and methylenecyclopropane is 27.5 and 40.9 kcal/mol, respectively.[2)] In this study, we found that the reaction of indene **4** with tributylstannylated propargylic acetates **1** in the presence of gold(I) catalyst yielded 2-vinyl-substituted naphthalene derivatives **5** (eqn 2). Interestingly, the reaction proceeded when JohnPhos or IPr ligands were used. On the other hand, the use of phosphine ligands other than JohnPhos or IPr provided cyclopropanation reaction products. Next, the ring expansion reaction of **4a** was examined to determine whether this reaction proceeds via the vinylidene cyclopropane derivative **3** (eqn 3). As a result, **5a** was obtained in 79% yield. This control experiment revealed that the present reaction proceeds in a tandem fashion.
The detail of this reaction mechanism will be presented.

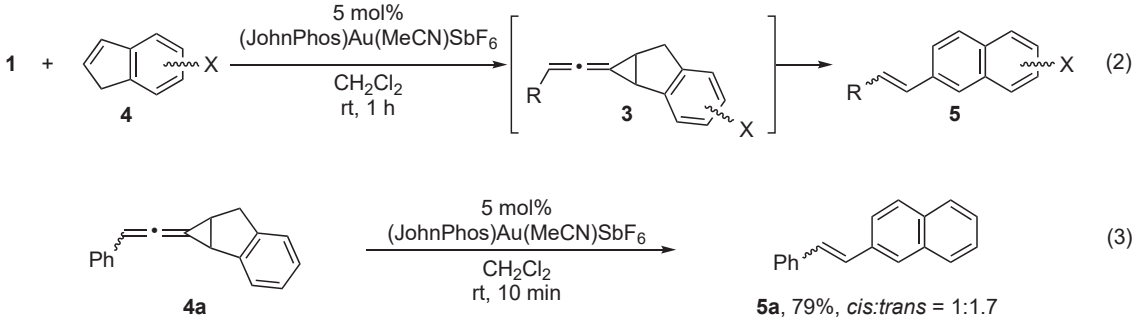

1) H. Mori, Y. Ono, S. Nakagawa, S. Akima, M. Murakami, T. Korenaga, T. Nakaji-Hirabayashi, M. Kyogoku, Y. Horino, *submitted.*
2) R. D. Bach, O. Dmitrenko, *J. Am. Chem. Soc.*, 2004, **126**, 4444–4452.

Transition-Metal-Free Synthesis of Homopropargylic Alcohols

Haruya Hirano[1] and Yoshikazu Horino*[1]

[1] Department of Applied Chemistry and Bioscience Chitose Institute of Science and Technology, Chitose 066-8655, Japan

y-horino@photon.chitose.ac.jp

Homopropargyl alcohols are not only used as useful synthetic building brocks, but also privileged structure in many biologically active natural products and agrochemicals. Given the importance of homopropargyl alcohols, efforts have been devoted to the development of efficient and practical methods for their synthesis. Despite remarkable progress, there are still few reports on the synthetic methods under transition metal-free conditions.

Previously, our laboratory has reported a transition-metal-free three-component process that combines aldehydes **1**, 3-(tributylstannyl)propargyl acetates **2** formed in situ from readily available propargyl acetates, and trialkylboranes **3** provides access to a range of 1,2,4-trisubstituted homopropargylic alcohols **4** (eqn 1).[1)] Considering the environmentally benign processes, avoiding the use of organostannanes is desirable and more environmentally benign alternative protocols are required. We herein report a novel and green route for the synthesis of homopropargyl alcohol derivatives **4** without the use of transition metals and organostannanes (eqn 2).

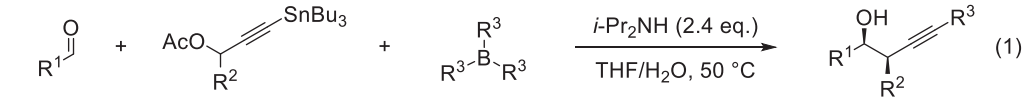

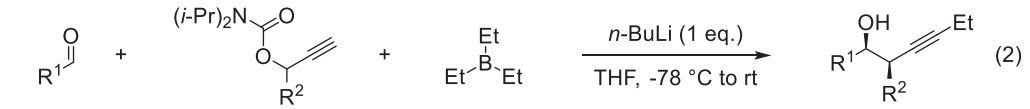

Reference

1) Y. Horino, *et al*. *Org*. *Lett*. **2019**, *21*, 9564-9568.

Synthesis of new reusable cage-shaped phosphine ligands

Mizuki Oda[1] and Yoshikazu Horino*[1]

[1] Department of Applied Chemistry and Bioscience Chitose Institute of Science and Technology, Chitose 066-8655, Japan

y-horino@photon.chitose.ac.jp

Palladium metal-catalyzed cross-coupling reactions are very useful for the synthesis of functional materials.[1)] Usually, phosphine ligands are used to stabilize the catalytically active Pd(0) species. However, phosphine ligands are easily oxidized, producing inactive palladium black and phosphine oxide at the end of the reaction. On the other hand, phosphine sulfide ligands, in which the phosphorus ligands are sulfurized, are not easily air oxidized and the catalyst can be recycled, but the oxidation of the central metal cannot prevent a decrease in catalytic activity.[2)]

Therefore, the aim of this study is to synthesize cage-shaped phosphine ligands, which are highly stable and can maintain catalytic activity for a long time. Here we report a route to synthesize bowl-shaped ligand precursors (Fig. 1), which are precursors of cage-shaped phosphine ligands (Scheme1).

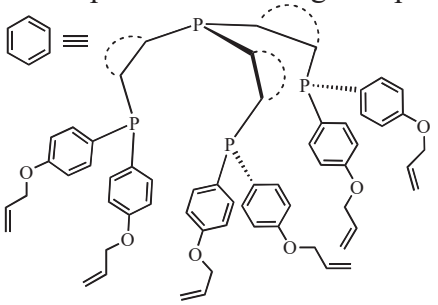

Fig. 1 bowl-shaped ligand precursors

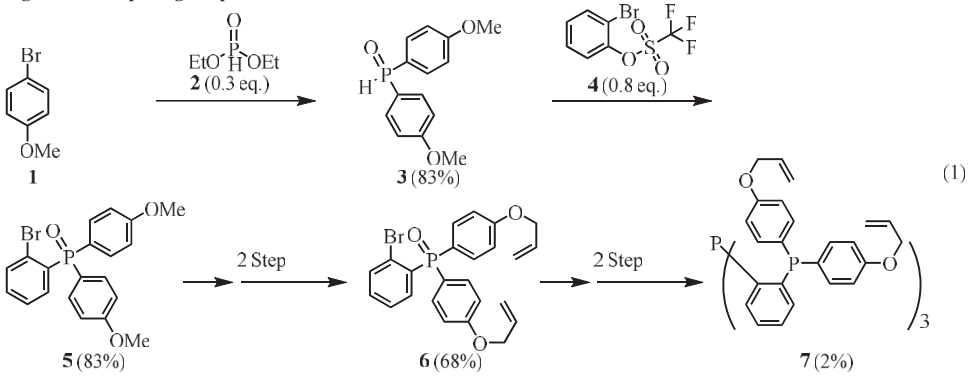

Scheme 1 Synthetic route to ligand precursor

References

1. R. Sato, T.Kanbara, J. Kuwabara, *Organomet*, **2020**, *39*, 235-238.
2. S. Aizawa, A. Majumder, Y. Yokoyama, M. Tamai, D. Maeda and A. Kitamura, *Organomet*, **2009**, *28*, 6072-6067.

Evaluation of Source Code that Includes Perspectives of Ease of Handover Measured by Class Cohesion

Mayu Sudo[1], and Hiroto Yamakawa[1]

[1] Graduate School of Science and Technology, Chitose Institute of Science and Technology, Chitose 066-8655, Japan

m2240300@photon.chitose.ac.jp

In Project-Based Learning (PBL) in higher education, which aims to train IT engineers, there are cases where part of software development is handed over to a new project, and development continues. Therefore, the software should be made with source code that is easy to hand over from an objective viewpoint. The purpose of this study is to reveal the methods to incorporate "ease of source code handover". In PBL, learners continue the advanced development of software by reading maps between requirements for the implementation of the request of customer role and the internal structure of software. Therefore, we assumed that the source code that is easy to hand over has the following three objectively high perspectives: 1. Understandability of modules responsibility, 2. Understandability of the structure of source code based on requirements, and 3. Understandability of software behavior. To incorporate perspectives 1 and 2, we used domain-driven design methods that prepare the requirements document supervised by customers and developers and reflect it in modeling and source code. To incorporate perspective 3, we used the test-driven development methods.

Based on the source code as legacy code made by the learner and the journal article of HANASHI-KOTOBA Checker[1], modeling and refactoring were performed with experts aiming to include three perspectives. In the expert's source code, classes that corresponded to the keywords used by the customer and the procedures for the requirements were created by modeling from the journal article, and a test case was provided to observe the behavior. We have confirmed perspective 1 using class cohesion that was measured using five metrics of jPeek[2](Table 1). The legacy code changed that there are a large number of highly cohesive classes that reflect the requirements implementation procedure. We were able to satisfy perspective 1 to some extent. In the future, we will evaluate and verify perspectives 2 and 3 and build methods to incorporate the ease of handover source code into learners' actual development.

Table 1. Comparison of number of classes and class cohesion score

	Number of classes	CAMC	LCOM5	MMAC	NHD	SCOM
Legacy code	30	0.97	0.50	0.50	9.32	0.50
Expert's source code	89	2.81	1.06	1.24	6.62	2.42

References

[1] Yamashita, Y., et al. (2021), *Development and Evaluation of Japanese Colloquial Writing Checker, Transactions of Japanese Society for Information and Systems in Education,* Vol. 38, No.4, pp. 369-374

[2] jPeek, https://github.com/cqfn/jpeek (accessed Aug. 17, 2024)

Development and Implementation test of LTI Gateway System to Improve Interoperability of Educational Systems

Toshinobu Kamada[1] and Hiroto Yamakawa[1]

[1]Graduate School of Science and Engineering, Chitose Institute of Science and Technology, Chitose 066-8655, Japan

m2240190@photon.chitose.ac.jp

For the demand for highly interoperable educational systems, it is important to find ways to make various educational systems easily used as Learning Tools Interoperability (LTI)[1] based systems. The purpose of this study is to develop an LTI gateway system that will enable educational systems that have yet to be LTI-tooled to be used as LTI tools.

Figure 1 shows a system overview of the architecture of the LTI gateway tool proposed in this study. The proposed method is to prepare an LTI gateway system for an educational system (we call it External Tool) that we wish to convert into an LTI tool. The LTI Gateway System provides basic LTI features to the LTI platform. On the other hand, it represents requests and responses to the External Tool. This method will provide services from the External Tool to the LTI platform as if they were by the LTI Tool.

This paper reports the results of two implementation test of represents external tools from the LTI gateway System. The first implementation is the LTI Gateway System redirects requests from the LTI platform directly to the External Tool. The second implementation is instead of redirecting, the LTI Gateway System executes a new request based on the request from the LTI platform and returns the results to the LTI platform.

As a result, it was found that both methods could represent the External Tool's service to the LTI platform side. However, when considering the support for the more diverse functions of LTI, it became clear that the second method was more suitable.

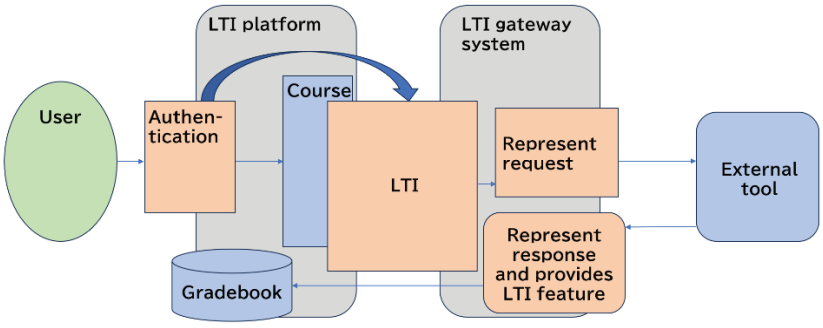

Figure 1. System Overview

References

[1] 1EdTechConsortium : ” Learning Tools Interoperability” https://www.1edtech.org/standards/lti(accessed Aug 2024)

Investigation of the inactivation effects of different UV intensity at 213 nm and irradiation time.

Tatsuro Kagawa[1], Kazuhiro Dainaka[1] and Nobuhiro Umemura[1]

[1] Chitose Institute of Science and Technology, Bibi 758-65, Chitose, Hokkaido 066-8655, Japan
E-mail address : umemura@photon.chitose.ac.jp

1. Abstract

We study on sterilization in agar medium by irradiating pulsed deep ultraviolet(UV) laser radiation at 213 nm. Based on previous research results [1,2], we examine high UV pulse energy with short irradiation time and low UV pulse energy with long irradiation time.

2. Material and Experimental Method

Microorganisms used in this experiment were Staphylococcus aureus (NBRC 13276) strains. S. aureus were cultured in 50 mL LB medium for 16 hours at 37℃ to achieve stationary phase. Next, we exerted E. coli from LB medium and diluted in 1×PBS buffer to achieve optical density to 0.01 at 600 nm wavelength. Prior to UV dose, 100μL solution was taken and spread on agar medium. After UV dose, agar medium was incubated for 24 hours at 37℃ and the sterilization effect was evaluated from a ratio of cultured colony area on a petri plate analyzed by Image-J software.

In this study, we used Nd:YAG laser operating at a repetition rate of 10Hz were used as an UV light source. The experimental setup for 5HG is shown in Fig. 1. We expanded the UV beam to cover all area of a petri plate.

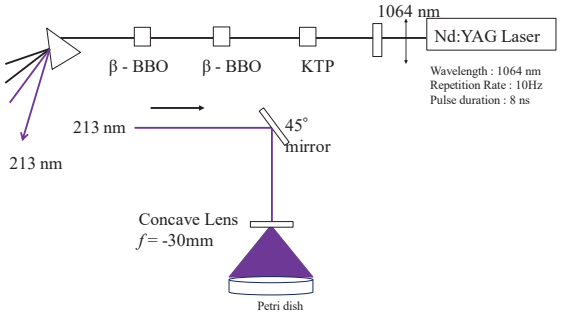

Fig 1 Experimental setup for 5HG at 213 nm

3. Experimental Results

Fig. 2 shows the results for the sterilization effect of S. aureus. We confirmed that low UV pulse energy with long irradiation time shows higher sterilization effect than that of high pulse energy with short irradiation time. The tendency of this result had been reported in Nagoya City University in 2022 [2].

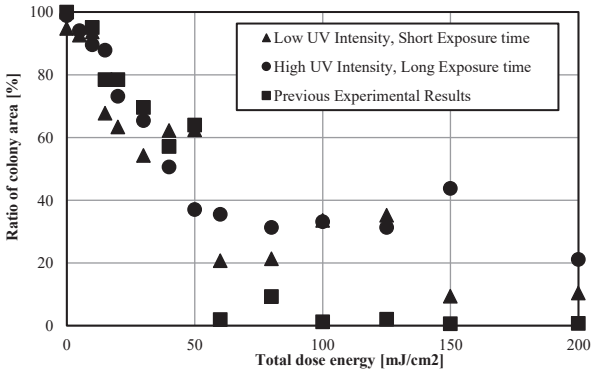

Fig 2 Sterilization effect of S. aureus

References

[1] N. Umemura et al., ALPSp1-05 (2023)

[2] K. Dainaka, Masters Thesis of CIST (2024)

[3] T. Matsumoto et al., Scientific Reports (2022)

Elucidation of anomalous fluorescence properties of 2,4-bis(1,3-benzothiazolylphenol derivatives

Yuma Hirose[1], Haruto Yamakawa[1], Ken-ichi Sakai[1] and Tomoyuki Akutagawa[2]

[1] Chitose Institute of Science and Technology
[2] IMRAM, Tohoku university

m2240400@photon.chitose.ac.jp

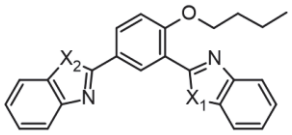

$X_1 = X_2 = S$: Alkoxylated 2,4-DBTP

2,4-bis(1,3-benzothiazol2-yl)-phenol (2,4-DBTP) emits yellow fluorescence with a large Stokes shift due to excited-state intramolecular proton transfer (ESIPT). Alkoxylation of the hydroxy group at the ESIPT site of this molecule results in a comparable Stokes shift in the crystalline state and orange fluorescence with a maximum around 570 nm, even though ESIPT is no longer assumed(Fig. 1, left). In solution, it emits a variety of fluorescence depending on the type of solvent and dye concentration. In acetone solution, blue-violet fluorescence with a maximum around 400 nm appears (Fig. 1, right). As the concentration of the dye increased, the intensity of this fluorescence decreased markedly, while blue-green fluorescence with a maximum near 500 nm appeared. At that time, the colorless solution also turned yellow, and the absorption and fluorescence spectra were found to have a mirror image relationship with a small Stokes shift, probably originating from the aggregates. We believe that the benzothiazole group in the para-position of the alkoxy group is responsible for this unique fluorescence, and we are currently synthesizing molecules with other benzoazole groups($X_1, X_2 = O, NH$) by changing the benzothiazole groups in the para and ortho positions and investigating their fluorescent properties.

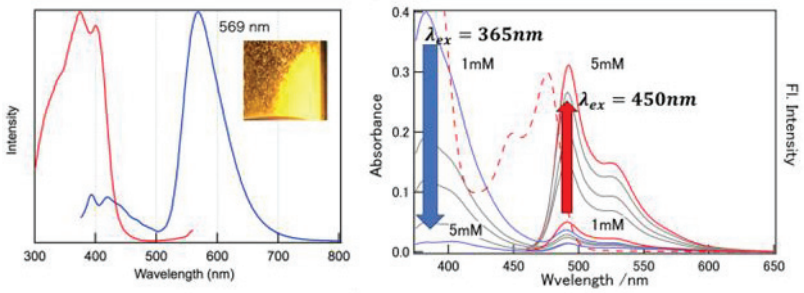

Figure 1. Fluorescence and excitation spectra of (left) powder of alkoxylated 2,4-DBTP and (right) fluorescence spectrum in acetone solution as a function of dye concentration.

Analysis of the Aggregated Structure of C_3-Symmetric Molecules with a Cyclic Hydrogen Bonding Network

Akihiro Kakiyama[1], Manami Uemura[1], Ken-ichi Sakai[1] and Tomoyuki Akutagawa[2]

[1]Department of Applied Chemistry and Bioscience, Chitose Institute of Science and Technology, [2]IMRAM, Tohoku university

Email: b2210620@photon.chitose.ac.jp

In this study, we synthesized C_3-symmetric molecules with a cyclic hydrogen bonding network centered in the structure (**Figure 1**) and observed their aggregate formation in $CHCl_3$ solution using ultraviolet-visible absorption spectroscopy. Additionally, we analyzed the molecular aggregation structures in the solvent using Raman spectroscopy. As a result, for both molecules—one with methoxy substituents at the terminal and the other with methyl substituents—a new absorption peak appeared in the visible light region (at 530nm) with increasing solution concentration, which was absent at low concentrations, confirming aggregate formation in both cases. Notably, the rate of absorbance increase was greater for the methoxy-substituted molecule than for the methyl-substituted one, suggesting that intermolecular interactions involving the terminal substituents may influence aggregate formation. Furthermore, in the Raman spectrum within the range of 1200–1900 cm^{-1}, no peak shifts corresponding to functional groups were observed with increasing concentration, indicating the need for reevaluation of the solvent and measurement conditions.

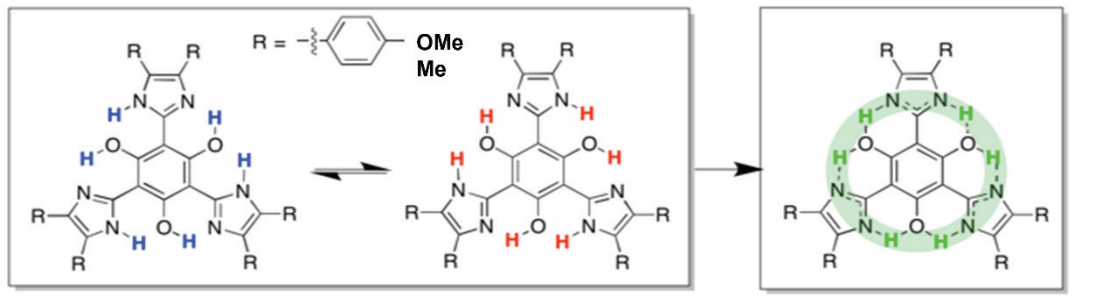

Figure 1: The chemical structure of the synthesized molecule.

Thermal and Fluorescence Properties of Methyl Salicylate Derivatives with an Anchor Site for Self-Assembling

Kei Kobayashi[1], Ken-ichi Sakai[1] and Takashi Nakanishi[2]

[1] Chitose Institute of Science and Technology
[2] National Institute of Materials Science

m2230130@photon.chitose.ac.jp

Supramolecular aggregates are formed through noncovalent intermolecular forces such as π-π, dipole-dipole, and intermolecular hydrogen bonding interactions. Molecules with a large π-system and dipole moment tend to self-assemble into aggregates. On the other hand, we recently found an exception: methyl salicylate (MS) can form aggregates with optical properties characteristic of excitons spread over multiple MS molecules, despite being a small π-system [1].

In this study, we synthesized MS-OC_n that is attached alkoky chain to MS. In case of alkoxy chain length of MS-OC_n is n=4~7, they obtained as molecular liquids. Herein, we report thermal and fluorescent properties of MS-OC_n in order to be revealed characteristics their molecular liquids. Their molecular liquids have absorption and fluorescence spectra in the peak at 340nm and 410nm in dilute solutions. On the other hand, in case of high concentration solutions or neat state, new absorption and fluorescence spectra appeared 400-500nm and 500-600nm region. Their results suggested that MS-OC_n(n=4~7) have aggregation form. Furthermore, MS-OC_3 of solid state at room temperature didn't appear optical properties by aggregation form, but MS-OC_3 of liquid state at about 90°C appeared optical properties similar to MS-OC_n(n=4~7). In addition to, IR spectra of MS-OC_3 of liquid state was very similar to MS-OC_4 too (**Fig. 1**). Therefore, MS-OC_4 and MS-OC_3 can be considered to have similar structure in liquid state. We currently considered to characteristics of MS-OC_n includ DSC and XRD results too.

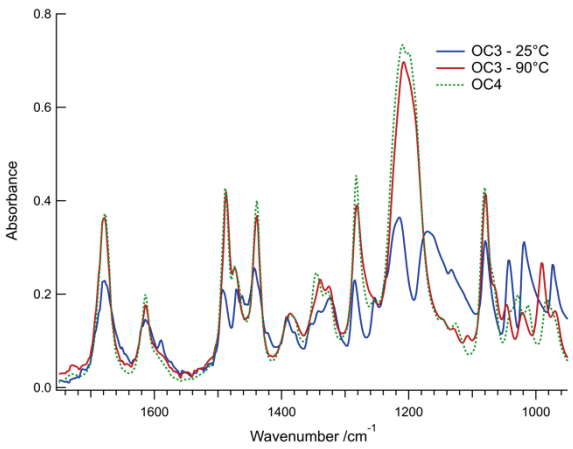

OC_3 and MS-OC_4 of neat state. MS-OC_3 and MS-OC_4 at the 25°C are appeared blue solid lines a nd green dotted lines. MS-OC_3 at the 90°C is olid lines.

References

[1] M. Takahashi, K. Sakai, K. Sambe, T. Akutagawa, *J. Phys. Chem. B*. **126**, 3116 (2022).

Performance Verification of an RSSI Indoor Localization Technique using a Two-Step Estimation Algorithm

Reiya Muraguchi[1], Yasuhiro Takano[1], Hsuan-Jung Su[2], and Yoshiaki Shiraishi[3]

[1] Chitose Institute of Science and Technology
[2]National Taiwan University, [3]Kobe University

{m2240460, y-takano}@photon.chitose.ac.jp

Receive Signal Strength Indicator (RSSI)-based localization technique is one of the most popular solutions to indoor positioning problems since the RSSI is measured as default in most wireless standards such as 802.11 [1]. It is expected that, in general, the more anchor nodes there are, the more accurate the estimate will be. According to our experiments, however, the improvement may not always be significant for more than five anchor nodes due to noisy measurements in actual system setups. Motivated by the observation, this study investigates if the estimation performance can be improved by using two-step estimation algorithms that aim to extract reliable samples from noisy measurements. Recently, Kosaka et al. showed in [2] that their two-step technique, referred to as eXtreme Gradient Boosting (XGBoost), outperforms the conventional techniques. However, the verification in [2] assumes that RSSI samples are obtained in Log Norma Shadowing Model (LNSM). Note that the LNSM can be irrelevant to capture structure of indoor enviornment since it is based on the Rician channels widely used for outdoor propagation scenarios. To confirm the benchmarks, we re-verify the XGBoost, by comparing a Deep Neural Network (DNN)-based algorithm [3], in Ray-tracing channel models that can compute RSSIs from line-of-sight paths and reflection paths based on specific room structure. According to our verification, XGBoost does not improve Mean Absolute Error (MAE) performance over the DNN in the LNSM. However, in ray-tracing channels, MAE performance obtained from XGBoost and DNN are 0.6m and 0.7m, respectively. For future work, we improve the two-step strategy aiming to obtain further accurate location estimates.

References

[1] S. R. Jondhale, R. S. Deshpande, S. M. Walke and A. S. Jondhale, "Issues and challenges in RSSI based target localization and tracking in wireless sensor networks," 2016 International Conference on Automatic Control and Dynamic Optimization Techniques (ICACDOT), Pune, India, 2016, pp. 594-598, doi: 10.1109/ICACDOT.2016.7877655.

[2] T. Kosaka, S. Wandale and K. Ichige, "RSSI-Based Indoor Localization Using Two-Step XGBoost," in IEICE Communications Express, vol. 12, no. 12, pp. 647-650, December 2023, doi: 10.23919/comex.2023XBL0123.

[3] Z. Munadhil, S. K. Gharghan, A. H. Mutlag, A. Al-Naji and J. Chahl, "Neural Network-Based Alzheimer's Patient Localization for Wireless Sensor Network in an Indoor Environment," in IEEE Access, vol. 8, pp. 150527-150538, 2020, doi: 10.1109/ACCESS.2020.3016832.

A Survey on Colorization Techniques for Near-Infrared Images

Shunsuke Shimada[1], Yasuhiro Takano[1] and Yoshiaki Shiraishi[2]

[1] Grad. School of Sci. & Tech., Chitose Institute of Science and Technology
[2] Grad. School of Engineering, Kobe University

{m2240260, y-takano}@photon.chitose.ac.jp

Near-infrared (NIR) cameras are widely used for foreign object detection-, smart vehicular-, and night vision security-systems, since they can capture NIR spectrums of which reflection response corresponds to the materials of target objects. NIR images are often recoded in a gray-scale format by converting the NIR spectrums that invisible for human. It is, however, preferable for human to easily recognize the image in a color format like the red-green-blue (RGB) model. In this initial technical report, we verify conventional colorization techniques for NIR images to confirm those accuracy and potential problems. Specifically, autoencoder (AE)-based [1] and deep-convolutional generative adversarial network (DCGAN)-based [2] colorization techniques are investigated. Figure 1 illustrates the verification results for five cases according to the columns, where input NIR images in the gray-scale format and the ground truth images in RGB format are respectively shown in the first and second rows. According to our verification, the DCGAN-based technique obtains a 10 dB gain over the AE in terms of average peak signal-to-noise ratio (PSNR) performance. This is because, as shown in the 4th row of Figure 1, DCGAN-based technique achieves PSNR=22.9 dB after learning NIR images expectedly. However, as shown in the 3rd row, the AE-based technique deteriorates PSNR=12.4 dB. NIR images have unique spectral properties that differ significantly from those of visible light images. Since AE assumes input images to be grayscale representations of visible light, it cannot accurately map the NIR spectral data to corresponding RGB colors, resulting in a noticeable drop in PSNR.

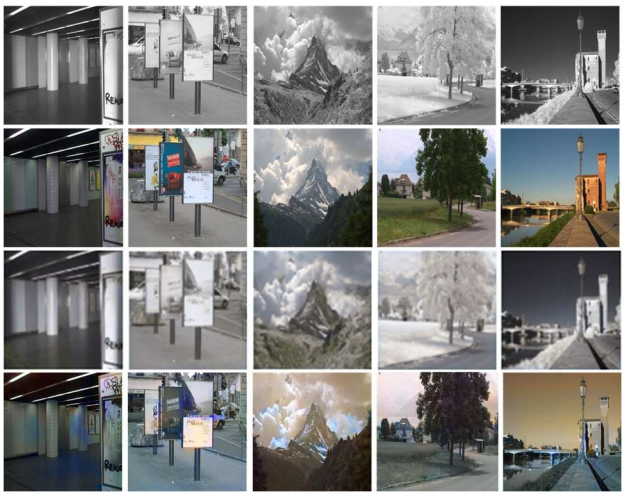

Figure 1. Verification results for 5 cases by columns. 1st row: NIR inputs, 2nd row: ground truth data in RGB, 3rd row: outputs with AE, 4th row: outputs with DCGAN

References

[1] G. E. Hinton, R. R. Salakhutdinov, “Reducing the Dimensionality of Data with Neural Networks,” Science, vol. 313, pp.504-507, 2006.

[2] A. Radford, L. Metz and S. Chintala, “Unsupervised Representation Learning with Deep Convolutional Generative Adversarial Networks,” arXiv, 2016. https://arxiv.org/abs/1511.06434

Control of Photoinduced Electron Transfer via Supramolecular Complex Formation of Polymers with Electron-Donor Molecules

Hiroyasu Yamaguchi[1,*], Yilin Cao[1], Hikaru Sotome[2] and Syoji Ito[2]

[1]Graduate School of Science, Osaka University, Osaka 560-0043, Japan
[2]Graduate School of Engineering Science, Osaka University, Osaka 560-0043, Japan

hiroyasu@chem.sci.osaka-u.ac.jp

To transfer electrons efficiently from electron donors to electron acceptors, the distance between the two must be maintained appropriately to prevent reverse electron transfer. In this study, we report our finding that the amount of electron transfer products can be increased by adding polymers that can specifically form complexes with electron donors through various types of non-covalent bonds (**Figure 1**).

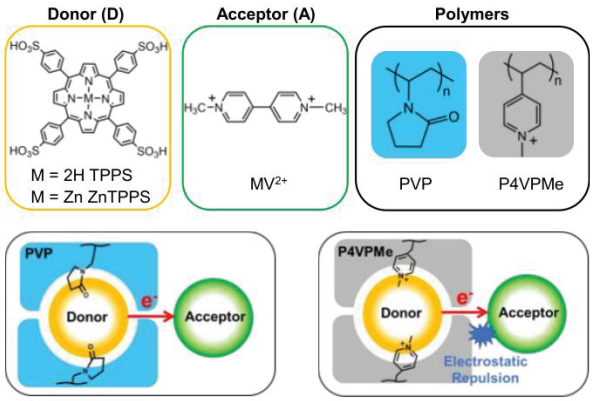

Figure 1. The chemical structures of electron donors (TPPS and ZnTPPS), electron acceptor (MV^{2+}), and polymers used in this study (PVP and P4VPMe).

Polyvinylpyrrolidone (PVP) was found to form complex with pigments 5,10,15,20-tetrakis-(4-sulfonatophenyl) porphyrin (TPPS) and its zinc complex (ZnTPPS) quantitatively through different interactions (hydrogen bonds and coordination bonds, respectively) (**Figure 2**). These complex formations hinder the interaction between ground-state TPPS or ZnTPPS and an electron acceptor (methyl viologen, MV^{2+}) and could control the photoinduced electron transfer from TPPS or ZnTPPS to MV^{2+}, giving more electron transfer products methyl viologen cationic radical ($MV^{+\bullet}$).[1]

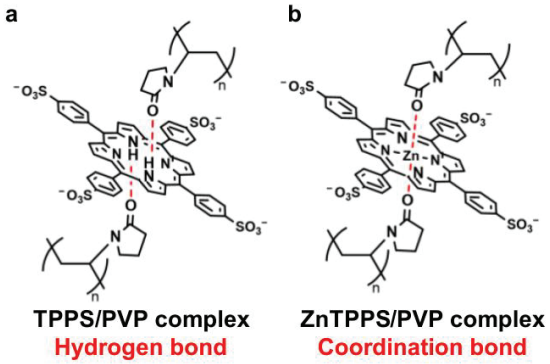

Figure 2. Conceptual figures of (a) TPPS/PVP and (b) ZnTPPS/PVP complexes.

An artificial photoinduced electron transfer system within a poly(*N*-methyl-4-vinylpyridinium) (P4VPMe) polymer matrix was also developed. In the presence of an excess of P4VPMe, ZnTPPS exists as individual molecules rather than self-aggregating, favoring photoinduced electron transfer. Under these conditions, P4VPMe inhibits the formation of ground-state charge-transfer complex between ZnTPPS and MV^{2+}. This shifts the main electron transfer process from singlet to triplet states. ZnTPPS with an excess of P4VPMe increased the catalytic activity of photoinduced oxidation of MV^{2+} more than 10-fold compared to ZnTPPS alone (**Figure 1b**).[2]

References

1 Y. Cao, T. Takasaki, S. Yamashita, Y. Mizutani, A. Harada, H. Yamaguchi, *Polymers* **14**, 1191 (2022).
2 Y. Cao, H. Sotome, Y. Kobayashi, S. Ito, H. Yamaguchi, *J. Photochem. Photobiol. A* **452**, 115593 (2024).

Functionalization of Supramolecular Complexes by Hybridization of Transition Metal Complexes with Biomolecules

Hiroyasu Yamaguchi[1,*], Yuichiro Kobayashi[1] and Akira Harada[2]

[1]Graduate School of Science, Osaka University, Toyonaka, Osaka 560-0043, Japan
[2]SANKEN, Osaka University, Ibaraki, Osaka 567-0047, Japan

hiroyasu@chem.sci.osaka-u.ac.jp

In biological systems, life processes are led by the unique behavior of macromolecules such as proteins and DNA. Molecular recognition by macromolecules plays an important role, for example, in substrate specificity of enzymes and antigen-antibody reactions in human life. Selective molecular recognition among macromolecules is achieved through a large number of weak interactions. We have developed novel materials through hybridization of bio-related macromolecules with synthetic small molecules. We constructed functionalized catalytic systems based on specific molecular recognition of bio-related polymers and selective assembly of bio/synthetic molecules.

Horseradish peroxidase (HRP) exhibits catalytic activity when L-histidine, at the active site of apohorseradish peroxidase (apoHRP), and iron porphyrin (FePor) form a complex via a metal–ligand interaction. The catalytic activities cannot be expressed by apoHRP alone. One clear challenge in developing catalysts is the ability to control their activity on demand. A controlled catalytic system, operated via mechanical forces, is versatile. However, there are few reports concerning catalytic activity via mechanical forces. Here, we report a system to express catalytic activity by adhesion of an apoenzyme gel and a cofactor gel. The apoenzyme- and cofactor gels (**Figure 1a**) act as catalysts when they form an assembly, but they lose catalytic ability upon manual dissociation (**Figure 1b**). We successfully constructed a system with controllable catalytic activity via the adhesion of gels at the macroscale.

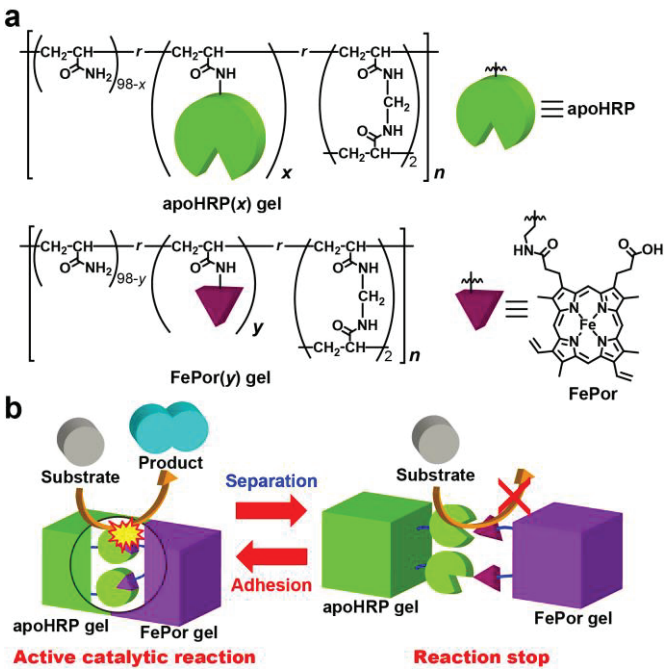

Figure 1. Chemical structures of apoHRP(*x*) gel and FePor(*y*) gel. **a** ApoHRP or FePor moieties are modified with poly(acrylamide) based gels. *x* and *y* indicate the mol% of apoHRP and FePor moieties, respectively. **b** Switchable catalytic activity system via adhesion and separation of apoHRP gel with FePor gel.

Convex-tape Driven Parallel Robot For 3D Shape Reconstruction

Reo Yamada[1]* and Hirooki Aoki[1]

[1] Graduate School of Science and Technology, Chitose Institute of Science and Technology, Chitose 066-8655, Japan
[2] Faculty of Science and Technology, Chitose Institute of Science and Technology, Chitose 066-8655, Japan

m2230360@photon.ac.jp

This study aims to construct a system to acquire 3D shape information of the entire circumference of plants without deforming them, which can be used for monitoring growth in plant factories. We propose a method to acquire 3D point clouds of plants from multiple directions using Convex-tape Driven Parallel Robot. Furthermore, all-surrounding 3D shape reconstruction is performed. Convex-tape Driven Parallel Robots use convex tapes as a force transmission medium [1]. Convex tape can increase the range of motion. Using a prototype robot (Fig 1) to move an RGB-D camera, multiple-frame 3D point clouds were reconstructed from RGB and depth images. These point clouds were then aligned and combined using the ICP algorithm, and a detailed all-surrounding 3D shape was reconstructed (Fig 2).

References

1 R. Yamada, H. Aoki: "Construction of New Cable-Driven Parallel Robot Using Convex Tapes for 3D reconstruction", *International Workshop on Frontiers of Computer Vision* (2024)

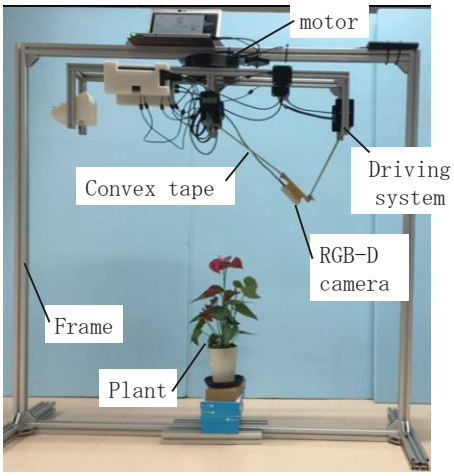

Figure 1. Prototype robot

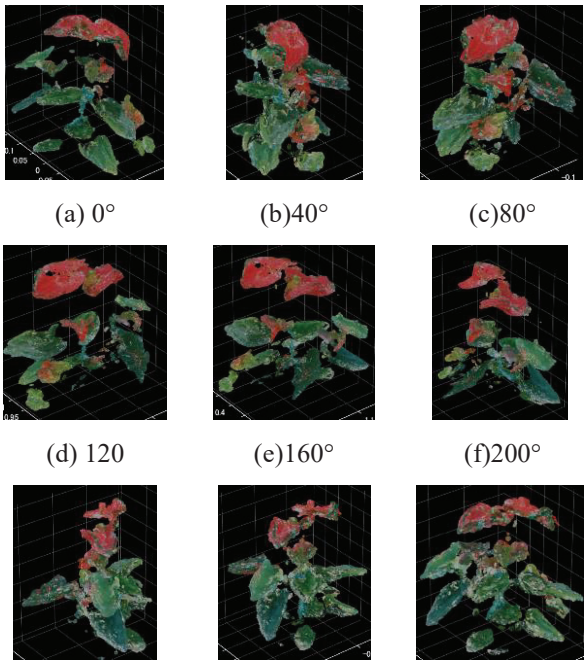

Figure 2. Reconstructed 3D point cloud.

Proposal for estimating the Volume of Cherry Tomatoes by 3D Image Measurement

Shimpei Okado[1], Hirooki Aoki[2]

[1]Graduate School of Science and Technology, Chitose Institute of Science and Technology, Chitose, 066-8655, Japan
[2]Faculty of School of Science and Technology, Chitose Institute of Science and Technology, Chitose, 066-8655, Japan

m2240110@photon.chitose.ac.jp

Quantitative evaluation of plant growth is useful in optimizing the growth environment in plant factories. As a method for quantifying plant growth, 3D shape measurement using 3D image sensors has been reported in many cases. To evaluate the growth of fruit vegetables we have conducted a study to quantify the growth by calculating the volume of fruits using a 3D image sensor. In this study, we propose a method to quantify the growth of cherry tomatoes.

The measurement system is shown in Figure 1. A 3D image sensor, Intel RealSense Depth Camera D415, was used to acquire the 3D point cloud of cherry tomatoes. The D415 images target on the plane from an oblique upward direction, and the reconstructed 3D point cloud is rotated so the plane is horizontal. By projecting the 3D point cloud toward the plane, orthographic projection is performed and an ortho image is obtained. In our proposed method, dimensional information is added to the ortho image by mapping one pixel to 1mm x 1mm. Semantic segmentation using SegNet was applied to the ortho image to extract the regions of cherry tomato fruit. The 3D point cloud of cherry tomato fruit was reconstructed from the pixels corresponding to the regions. After complementing the occluded region, the volume was estimated by approximating the ellipsoid sphere using the iterative least-squares method. Initial and lower bounds for unknowns in the iterative calculations were set from the number of pixels in the regions of cherry tomato fruit.

The volume of five cherry tomatoes was estimated, and the errors between the estimation results and ground truth of the volume was determined. Ground truth was measured from the change in the volume of water using a measuring cylinder. The results are shown in Table 1. For all samples, the error was less than 1 ml, indicating that volume estimation was feasible. In the future, we plan to measure changes in the volume of cherry tomatoes over time to quantify their growth.

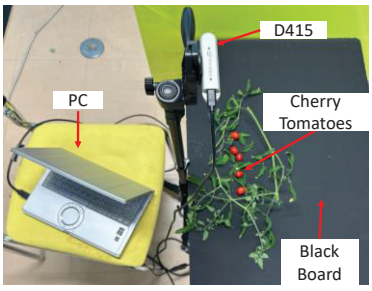

Figure 1. Measurement System

Table 1. Volume Estimation Results [ml]

	CT1	CT2	CT3	CT4	CT5
Estimation Results	6.47	4.35	6.02	6.53	4.35
Ground Truth	7.0	4.9	6.9	6.8	4.9
Error	-0.53	-0.55	-0.88	-0.27	-0.37

Sample preparation for characterizing soft and hard tissues using Fourier transform infrared spectroscopy in attenuated total reflection mode

Miu Murao and Hiromi Kimura-Suda

Graduate School of Science and Technology, Chitose Institute of Science and Technology, Chitose 066-8655, Japan

e-mail: kimurasu@photon.chitose.ac.jp

Fourier transform infrared (FTIR) spectroscopy is a powerful tool for the characterization soft and hard tissues. We have been working on development of methods for assessing bone quality, including structural and material properties, using FTIR imaging. The FTIR image can provide information on the distribution of chemical composition and is therefore useful for determining the distribution of bone quality factors in bone tissue with heterogeneous compositional distribution. On the other hand, FTIR imaging is not suitable for clinical applications because of the time-consuming sample preparation required. Attenuated total reflection (ATR) mode has potential as an easier and faster method to evaluate bone quality using FTIR spectroscopy. In this study, we investigated sample preparation for the clinical application of the ATR mode for the evaluation of soft and hard tissues. Vertebrae and cartilage of adult kokanee salmon caught in Lake Shikotsu were removed and characterized before and after drying using FTIR spectroscopy in ATR and transmission modes. The ATR spectra of the fresh vertebrae showed significant shifts in both the amide l and PO_4^{3-} bands compared to the transmission spectra. To investigate the influence of water on the band shifts observed in the FTIR spectra of vertebrae, we compared the ATR spectra of cartilage before and after drying. With or without drying, the amide bands were shifted compared to those obtained in transmission mode (Figure 1). These results indicated that when evaluating cartilage and bone using the ATR mode, it may not be necessary to take into consideration the influence of water contained in the sample.

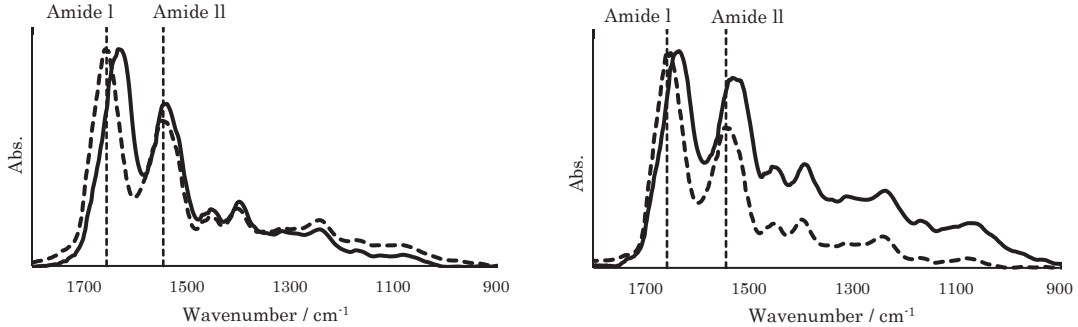

Figure 1. FTIR spectra of nucleus pulposus in kokanee salmon before (left) and after (right) drying, acquired in the ATR (bold line) and transmission (dashed line) modes.

References

1 Kimura-Suda H, Takahata M, Ito T, Shimizu T, Kanazawa K, Ota M, et al. PLoS ONE 13(2): e0189650 (2018).

Single-Shot Chirped Pulse Phase-Shifting Digital holography for Capturing Ultrafast Optical Wavefront Sequences

Wataru Fukuda* and Naoki Karasawa
Graduate School of Science and Technology, Chitose Institute of Science and Technology, 758-65 Bibi Chitose, 066-8655, Japan
m2230300@photon.chitose.ac.jp

In our laboratory, we previously demonstrated the capture of ultrafast optical wavefront sequences using chirped pulse phase-shifting digital holography [1]. In this study, we demonstrated the capture of ultrafast optical wavefront sequences using single-shot chirped pulse phase-shifting digital holography.

Figure 1 shows the experimental optical system. The object pulse divided by BS2 passes through a pentagon-shaped slit with a concave lens of 2 m focal length and a star-shaped slit with a convex lens of 2 m focal length, respectively. The reference pulse is chirped by high refractive index glass and becomes circularly polarized by a 1/4 plate. The timing of the reference light is adjusted such that it interferes with the object light passing through the pentagon-shaped slit on the long wavelength (802 nm) side and with the object light passing through the star-shaped slit on the short wavelength (791 nm) side. The interference light is split into two by the DOE, and each light wave is incident on the BPF at different angles, allowing only light of a specific wavelength to pass through. The split light is recorded by a polarization camera in different regions as intensity images in four different linear polarization directions. A pulse picker is used to select one pulse every 1/8 s, and its output signal is used to trigger the exposure of a polarization camera. The exposure time of the camera is set to be 1.048 μs and the delay time of the pulse is set to be 124.778 ms. The light wavefront of each object light is reconstructed using a computer.

Figure 2 shows the reconstructed images. (a), (a') are amplitude and phase images of the object pulse on the long wavelength side, while (b), (b') are those on the short wavelength side. From the results, it is shown that the ultrafast optical wavefront sequences can be recorded by single-shot chirped pulse phase-shifting digital holography.

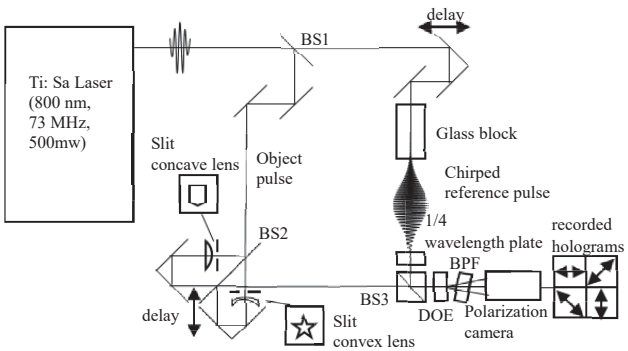

Figure 1. Experimental Setup, BS: Beam Splitter, DOE: Diffractive Optical Element, BPF: Band Pass filter

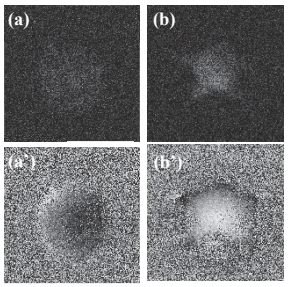

Figure 2. (a), and (b) show the reconstructed amplitude images. (a'), and (b') show the reconstructed phase images. (a), and (a') show the long wavelength images. (b), and (b') show the short wavelength image.

References

[1] W. Fukuda and N. Karasawa, "Demonstration of chirped pulse phase-shifting digital holography for capturing the sequence of ultrafast optical wavefronts," Applied optics, Vol. 63, Issue 20, pp. 5472-5478 (2024)

Corrosion protection of damaged metal covered with self-healing coating in freezing situation

Runa Hiraki[1*], Rin Takada[1], Kanon Kato[1] and Makoto Chiba[1,*]

[1] National Institute of Technology, Asahikawa College,
Shunkodai 2-2-1-6, 071-8142, Japan

[*]makoto@asahikawa-nct.ac.jp

In our laboratory, a "self-healing coating", this is an organic coating dispersing many capsules containing a healing agent, is currently developing. When a defect formed in this coating, the capsules dispersed in this coating are broken at the same time, and the healing agent containing in the capsules is released to the defected area of the coating, then this reacts with moisture in the air to form a self-healing structure. By formation of this coating, corrosion protection of metals is improved for long term. On the other hand, when such coating are used in cold regions such as Hokkaido, rainwater adhere in the defected area, will freeze, and the stress by the volume change of freezing of water will generate. And this stress may break the self-healing structure formed at defected area of coating, as shown in Fig. 1. In this study, we investigated the effects of freezing of water in damaged area of coating on the corrosion protection of Al materials covered with self-healing coating. Fig. 2 (a) shows a surface SEM image of the normal coating, (b) self-healing coating, and (c) self-healing coating with freezing treatment after immersion testing and removal of all surface layers. From (a), pit formed by corrosion of Al substrate with about 250 μm was observed. However, from (b) and (c), no corrosion was observed and only clear defects were observed. These results suggest that when a defect formed in the self-healing coating, high corrosion protection. Moreover, by formation of the self-healing structure, high corrosion protection can be maintained even after the freezing treatment.

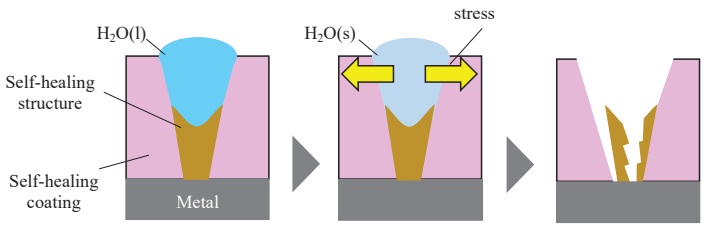

Fig. 1 Problems with self-healing coatings in cold regions

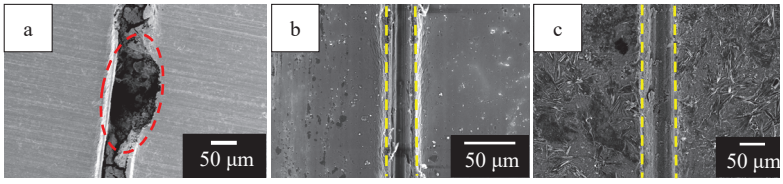

Fig. 2 Surface SEM image after immersion testing and removal of all surface layers

(a) Nomal coating

(b) Self-healing coating

(c) Self-healing coating with freezing treatment

Shape transient of defect formed on self-healing coating for corrosion protection of substrate metal

Shin Tamura[1*], Rin Takada[1], Jotaro Sato[1] and Makoto Chiba[1,*]

[1] National Institute of Technology, Asahikawa College,
Shunkodai 2-2-1-6, 071-8142, Japan

[*]makoto@asahikawa-nct.ac.jp

Organic coating is one of the most important surface treatment techniques for corrosion protection of metals. If this coating is damaged, however, the corrosion protection of substrate metals by formation of organic coatings will be lost soon. Therefore, organic coating with self-healing property, this coating can automatically heal without any treatment when the coated layer damaged, are strongly demanded from many industrial fields. This coating can be realization by dispersion many micro-capsules containing in healing agent of coating to the coating, as shown in Fig. 1-a. If this coating was damaged, capsules in this coating also break, simultaneously, and healing agent in the capsules is released to the damaged area of coating, as shown in Fig. 1-b. Moreover, the healing agent reacts with moisture in the air to form the self-healing structure and the damaged area of coating is covered again by this self-healing structure, without any treatment, shown in Fig. 1-c. In our previous study, this coating has a self-healing property if the coated layer is damaged. However, it is unknown how long time needs for formation of self-healing structure. The volumes of defects formed by micro-indentation test were measured and these changes were traced, in order to investigate the rate of self-healing of these coatings.

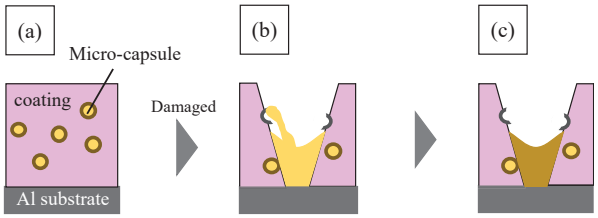

Fig. 1 Schematic illustration of self-healing coating developed in our research group

Fig. 2 shows the indentation volume of the Vickers indenter formed on the surface of normal coating and self-healing coating, measured by 3D-OM, and the Self-healing property calculated from the indentation volume vs. time. The values of self-healing property of a normal coating costing increase with time, up to 3 h after formation the defect. And then the value reached to the steady state value of 10 %. This value of the self-healing coating also increases during only first 3 h after the formation of the defect and reached to the steady state value. The steady state value of self-healing property of self-healing coating is about 75 %, and this value is much larger than that of normal coating.

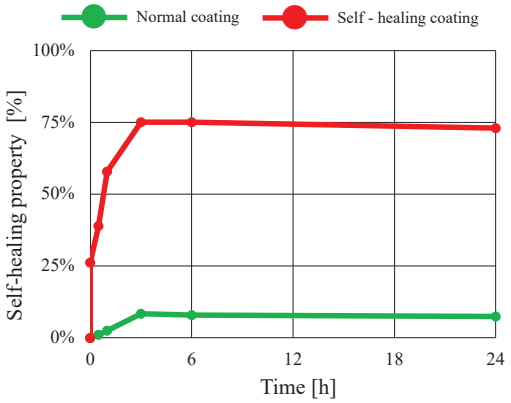

Fig. 2 Self-healing property vs. time

Corrosion morphology of aluminum formed during wet-dry cycling tests with solution containing anions

Saki Kawashima[1], Koharu Higashide[1], Fuka Kawamura[1], Koki Saito[1], Keishou Nishida[1] and Makoto Chiba[1,*]

[1] National Institute of technology, Asahikawa college, Shunkodai 2-2-1-6, 071-8142, Japan

[*]makoto@asahikawa-nct.ac.jp

Aluminum alloys are used as many products, such as bodies of automobile, because their weight is light and processability of them is excellent. However, atmospheric corrosion of aluminum materials sometime causes quite severe problem, because corrosion protection of aluminum alloys, itself is not so high. Under atmospheric condition, it is well known that aluminum materials undergo repeated wet–dry cycles, because contacting of the rain-water, containing with any kinds of salts, leads to corrosion under these wet–dry cycle conditions. In this study, corrosion morphology of aluminum alloys after wet-dry cycling condition with NaCl, $NaNO_3$, and Na_2SO_4 solutions were observed, in order to clear the corrosion mechanism of aluminum alloys under wet-dry cycling conditions. The wet-dry cycling condition can be simulated by following procedure. First, a single droplet of these solution is dripped on the sample surface. After a while, the water of the droplet dries out and leaves island of salt particles, by evaporation of water. After that, a droplet of pure water is placed at the same position on the specimen. Soon deposited particles are dissolved and sample is contact with solution, again.

The sample was a 20 × 20 mm piece of 1050-Al alloy (99.5% purity, 1.0 mm thick), after polishing mechanically. As wet-dry cycling corrosion test, the sample was placed on a stage held at 323 K of temperature. One drop (about 20 mm^3) of 0.02 M of NaCl, $NaNO_3$, or Na_2SO_4 solution was dropped on the surface of sample. After about 6 min, the droplets were almost completely dried. After 3 min of drying time, a drop of pure water was dripped to the same position of the sample again, and the wet and dry cycles were repeated for 150 cycles. After above corrosion test, the surface morphology is observed by a three-dimensional optical microscope (3D-OM). The sample were immersed in a 10 %-H_3PO_4 / 4 %-K_2CrO_4 solution (373 K) for 7.5 min to remove only the corrosion products.

Fig. 1 shows the optical image of a sample after 50 (-a) and 150 cycles (-b) of wet and dry cyclic testing in 0.02 M Na_2SO_4 solution and washing with acetone and the optical image. From Fig. 1, a dark colored circle can be observed at the center of these images. These are a corrosion products formed during wet-dry cycling corrosion test of Al materials. After removing the corrosion products, corrosion morphology can be observed. The maximum depth of the corrosion at 50 cycles was 17 μm and at 150 cycles was 24 μm, suggesting that the depth of corrosion increases with the number of cycles.

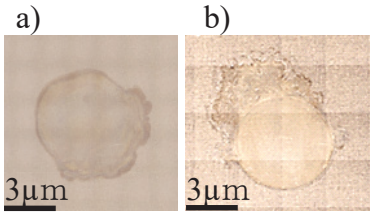

Fig. 1 Optical images after repeated wet and dry tests with 0.02M Na_2SO_4 solution and after acetone washing
a) Optical image after 50 cycles of repeated dry/wet testing
b) Optical image after 150 cycles of repeated dry/wet testing

Difference of Corrosion Morphology between that of Pure Iron during Immersion and Wet-Dry Cycling Tests

Reina Shibata[1], Fuka Kawamura[1], Koki Saito[1] and M. Chiba[1,*]

[1] National Institute of technology, Asahikawa college,
Shunkodai 2-2-1-6, 071-8142, Japan

[*]makoto@asahikawa-nct.ac.jp

Steels and iron based alloy are generally used as structural materials, such as bridges, but some bridges have been built, a half century ago. Thus, atmospheric corrosion of these materials may reduce safety. However, the mechanism of corrosion in atmospheric environments is still uncleared yet. This is because atmospheric corrosion occurs under repetitive dry and wet conditions. In order to investigate the corrosion mechanism, especially the effect of anions, such as NO_3^-, this is expected to be contained in the adhered water, this paper reports the corrosion morphology of iron after immersion test or wet-dry cycling test were observed. By the wet-dry cycling test, atmospheric conditions can be simulated. The wet-dry cycling test is done by following procedure. First, a single droplet of $NaNO_3$ solution is dripped on the iron surface. After a while, the water of the droplet dries out and leaves island of $NaNO_3$ particles, by evaporation of water. After that, a droplet of pure water is placed at the same position on the specimen. Soon deposited $NaNO_3$ particles are dissolved and specimen is contact with $NaNO_3$ solution, again.

Highly pure Fe after polishing mechanically, was used as a specimen. As wet-dry cycling corrosion test, the sample was placed on a stage held at 323 K of temperature. One drop (about 20 mm^3) of 0.02 M of $NaNO_3$ solution was dropped on the surface of sample. After about 6 min, the droplets were almost completely dried. After 3 min of drying time, a drop of pure water was dripped to the same position of the sample again, and the wet and dry cycles were repeated for 150 cycles. The specimens were then washed, and the surfaces were observed with a three-dimensional optical microscope (3D-OM). As the immersion test, the specimens were immersed in 35 mL of pure water or 0.02 M-$NaNO_3$ solution for 24 hours. After the wet-dry cycling test and immersion test, these specimens were washed and observed using a three-dimensional optical microscope (3D-OM).

Fig. 1 shows the optical images of the surface of the specimens after 150 cycles of wet-dry cycling test with pure water (a) and with $NaNO_3$ solution (b). From Fig. 1-a) reddish-brown colored corrosion product formed during wet-dry cycling test with pure water can be observed. However, less corrosion product formed during the corrosion test with $NaNO_3$ solution can be observed.

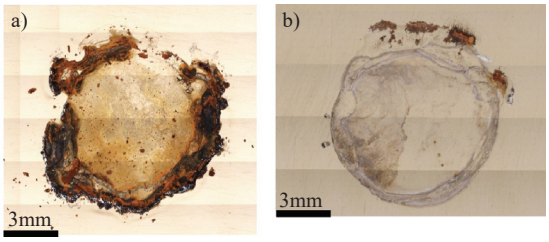

Fig. 1 Optical image of iron specimens after wet-dry cycling test
a) with pure water
b) with $NaNO_3$ solution

Development of medical adhesive materials with removability by external stimulation

Eri SEITOKU[1], Sirus SAFAEE[1], Mahdis NESABI[1], Ko NAKANISHI[2], Yuko ERA[3]
Alireza VALANEZHAD[1], Shigeaki ABE[1,*], Tomoya TAKADA[4],
Hiroshi MURATA[1] and Ikuya WATANABE[1]

[1] Graduate School of Biomedical Science, Nagasaki University, Nagasaki 095-8102, Japan
[2]Faculty of Dentisity, Hokkaido University, Sapporo 060-8586, Japan
[3] Saitama Prefectural University, Sannomiya 820, Kawagoe 343-8540, Japan
[6]Graduate School of Science and Technology, Chitose Institute of Science and Technology, Chitose Japan

sabe_den@nagasaki-u.ac.jp

In general, medical/dental adhesive materials in surgical fields are required strong mechanical property and adhesive property to the hard tissue. Based on these viewpoints, many researchers investigated then some adhesives were developed, such as PMMA resin cement. In contrast, the strong adhesion property sometimes generated some problems when removal the attached materials. In case of dental orthodontic fields, the strong adhesion sometimes induced invasive procedures on tooth when orthodontic anchoring screws were removed [1]. Therefore, it is required to reduce the adhesion strength on the screw removal. In this study, we investigated to control the adhesive property by external stimulation such as thermal process. For example, we have developed polyacrylamide derivatives hydrogel composite in previous study [2]. They can indicate reversive sol-gel conversion by external stimulation such as temperature change generated by IR light. Because carbon nanotube (CNT) can carry out effective light-thermal conversion under IR irradiation, the light irradiation induced thermal sol-gel conversion on the hydrogel composite contained CNT. Thus, the compounds are mixed into the adhesive materials then estimated the mechanical strength with/without external stimulation.

References

1 S. Yamagata et al., *Nano Biomedicine*, **8**, 35-40, (2016).
2 S. Abe et al., *Molecular Crystals and Liquid Crystals*, **763**, 73-79, (2023).

Effects of tree species on nitrogen deposition in forest stands around the livestock area

Masaharu Kato[1], Jun'ichiro Ide[1] and Izuki Endo[1]

[1]Department of Applied Chemistry and Bioscience, Chitose Institute of Science and Technology, Chitose 066-8655, Japan

m2240170@photon.chitose.ac.jp

In livestock areas, ammonia volatilization occurs during the composting process of livestock manure, which provides large amounts of nitrogen (N) to the surrounding land cover, such as forests. N emissions sometimes exceed the N saturation standard[1] (10 kgN ha^{-1} y^{-1}), which can in turn impact the nearby forests and thereby result in high levels of nitrate in forest streams. Previous studies have shown that different forest species, such as birch and oak, can change the rainfall partitioning and affect the deposition of N and other air pollutants. However, few studies have addressed how much differences in N deposition are there between forest stands with different tree species in livestock areas with high N deposition. Therefore, the purpose of this study was to clarify the extent to which N deposition differs between forest stands with different tree species in the livestock area.

Rainwater samplers were installed in Bibi park, located in Chitose, Japan, as a livestock area to collect throughfall water (TF) in the birch and oak forest stands (n = 3 for each) fortnightly from June to November 2023. Simultaneously, rainwater (RF) was also collected using the same samplers (n = 3) in the open area near the park. In collecting water samples, the amount of RF and TF were measured. After that, nitrate (NO_3^-) and ammonium (NH_4^+) concentrations in the samples were measured using ion chromatography in the laboratory. In this study, N depositions through RF and TF were calculated by multiplying the amount of RF and TF and the sum of NO_3^--N and NH_4^+-N concentrations obtained fortnightly, summing those fortnight values during the observation period, and converting the duration values to the annual values, respectively.

N deposition through RF was calculated to be 12.4 kgN ha^{-1} y^{-1}, indicating that it could be higher than the national average of bulk deposition (10.5 kgN ha^{-1} y^{-1}). The average N deposition through TF was 6.2 kgN ha^{-1} y^{-1} in the oak stand and 5.9 kgN ha^{-1} y^{-1} in the birch stand, which showed no significant difference. It is predicted that the similar physical characteristics of the two species, such as tree height and crown structure, affected dry and wet deposition processes rather than physiological characteristics, resulting in the similar N deposition through TF between the species in this study. The large differences in N deposition between RF and TF were attributable to the N absorption by the tree canopy[2]. Because of ammonia volatilization from the livestock manure, it is highly possible that tree canopy adsorbs the large amount of NH_4^+ through dry and wet deposition in the forests in the vicinity of the livestock area.

References

1. Tokuchi N, et al. *J Jpn For Soc* 105(6), 199-208. (2023).
2. Otuki K et al. (eds.) *An introduction to forest hydrology* (2022).

Low-cost maskless lithography process for flexible devices

Yuzuki Mikami, Gakuto Ito, Makito Haruta
Department of Opto-Electronic System Engineering, Institute of Science and Technology,
Chitose 066-8655, Japan

m-haruta@photon.chitose.ac.jp

Flexible devices are expected in the fields of medical health care and human interface. Their flexible structure is important for attaching wearable and implantable devices to body surfaces or organs, which measure vital data such as heartbeat and myoelectric activity. This research has developed a fabrication process for flexible devices with thin-film and CMOS sensors. This process creates a sensor circuit on a thin-film substrate by distributing small pieces of CMOS chips to provide flexibility. We create metal patterns on a thin-film substrate, using a polymer as the base substrate, through lithography and deposition. Then, CMOS chips are mounted on the flexible circuit. We have developed a low-cost maskless lithography process using an exposure device with an LCD monitor in Fig. 1. This exposure device uses a digital image created on a computer instead of a photo mask. This process reduces costs and saves time from making a photo mask. We successfully created circuit patterns with this device, as shown in Fig. 2.

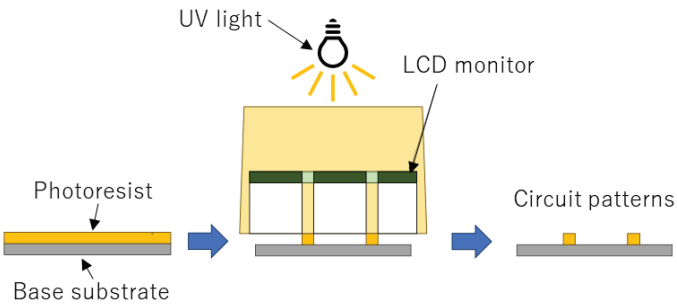

Fig. 1 Low-cost maskless lithography process

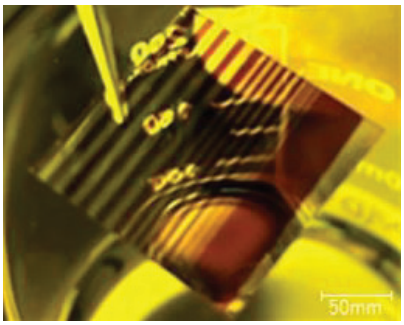

Fig. 2 Created circuit patterns

Reference

[1] Sugiyama, M., Uemura, T., Kondo, M. et al. An ultraflexible organic differential amplifier for recording electrocardiograms. Nat Electron 2, 351–360 (2019). https://doi.org/10.1038/s41928-019-0283-5

Development of the deep brain imaging device with the FOP probe

Ryusei Yago, Makito Haruta

Department of Opto-Electronic System Engineering,
Institute of Science and Technology, Chitose 066-8655, Japan

m-haruta@photon.chitose.ac.jp

Neuroscience studies have used optical methods to understand neural activities and elucidate the complex information-processing function of the interlaminar network of the cortex. Previous research developed a deep brain measurement method using a miniaturized fluorescence microscope and a prism probe [1]. The method observed neural activities in the depth direction but could not get a sufficient field of view to observe one to six layers of the cortex.

Our research has developed a deep brain imaging device that uses a Fiber Optic Plate (FOP) to observe six layers of the cortex. Using the FOP probe instead of a prism probe gives the device a wide field of view in the depth direction. The FOP probe can transmit clear optical images to a CMOS image sensor with a small and less invasive structure because the tip angle can be changed freely, as shown in Fig. 1.

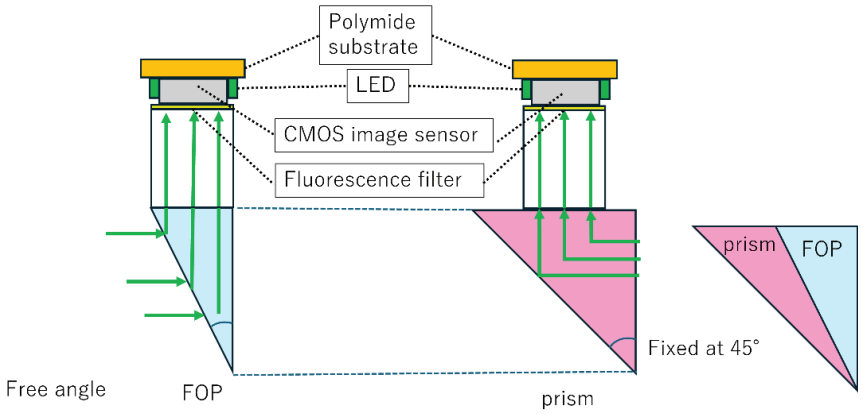

Figure 1: The deep brain imaging device with the FOP probe

Reference

[1] Gulati, S., Cao, V. Y., Otte, S. Multi-layer Cortical Ca2+ Imaging in Freely Moving Mice with Prism Probes and Miniaturized Fluorescence Microscopy., June 13, 2017.

Acknowledgment

This work was supported by JSPS KAKENHI Grant No. JP 23K06786.

Development of microchannels to integrate with a semiconductor sensor for Aquaponics

Airi Fukuhara, Ryusuke Sakuma, Iria Ito, Makito Haruta

Department of Opto-Electronic System Engineering Institute of Science and Technology, Chitose 066-8655, Japan
e-mail: m-haruta@photon.chitose.ac.jp

Aquaponics is a recirculating growth system that uses water from a freshwater fish tank for hydroponics (Fig. 1a). Toxic ammonia from fish waste is decomposed by microorganisms into nitrite ions, which plants then absorb. The plants act as a filtration system, enabling the efficient growth of both plants and fish. However, few newcomers to the aquaponics industry have entered the market because the method requires specialized knowledge, experience, and equipment in agriculture and aquaculture. We propose an IoT-based aquaponics system using semiconductor sensors. The concentration of nitrite (NO_2^-) in the water indicates the level of pollution. Based on the data acquired from the sensors, an environment optimized for plant and fish growth will be established. In this study, we developed microchannels to integrate with a semiconductor sensor for measuring NO_2^- concentrations in the fish tank. We are considering a CMOS image sensor capable of optical detection and an ion detection sensor [1], as semiconductor sensors. We successfully established a hydroponic environment (Fig.1b) and developed methods for fabricating microchannels (Fig. 1c).

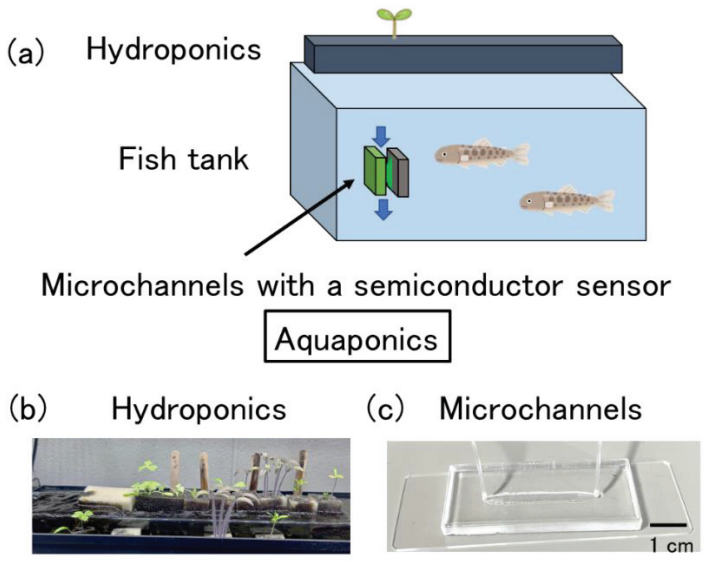

Figure 1 IoT-based aquaponics system using semiconductor sensors

Reference

[1] T. Hattori, F. Dasai, H. Sato, R. Kato, K.Sawada, Sensors 2019, Vol. 19, April 2019.

Acknowledgment

This work was supported by THE AKIYAMA LIFE SCIENCE FOUNDATION.